Detrital zircon geochronology and related evidence from clastic sediments in the Kyrenia Range, N Cyprus: Implications for the Mesozoic-Cenozoic erosional history and tectonics of southern Anatolia

Citation for published version:
Chen, G, Robertson, AHF & Wu, F 2022, 'Detrital zircon geochronology and related evidence from clastic sediments in the Kyrenia Range, N Cyprus: Implications for the Mesozoic-Cenozoic erosional history and tectonics of southern Anatolia', *Earth-Science Reviews*, vol. 233, 104167. https://doi.org/10.1016/j.earscirev.2022.104167

Digital Object Identifier (DOI):
10.1016/j.earscirev.2022.104167

Published In:
Earth-Science Reviews

Highlights

- Detrital zircon U-Pb and related analyses indicate the erosional history of S Anatolia
- The combined data indicate a switch from N to E sources related to Neogene collision
- The zircon and related data support tectonic development along N margin of S Neotethys

Abstract

Triassic to Pleistocene sandstones of the Kyrenia Range, N Cyprus provide an exceptional repository of the erosional history of Anatolia. The Kyrenia Range features in several different tectonic hypotheses of the Eastern Mediterranean region, which are tested here using a combination of new and recently published detrital zircon geochronology, zircon trace-element data and hafnium isotopic data. Minimum detrital zircon ages refine the ages of several formations in the Kyrenia Range. The new data also provide insights into sediment provenance including far-removed sources of Upper Paleozoic zircons, within-plate versus subduction-related sources (e.g., rift; oceanic/continental arc/ophiolite) and Neogene collision-related magmatism. Facies and paleocurrent data indicate a major switch in clastic sediment input from generally southwards to westwards during the Oligocene, which was mainly controlled by the collision of the Arabian promontory with Anatolia, leaving the S Neotethys as an isolated deep-water basin.

The U-Pb zircon age profiles indicate a prominent Late Neoproterozoic population, together with Carboniferous, Permian, Late Cretaceous and Miocene-aged clusters. Pan-African and Grenvillian-aged zircons were ultimately derived from Cadomian continental basement. Basement that rifted from Gondwana during the Triassic later became sources of detritus within Anatolia to the north. Devonian-Carboniferous zircons were originally supplied by active continental margin magmatism in southern Eurasia (Pontides) or

northern Gondwana (Afyon zone of the Anatolides). The proposed explanation is that detrital zircons were sequentially recycled, first to Upper Carboniferous-earliest Permian turbidites (within the Afyon zone to the east), later to Mid-Upper Triassic alluvium and turbidites (within the Taurides to the south), and finally to Triassic-Paleogene clastic sediments as now preserved in the Kyrenia Range. Upper Cretaceous zircons were derived from continental arc granitoids, oceanic arc and/or ophiolitic rocks and related metamorphic rocks, generally to the north of the Kyrenia Range. Paleogene zircons mainly represent late-stage continental margin arc magmatism in SE Turkey. During the Oligocene, the switch from mainly southward sediment supply to mainly westward sediment supply represents dominant input from the S Neotethyan suture zone in SE Turkey. Miocene zircons were mainly derived from post-collisional volcanics in SE Turkey. Paleoriver drainage systems in central/southeast Anatolia largely existed by the Late Miocene in response to collision-related surface uplift, in turn strongly influencing Miocene-Pleistocene zircon provenance in sub-basins within and adjacent to the Kyrenia Range.

The combined zircon and Hf data, together with assembled geological evidence, are used to discuss three contrasting tectonic hypotheses for the early Mesozoic-Eocene setting of the Kyrenia Range: (1) locally, in the easternmost Mediterranean (i.e., preferred interpretation); (2) far to the south, on the N African passive margin, and (3) far to the north, along (or near) the Eurasian margin. Overall, the present study exemplifies the diversity and complexity of clastic sediment sources within a developing orogen, with implications for some other regions.

Figure 1

Click here to access/download;Figure;Fig. 1.jpg

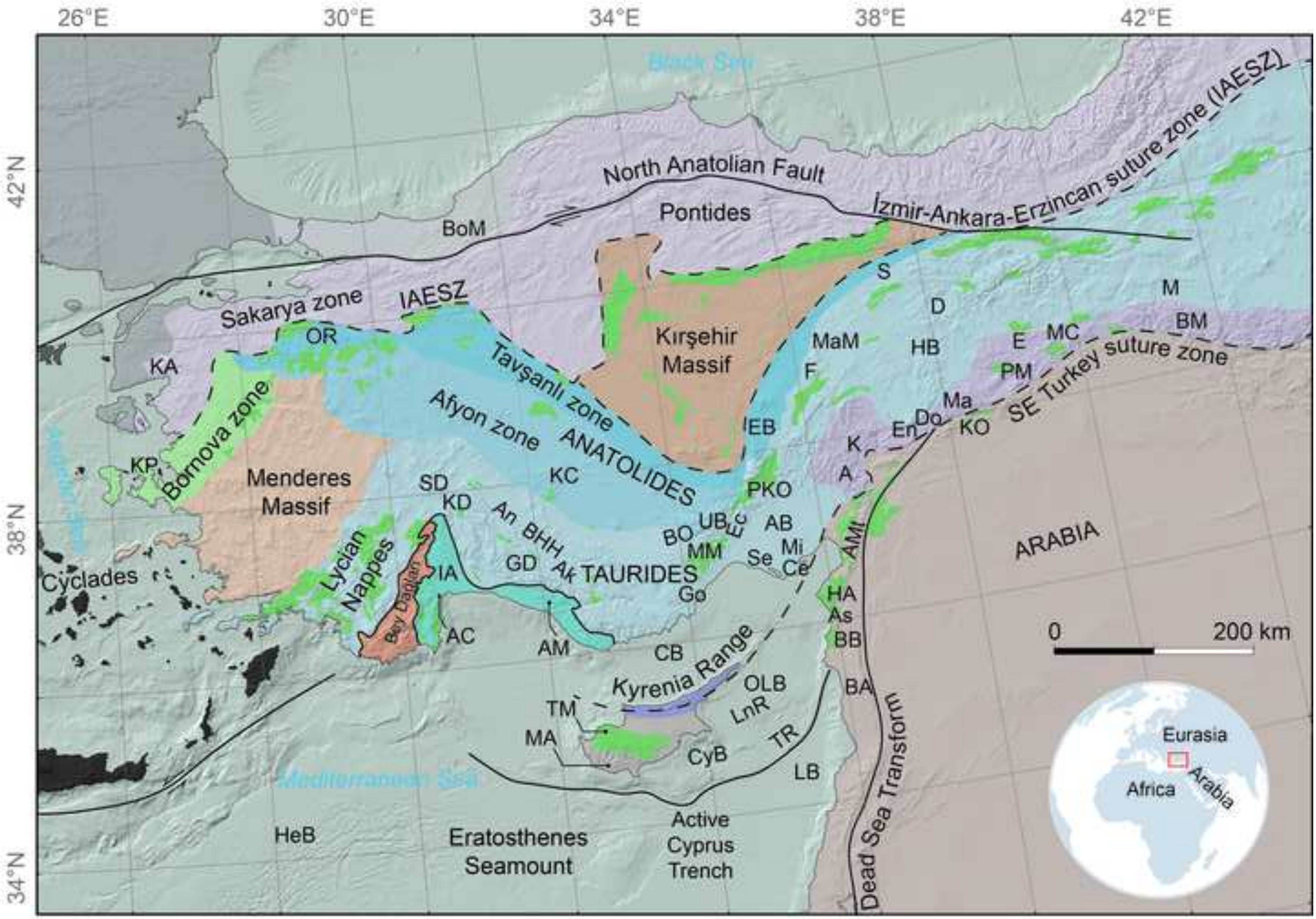

Figure 2 Click here to access/download;Figure;Fig. 2.jpg

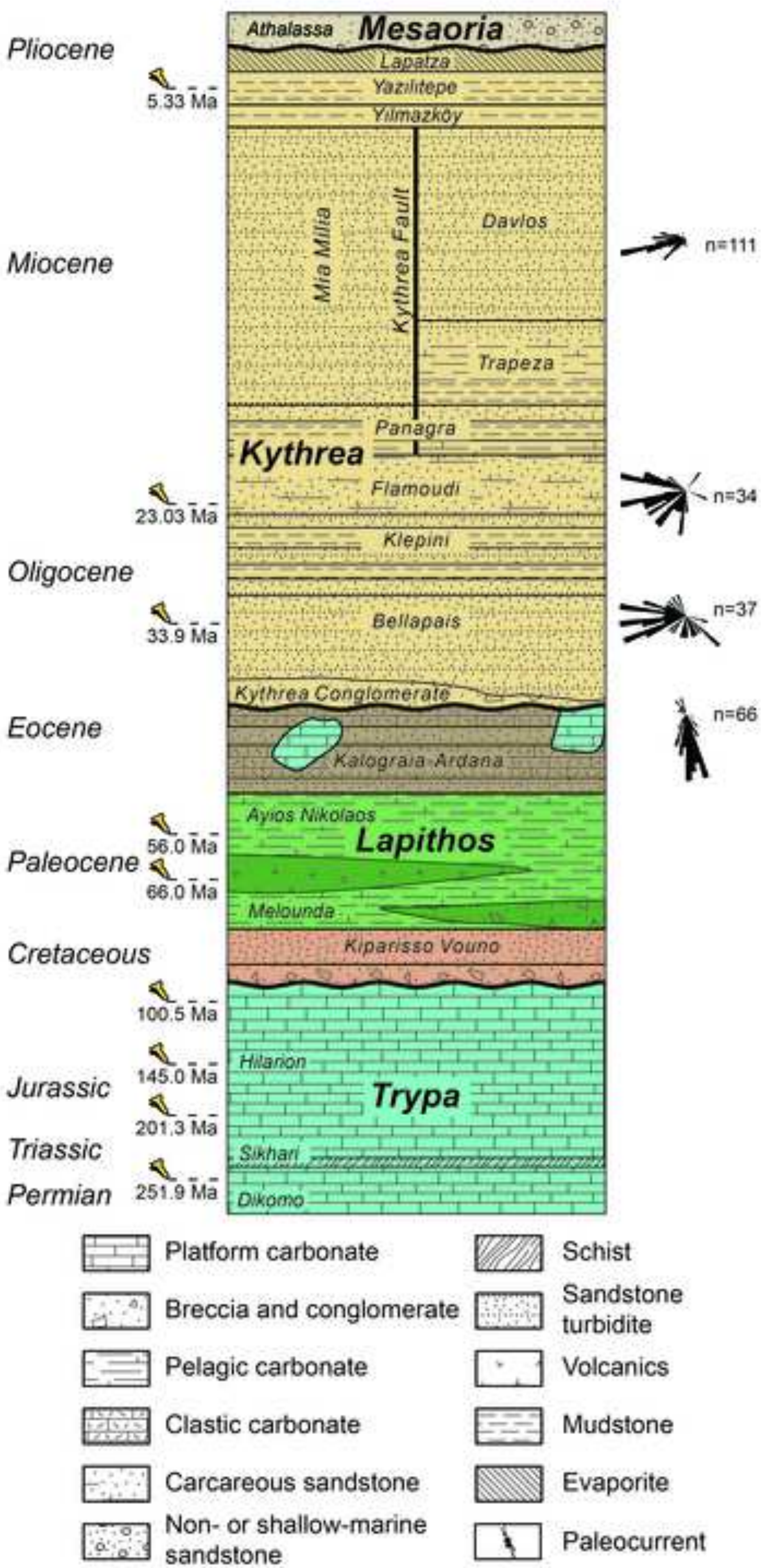

Figure 3 Click here to access/download;Figure;Fig. 3.jpg

Figure 4

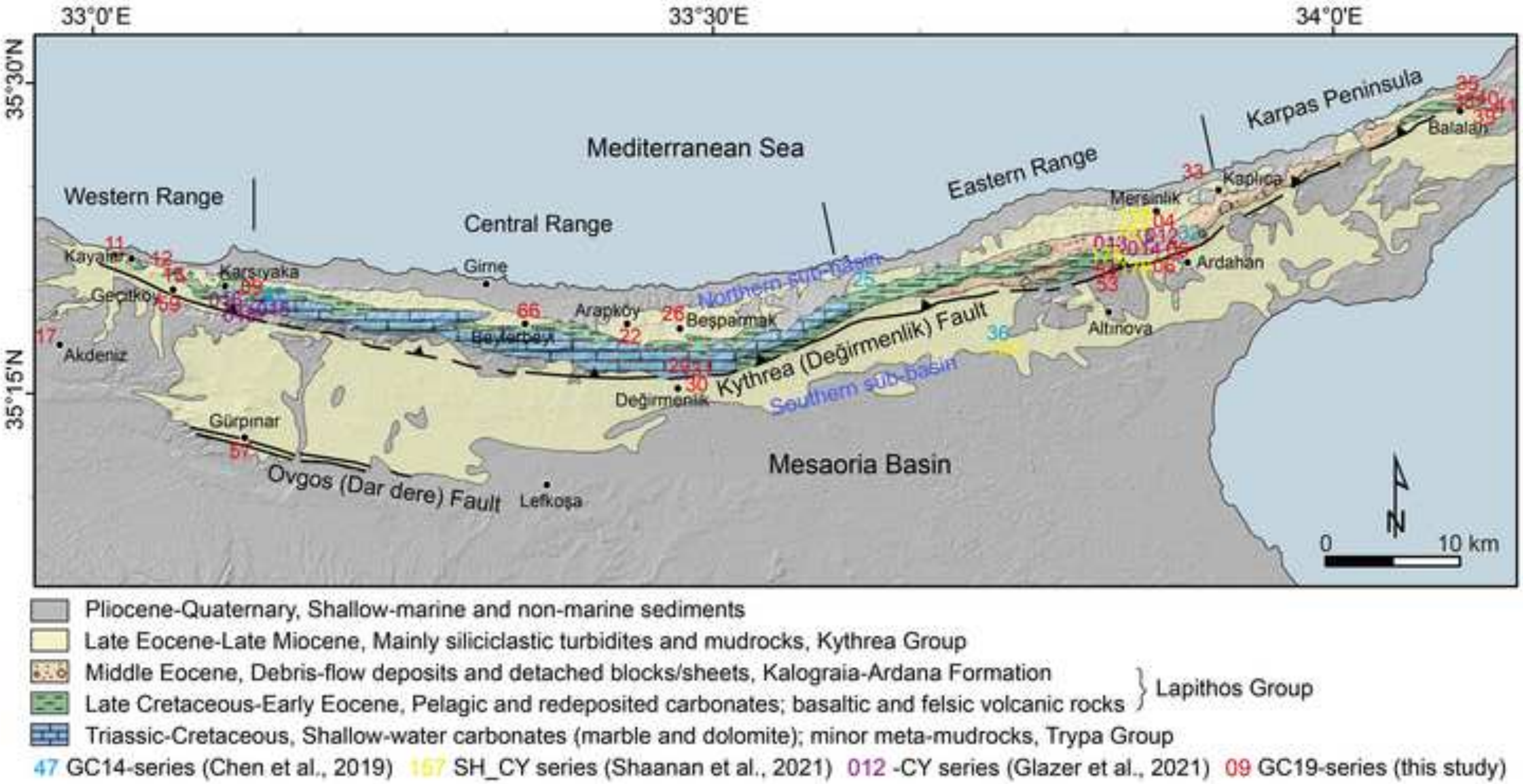
33°0'E
33°30'E
34°0'E
35°30'N
35°15'N
Mediterranean Sea
Western Range
Central Range
Eastern Range
Karpas Peninsula
Kayalar
Karşıyaka
Geçitköy
Akdeniz
Girne
Arapköy
Beşparmak
Beylerbeyi
Değirmenlik
Northern sub-basin
Southern sub-basin
Kythrea (Değirmenlik) Fault
Mersinlik
Kaplıca
Ardahan
Altınova
Balalan
Gürpınar
Ovgos (Dar dere) Fault
Lefkoşa
Mesaoria Basin
N
0
10 km
Pliocene-Quaternary, Shallow-marine and non-marine sediments
Late Eocene-Late Miocene, Mainly siliciclastic turbidites and mudrocks, Kythrea Group
Middle Eocene, Debris-flow deposits and detached blocks/sheets, Kalograia-Ardana Formation
Late Cretaceous-Early Eocene, Pelagic and redeposited carbonates; basaltic and felsic volcanic rocks
Lapithos Group
Triassic-Cretaceous, Shallow-water carbonates (marble and dolomite); minor meta-mudrocks, Trypa Group
47 GC14-series (Chen et al., 2019)
157 SH_CY series (Shaanan et al., 2021)
012 -CY series (Glazer et al., 2021)
09 GC19-series (this study)

Figure 5

Click here to access/download;Figure;Fig. 5.jpg

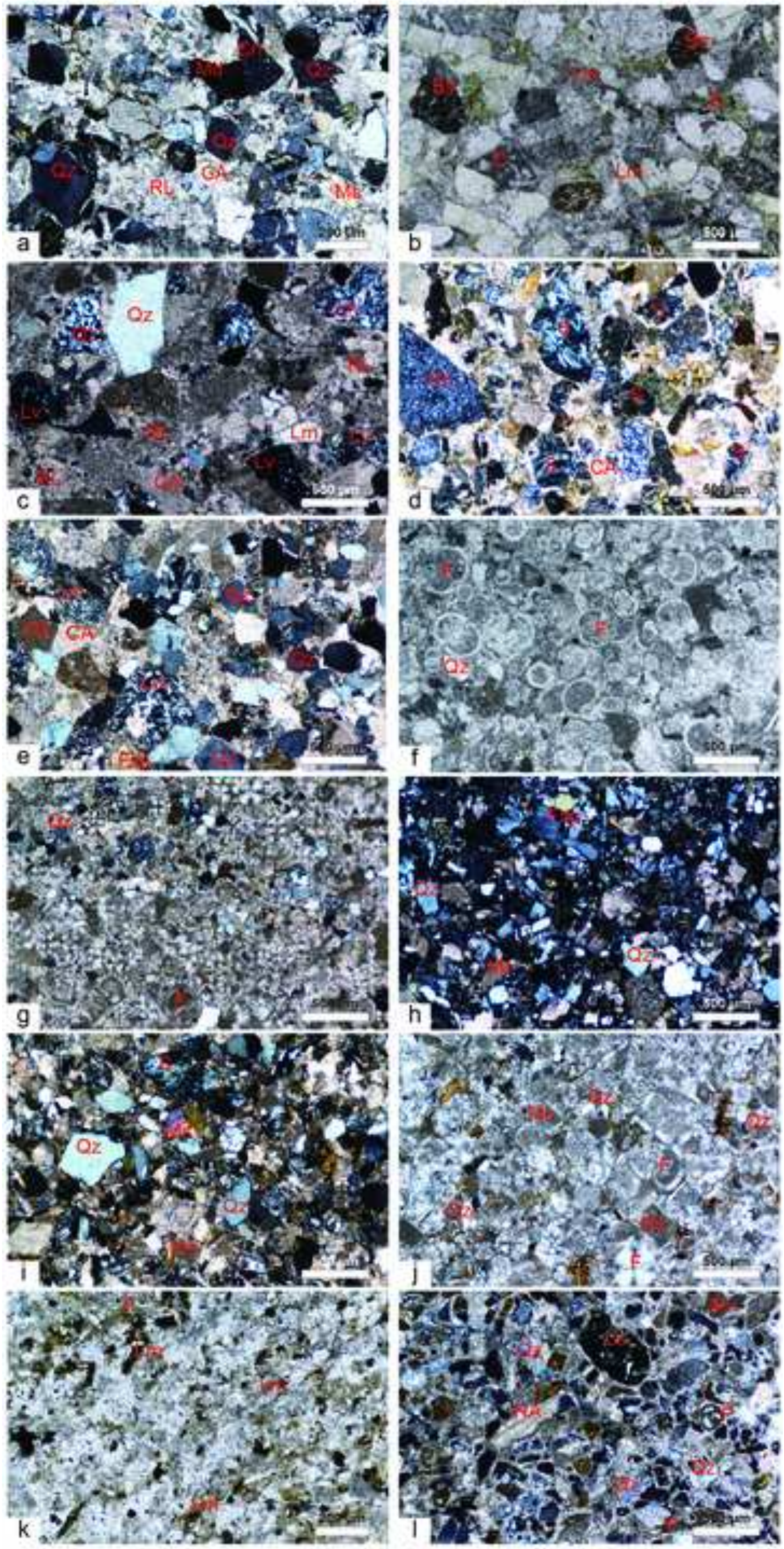

Figure 6

Click here to access/download;Figure;Fig. 6.jpg

Figure 7

Click here to access/download;Figure;Fig. 7.jpg

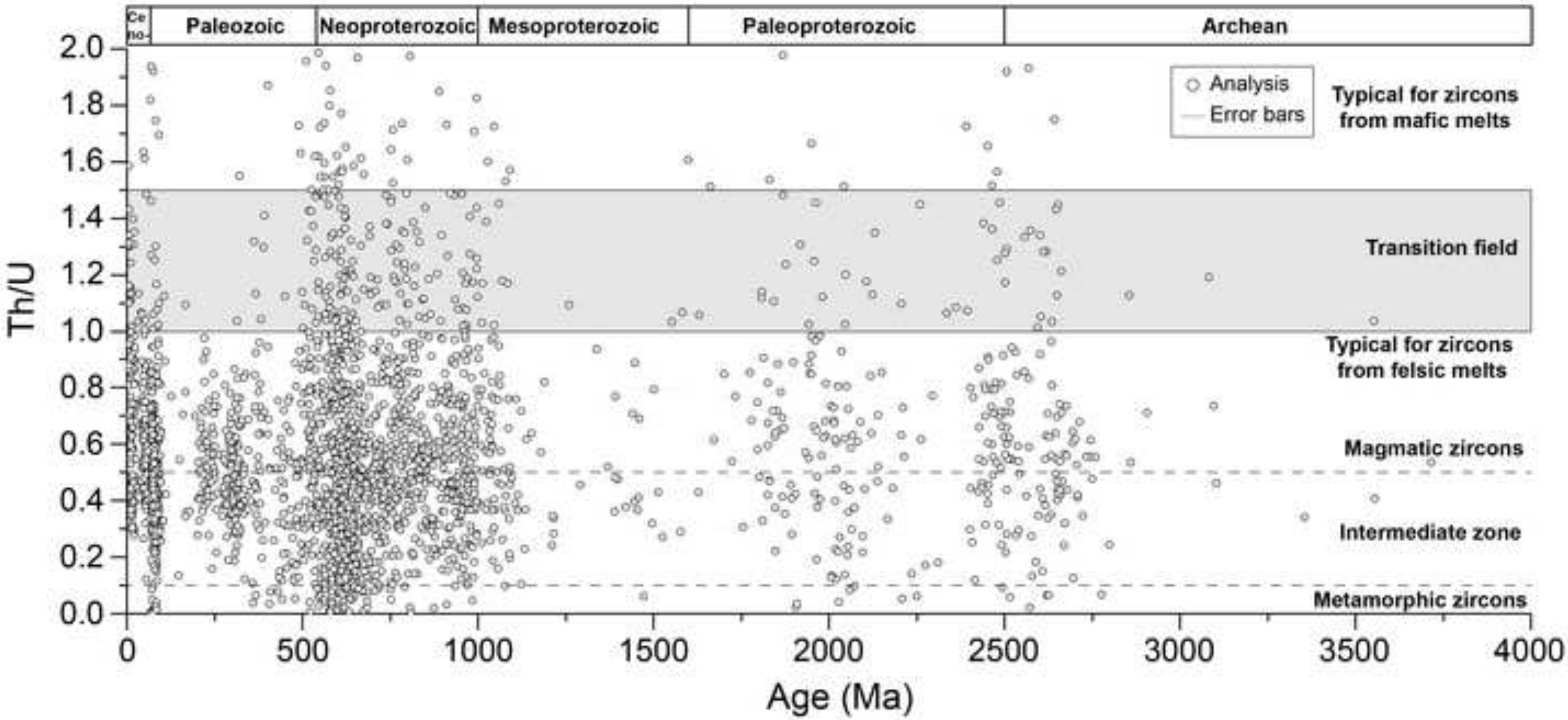

Figure 8

Click here to access/download;Figure;Fig. 8.jpg

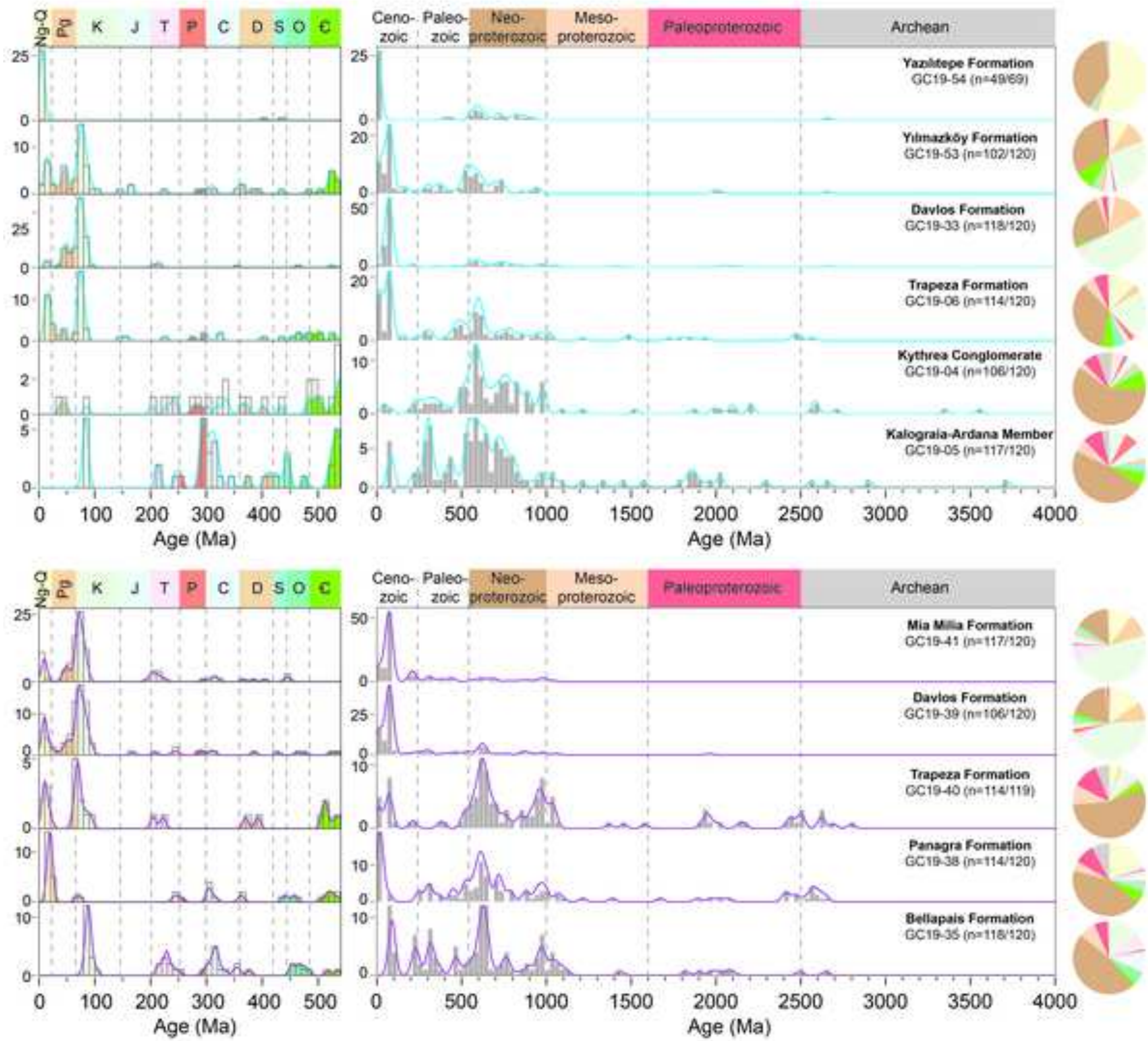

Figure 9

Click here to access/download;Figure;Fig. 9.jpg

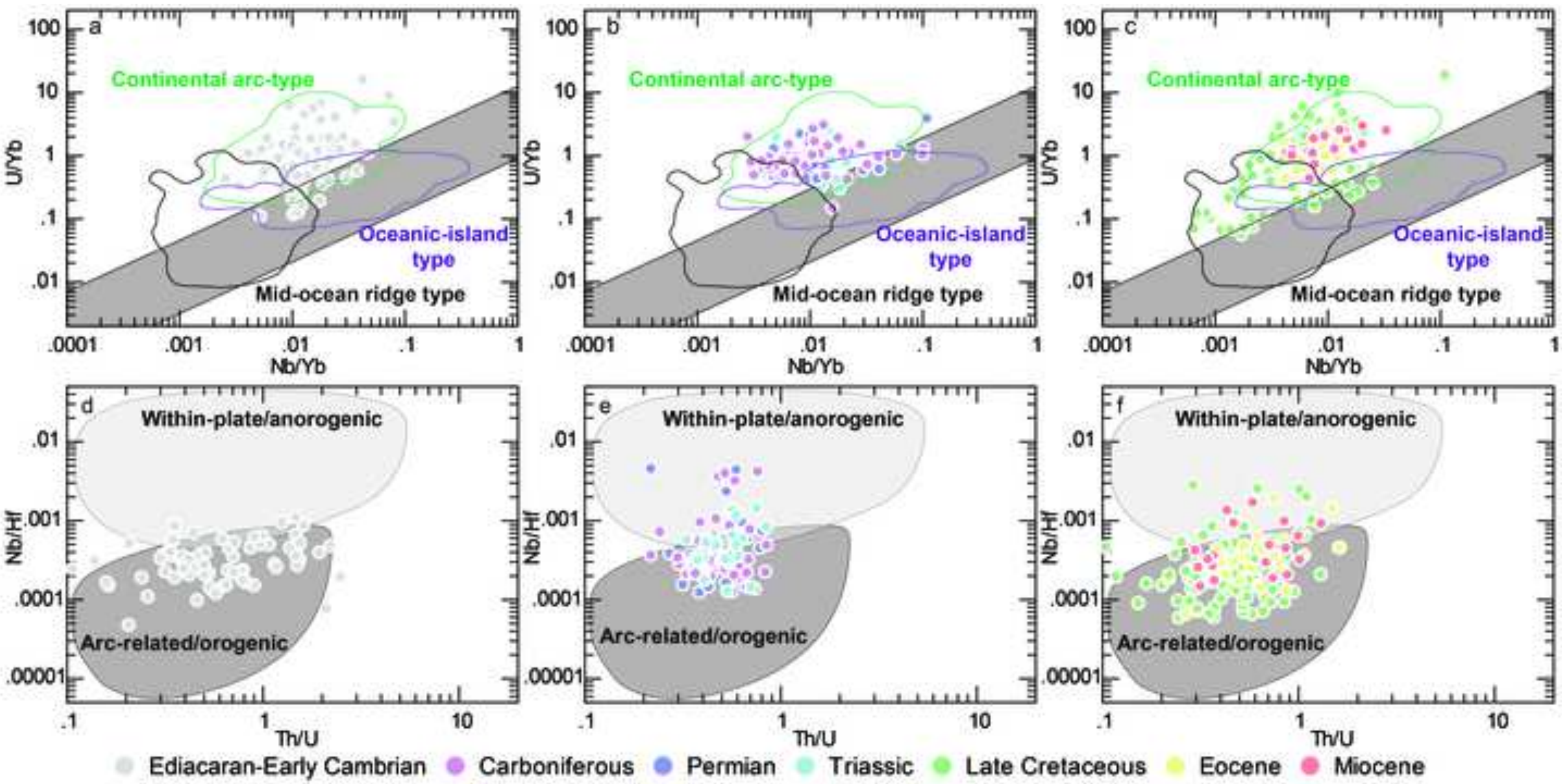

Figure 10

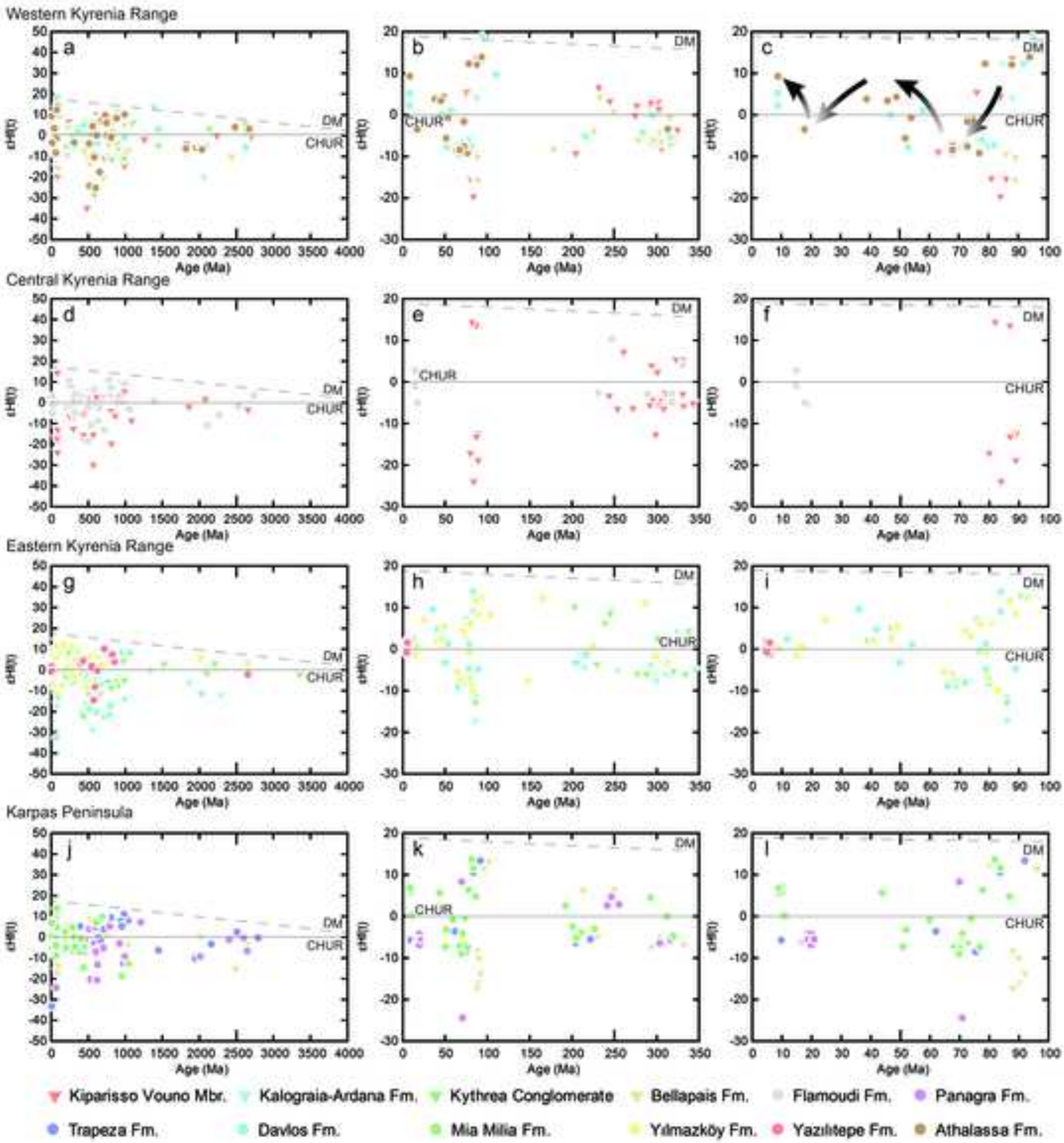

Western Kyrenia Range
Central Kyrenia Range
Eastern Kyrenia Range
Karpas Peninsula
a
b
c
d
e
f
g
h
i
j
k
l
DM
CHUR
εHf(t)
Age (Ma)
Kiparisso Vouno Mbr.
Kalograia-Ardana Fm.
Kythrea Conglomerate
Bellapais Fm.
Flamoudi Fm.
Panagra Fm.
Trapeza Fm.
Davlos Fm.
Mia Milia Fm.
Yılmazköy Fm.
Yazılıtepe Fm.
Athalassa Fm.

Figure 11

Click here to access/download;Figure;Fig. 11.jpg

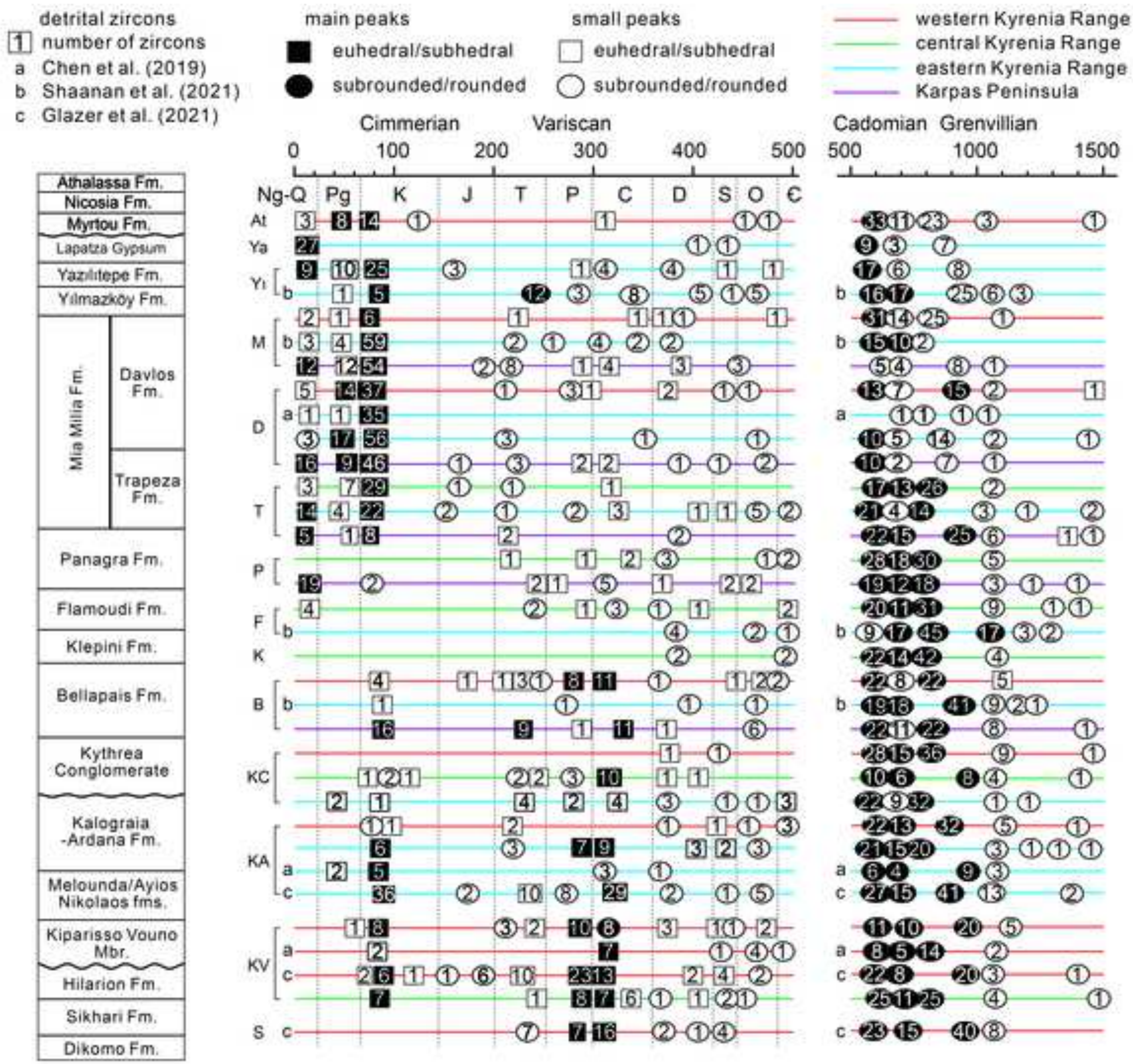

Figure 12

Click here to access/download;Figure;Fig. 12.jpg

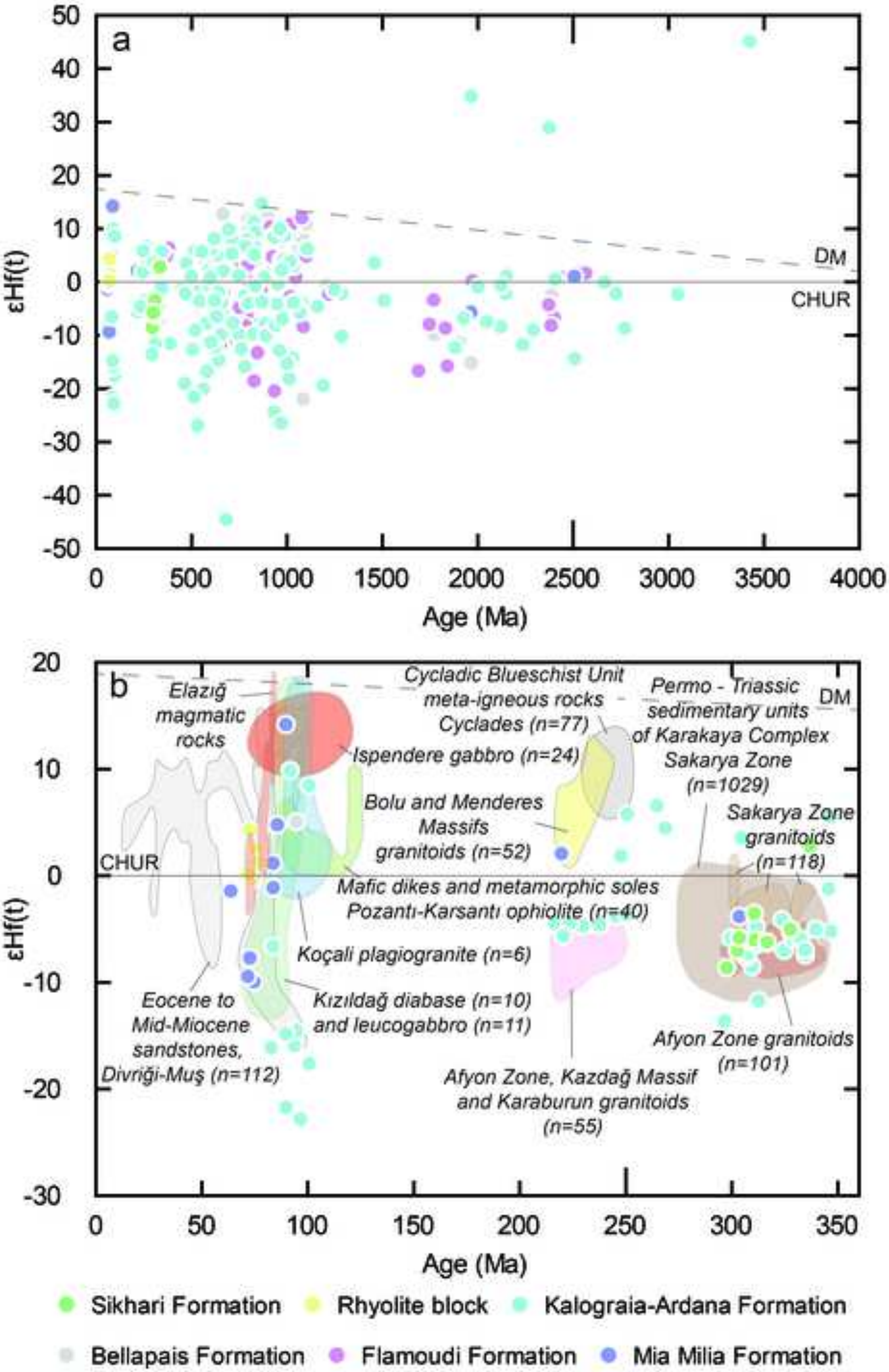

Figure 13

Click here to access/download;Figure;Fig. 13.jpg

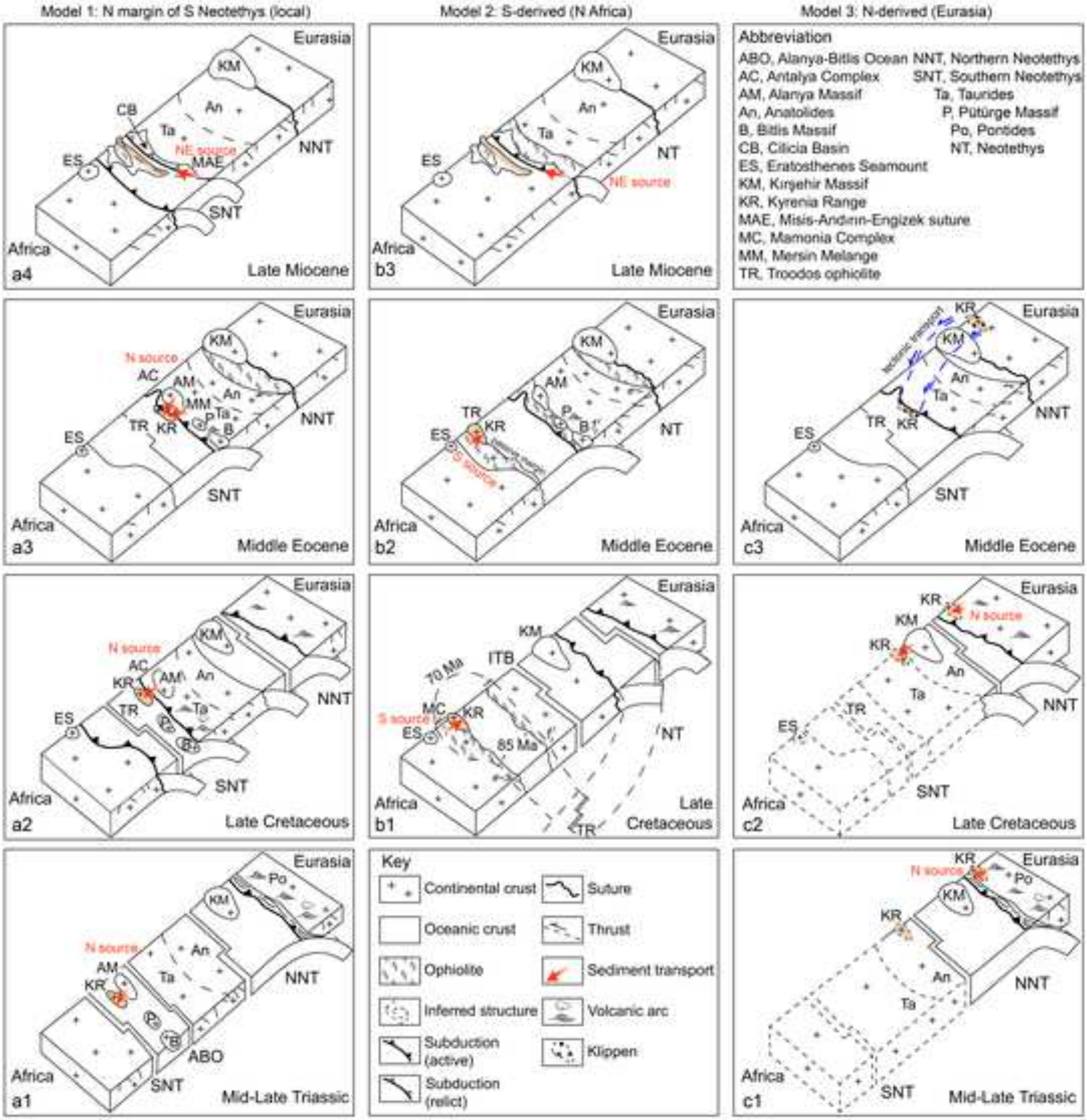

Declaration of interests

☒The authors declare that they have no known competing financial interests or personal relationships that could have appeared to influence the work reported in this paper.

☐The authors declare the following financial interests/personal relationships which may be considered as potential competing interests:

Detrital zircon geochronology and related evidence from clastic sediments in the Kyrenia Range, N Cyprus: implications for the Mesozoic-Cenozoic erosional history and tectonics of southern Anatolia

Guohui Chen[a,b], Alastair H. F. Robertson[c], Fu-yuan Wu[b]

[a] School of Earth Sciences and Engineering, Hohai University, Nanjing 210098, China

[b] State Key Laboratory of Lithospheric Evolution, Institute of Geology and Geophysics, Chinese Academy of Sciences, Beijing 100029, China

[c] School of GeoSciences, University of Edinburgh, Grant Institute, West Mains Road, Edinburgh EH9 3JW, UK

Corresponding author: Guohui.Chen@live.cn

Highlights

- Detrital zircon U-Pb and related analyses indicate the erosional history of S Anatolia
- The combined data indicate a switch from N to E sources related to Neogene collision
- The zircon and related data support tectonic development along N margin of S Neotethys

Abstract

Triassic to Pleistocene sandstones of the Kyrenia Range, N Cyprus provide an exceptional repository of the erosional history of Anatolia. The Kyrenia Range features in several different tectonic hypotheses of the Eastern Mediterranean region, which are tested here using a combination of new and recently published detrital zircon geochronology, zircon trace-element data and hafnium isotopic data. Minimum detrital zircon ages refine the ages of several formations in the Kyrenia Range. The new data also provide insights into sediment provenance including far-removed sources of Upper Paleozoic zircons, within-plate versus subduction-related sources (e.g., rift; oceanic/continental arc/ophiolite) and Neogene collision-related magmatism. Facies and paleocurrent data indicate a major switch in clastic sediment input from generally southwards to westwards during the Oligocene, which was mainly controlled by the collision of the Arabian promontory with Anatolia, leaving the S Neotethys as an isolated deep-water basin.

The U-Pb zircon age profiles indicate a prominent Late Neoproterozoic population, together with Carboniferous, Permian, Late Cretaceous and Miocene-aged clusters. Pan-African and Grenvillian-aged zircons were ultimately derived from Cadomian continental basement. Basement that rifted from Gondwana during the Triassic later became sources of detritus within Anatolia to the north. Devonian-Carboniferous zircons were originally supplied by active continental margin magmatism in southern Eurasia (Pontides) or northern Gondwana (Afyon zone of the Anatolides). The proposed explanation is that detrital zircons were sequentially recycled, first to Upper Carboniferous-earliest Permian turbidites (within the Afyon

zone to the east), later to Mid-Upper Triassic alluvium and turbidites (within the Taurides to the south), and finally to Triassic-Paleogene clastic sediments as now preserved in the Kyrenia Range. Upper Cretaceous zircons were derived from continental arc granitoids, oceanic arc and/or ophiolitic rocks and related metamorphic rocks, generally to the north of the Kyrenia Range. Paleogene zircons mainly represent late-stage continental margin arc magmatism in SE Turkey. During the Oligocene, the switch from mainly southward sediment supply to mainly westward sediment supply represents dominant input from the S Neotethyan suture zone in SE Turkey. Miocene zircons were mainly derived from post-collisional volcanics in SE Turkey. Paleoriver drainage systems in central/southeast Anatolia largely existed by the Late Miocene in response to collision-related surface uplift, in turn strongly influencing Miocene-Pleistocene zircon provenance in sub-basins within and adjacent to the Kyrenia Range.

The combined zircon and Hf data, together with assembled geological evidence, are used to discuss three contrasting tectonic hypotheses for the early Mesozoic-Eocene setting of the Kyrenia Range: (1) locally, in the easternmost Mediterranean (i.e., preferred interpretation); (2) far to the south, on the N African passive margin, and (3) far to the north, along (or near) the Eurasian margin. Overall, the present study exemplifies the diversity and complexity of clastic sediment sources within a developing orogen, with implications for some other regions.

Keywords: Eastern Mediterranean, Kyrenia Range, U-Pb zircon dating, Hf isotopic

analysis, sediment provenance, tectonic synthesis

1. Introduction

Provenance analysis of clastic sedimentary rocks, especially detrital zircon U-Pb geochronology and related analysis, provide important information concerning the erosional history of continents and their tectonic development including rifting, subduction and collision on variable scales (e.g., Cawood et al., 2012; Gehrels, 2014).

The Kyrenia Range in the north of Cyprus (Fig. 1) developed in response to successive rift, passive margin, active margin and collisional processes during opening and closure of a Neotethyan ocean basin (Robertson and Woodcock, 1986). Each one of these tectonic phases provided an erosional record that is investigated here using zircon geochronology and related data, especially Lu-Hf isotopic analysis. Where continents border ocean basins much detritus runs off into the deep sea, where it can be studied by deep-sea drilling at relatively shallow depths (several km) (e.g., Clift, 2002). Good examples in the modern oceans include the detrital record of the Himalayan region preserved within the Bengal Fan (Bay of Bengal) (e.g., Tripathy et al., 2014; Pickering et al., 2020; Bretschneider et al., 2021) and also farther west within the Indus Fan (Arabian Sea) (Clift et al., 2002; Yu et al., 2019; Kumar et al., 2020).

Following Triassic rifting to form a Neotethyan ocean basin, the Kyrenia Range documents passive margin development, followed by a switch to active margin and collisional settings from Late Triassic to Recent (Robertson and Woodcock, 1986;

Robertson et al., 2012a, 2014). The range runs parallel to the developing Tethyan collision zone for ca. 150 km and has been uplifted from the deep Mediterranean Sea during the Pleistocene (Palamakaumbura et al., 2016), providing access to a lengthy Triassic-Pleistocene erosional record. Ideally, detrital zircon geochronology allows unique provenances to be identified (e.g., Gehrels, 2004). However, the situation is more complex where erosional detritus is supplied and mixed from successive tectonic settings over a large region. In the Eastern Mediterranean region, erosional detritus potentially was supplied from multiple ocean basins, which may be challenging to recognised. The possibility of zircon recycling through different tectonic settings over a long time period needs to be considered. The present study provides a case history of zircon provenance in a tectonically complex region, where all aspects of the regional geology need to be taken into account in the interpretation.

Recently published zircon U-Pb geochronology for different time intervals in the Kyrenia Range confirms a close linkage with the geological development of Turkey (Chen et al., 2019; Shaanan et al., 2021; Glazer et al., 2021). Three contrasting tectonic hypotheses have been proposed for the tectonic development of the Kyrenia Range, which will be tested and developed here using a combination of zircon geochronology, trace-element analysis and Lu-Hf analysis, together with existing geological evidence mainly from the Kyrenia Range and Anatolia. The first hypothesis is that the Kyrenia Range represents the northern continental margin of the Southern Neotethys (McCay and Robertson, 2012; Robertson et al., 2012a, 2014; Barrier et al., 2018). The second hypothesis is that the Kyrenia Range represents part of the southern passive margin of the Mesozoic Tethyan ocean (i.e., N Africa) and then was transferred to the southern margin of Eurasia (S Anatolia) during the Neogene (McPhee and van Hinsbergen, 2019). The third hypothesis is that the Kyrenia Range is grossly allochthonous and was transported hundreds of km southwards during the Eocene from an initial position along, or near, the Eurasian continental margin (Glazer et al., 2021). The provenance of detrital zircons, especially their Upper Paleozoic fraction is a key to evaluating the above three contrasting tectonic hypotheses.

Here, we present a large body of new detrital zircon evidence from Upper Cretaceous to Pliocene sandstones (24 samples) from the Kyrenia Range. We compare data from four transects along the range to help identify specific provenances. We compare our new results with existing U-Pb detrital zircon data (10 samples) (Chen et al. 2019; Shaanan et al., 2021; Glazer et al., 2021), and utilise new (n=684) and existing (n=319) hafnium isotopic data. We also use zircon trace element data, particularly to help discriminate intra-plate versus convergent plate magmatic sources.

Our specific objectives for the Kyrenia Range are: (1) to test paleontologically determined ages; (2) to infer provenance for different time slices from Middle-Late Triassic to Pleistocene; (3) to investigate how provenance has changed through time; (4) to further help interpret tectonic development of Tethys in the easternmost Mediterranean region; (5) to test the three different tectonic hypotheses for the Kyrenia Range in its regional tectonic setting, and (6) to consider the wider implications of our preferred interpretation.

2. Geological setting and tectonostratigraphy of the Kyrenia Range

The island of Cyprus, located in the eastern Mediterranean, is made up of three tectonic terranes: the Troodos Massif in the centre, the Mamonia Complex in the west and the Kyrenia Range in the north (Fig. 1). The Kyrenia Range is characterised by a narrow, elongate topographic ridge (up to 5 km wide × 160 km long × 1.0 km high) that lies between the Troodos Massif to the south and the Cilicia Basin to the north, with the Tauride Mountains of southern Turkey farther north (Fig. 1). The Troodos Massif comprises an Upper Cretaceous, supra-subduction zone-type ophiolite (92-90 Ma; Mukasa and Ludden, 1987), overlain by an Upper Cretaceous to Recent deep-marine to shallow-marine and non-marine sedimentary cover (e.g., Robertson, 1990). The Mamonia Complex is dominated by highly deformed Upper Triassic to Lower Cretaceous sedimentary and igneous rocks, interpreted as a remnant of a deep-marine rifted passive continental margin (e.g., Robertson and Woodcock, 1979; Torley and Robertson, 2018). The easternmost Mediterranean including the Kyrenia Range was strongly affected by rifting that began in the Late Permian, continued during the Early-Middle Triassic and culminated in continental breakup to form oceanic crust during Late Triassic (Robertson and Woodcock, 1979; Şengör and Yılmaz, 1981; Robertson and Dixon, 1984; Garfunkel, 1998). The Kyrenia Range can be interpreted, either as a microcontinent capped by a small carbonate platform or as part of a larger regional, continental unit and carbonate platform (e.g., Robertson et al., 2012a; Barrier et al., 2018; van Hinsbergen et al., 2020).

2.1 Late Paleozoic-Mesozoic

The oldest rocks exposed in the Kyrenia Range are Upper Paleozoic blocks of carbonate rock that are exposed in a sedimentary melange (olistostrome) in the eastern part of the Range. No basal contact is exposed and entire lithostratigraphy of the Kyrenia Range is inferred to be allochthonous (Baroz, 1979; Robertson and Woodcock, 1986).

The intact succession, which is mainly exposed in the central and western part of the Kyrenia Range, is characterised by platform carbonate rocks of the Trypa (Tripa) Group[1], comprising the Dikomo (Dikmen), Sikhari (Kaynakköy) and Hilarion (Hileryon) formations (Fig. 2) (Henson et al., 1949; Ducloz, 1972; Baroz, 1979; Robertson and Woodcock, 1986). The Trypa Group is deformed into thrust sheets and blocks without any overall intact succession (Fig. 3a-b); also, the dominant carbonate rocks are variably recrystallised to marble and dolomite, hindering fossil age determination. The Dikomo Formation, which lacks supporting paleontological age data (Ducloz, 1972), comprises finely laminated calcilutite and silty marl, which is mostly recrystallised to grey, blue and white schistose marble. The overlying Sikhari Formation is laterally variable, comprising sugary textured dolostones, minor quartz and rare diagenetic feldspar, together with chert nodules. The formation is dark grey to black owing to a high content of organic carbon. A Triassic age is inferred based on lithological comparisons with similar dolomitic shelf facies

[1] For simplicity, we use the traditional stratigraphy for the formation names (more recent Turkish equivalents are mentioned initially). However, we use current Turkish names for settlements (previously used names are mentioned initially).

in the Taurides and elsewhere in the eastern Mediterranean region, and by the presence of Mesozoic ostracods (Ducloz, 1972). The conformably overlying Hilarion Formation comprises highly recrystallised, brecciated limestones, dolomites and marbles, with poorly preserved sedimentary structures including planar and cross-lamination (Ducloz, 1972; Baroz, 1979; Robertson and Woodcock, 1986). The Hilarion Formation is dated as Jurassic-Early Cretaceous based on neritic macrofossils; e.g., the corals *Lovcenipora, Diplocoenia* and *Cryptocoeuia* and the hydrozoan *Ellipsactinia* (Henson et al., 1949); also present is the branched sclerosponge *Cladocoropsis mirabilis* that is particularly abundant in the Late Jurassic (Baroz, 1979). The Hilarion Formation ends with a major structural and metamorphic break during which the Trypa Group underwent greenschist-facies metamorphism involving burial to ca. 5 km to 7 km (Baroz, 1979; Robertson and Woodcock, 1986). Detritus from the Trypa Group occurs in transgressive Maastrichtian sediments of the Lapithos (Lapta) Group, placing a pre-Maastrichtian upper age limit on the Hilarion Formation (Fig. 3c). The contact between the Trypa Group and the Lapithos Group is characterise by small, discontinuous thrust slices of ophiolitic rocks, chert, marble and meta-volcanic rocks (Ducloz, 1972; Baroz, 1979); these are interpreted as ophiolitic melange and retain indications of HP/LT metamorphism (Glazer et al., 2021).

The Mesozoic carbonate platform (Trypa Group) was deformed, brecciated, recrystallised and metamorphosed to greenschist facies, together with the emplacement of small volumes of ophiolitic melange (with HP/LT metamorphic relics), prior to Campanian-Maastrichtian transgression (Kiparisso Vouno

(Alevkaya Tepe) Member). The Upper Cretaceous the emplacement-related structure is overprinted and mainly obliterated by the later deformation events. The primary deformation and metamorphism are interpreted to related to regional subduction, which was followed by rapid exhumation and marine transgression (Robertson and Woodcock, 1986; Robertson et al., 2012b; Maffione et al., 2017; McPhee and van Hinsbergen, 2019; Glazer et al., 2021).

2.2 Latest Cretaceous-Middle Eocene

The Lapithos Group comprises basal carbonate breccias, pelagic carbonates, basic volcanics, calcareous sandstones and sandy carbonates (Figs. 2, 3c; Supplementary Figure S1), which are dated as Campanian to Early Eocene based mainly on planktonic foraminifera (Ducloz, 1972; Baroz, 1979; Hakyemez et al., 2000; Robertson et al., 2012b). Two structurally different units are present. The first unit is the Upper Campanian Fourkovouno (Selvilitepe) Formation. This crops out as thrust slices mainly in the western Kyrenia Range, comprising marine water-lain felsic tuffs and subaqueous felsic debris-flow deposits (Moore, 1960; Baroz, 1979; Huang et al., 2007; Robertson et al., 2012b; Chen and Robertson, 2021b). Uranium-lead radiometric dating has yielded an age of ca. 74 Ma (Late Campanian) (Chen and Robertson, 2021b; Glazer et al., 2021). The second unit, which is located at a higher structural position, is the Kiparisso Vouno (Alevkaya Tepe) Member of the Melounda (Mallıdağ) Formation (Lapithos Group) (Supplementary Figure S1a). This lithostratigraphic unit is locally exposed near the base of the Melounda Formation in the western and central Kyrenia Range (Baroz, 1979;

Robertson and Woodcock, 1986; Robertson et al., 2012b). The Kiparisso Vouno Member is dated as Late Campanian-Maastrichtian based on planktic foraminifera; e.g., *Rugoglobigerina sp.* and *Globotruncanita stuarti* (Robertson et al., 2012b). These clastic sediments are conformably overlain by basaltic and pelagic carbonate units (also within the Melounda Formation), which are dated as Maastrichtian using planktic foraminifera and calcareous nannofossils (Baroz, 1979; Hakyemez et al., 2000; Hakyemez and Özkan-Altıner, 2007; Robertson et al., 2012b, 2014). The succession continues upwards without a break into the Ayios Nikolaos (Yamaçköy) Formation (Fig. 2; Supplementary Figure S1b), which is dated as Paleocene-Middle Eocene, again using planktonic foraminifera and calcareous nannofossils (Hakyemez et al., 2000; Hakyemez and Özkan-Altıner, 2007; Robertson et al., 2012b). The succession continues transitionally within the Kalograia-Ardana (Bahçeli–Ardahan) Formation, which is mainly exposed in the eastern Kyrenia Range (Fig. 4; Supplementary Figure S1c-d) (Baroz, 1979; Robertson and Woodcock, 1986; Hakyemez et al., 2000; Robertson et al., 2014). The lower part of the formation is mainly sandstone turbidites and mudrocks, which pass upwards into thicker-bedded turbidites, debris-flow deposits. Associated large-scale mass-transport units (‘olistostromes’) encompass blocks and dismembered thrust sheets; these include Permian neritic carbonates (Kantara Limestone) and ophiolitic rocks, mainly serpentinite (Ducloz, 1972; Baroz, 1979; Robertson and Woodcock, 1986; Hakyemez et al., 2000; Robertson et al., 2014). Marls in the lower part of the Kalograia-Ardana Formation are dated as Middle Eocene using planktonic foraminifera (e.g., *Acarinina bullbrooki* and

Globigerinatheka sp.) and calcareous nannofossils (e.g., *Coccolithus pelagicus* and *Discoaster saipanesis*) (Baroz, 1979; Hakyemez et al., 2000; Robertson and Woodcock, 1986; Robertson et al., 2014).

According to most authors, there is a major Mid-Eocene unconformity (Ducloz, 1972; Baroz, 1979; Robertson and Woodcock, 1986; Robertson et al., 2014; Robertson and Kinnaird, 2016) that separates the underlying units (other than some frontal thrust slices of felsic volcanic rocks) from the Upper Eocene to Upper Miocene non-marine to deep-marine siliciclastic sandstones and mudstones of the Kythrea (Değirmenlik) Group (Weiler, 1970; McCay and Robertson, 2012; Robertson et al., 2012b, 2014; Robertson and Kinnaird, 2016). Evidence for Eocene compressional deformation has been reported from many parts of the Kyrenia Range, especially the northern flanks, where highly deformed older units are unconformably overlain by much less deformed younger units (Robertson and Kinnaird, 2016). There is also evidence of similar-aged deformation in SE Turkey/Anatolia to the north, notably the Amanos Mountains (e.g., Yılmaz, 1993; Robertson et al., 2006, 2016; Boulton and Robertson, 2008; Duman et al., 2017). The unconformity in the Kyrenia Range has been suggested to record initial suturing (continental collision) of the S Neotethys in the easternmost Mediterranean region, or far-field effects of suturing of the N Neotethys in central Anatolia (Robertson et al., 2014). Alternatively, Glazer et al. (2021) relate the inferred Mid-Eocene structural break in the Kyrenia Range to the emplacement of the entire Permian to Lower Eocene stratigraphy as a vast allochthonous body that transported from far to the north (see below). On the other hand, McPhee and van

Hinsbergen (2019) interpret all of the post-Upper Cretaceous deformation as Late Miocene and instead infer continuous passive margin deposition from the time of Upper Cretaceous deformation and metamorphism until the Upper Miocene thrusting. The Mid-Eocene ‘olistostromes’ of the Kalograia-Ardana Formation were explained by mass transport down a passive margin.

2.3 Late Eocene-Late Miocene

The Lapithos Group is unconformably overlain, or in fault contact with, an Upper Eocene-Upper Miocene siliciclastic succession known as the Kythrea Group (Fig. 3d-e; Supplementary Figure S2-S3). In the north, the succession unconformably overlies various older units within the Kyrenia Range (Fig. 3b). Within the Mesaoria Basin to the south (Fig. 3d-e), where the Kythrea Group is folded and imbricated, the total thickness is estimated utilising borehole evidence as up to 4000 m (Weiler, 1970; Cleintuar et al., 1977; Baroz, 1979; Hakyemez et al., 2000; Harrison et al., 2004; McCay, 2010; McCay et al., 2013).

Where exposed on the northern and southern flanks of the Kyrenia Range, the Kythrea Group is mainly composed of conglomerates (near basal), sandstone turbidites, bioclastic calciturbidites, mudstones, claystones and minor tuffaceous sediments. The formations present, both within the Kyrenia Range and the Mesaoria Basin to the south, are the Upper Eocene-Oligocene Kythrea (Büyüktepe) Conglomerate Member, the Upper Eocene-Oligocene Bellapais Formation, the Upper Oligocene Klepini (Arapköy) Formation, the Upper Oligocene Flamoudi (Tirmen) Formation, the Lower Miocene Panagra (Geçitköy) Formation, the

Middle-Upper Miocene Trapeza (Esentepe) Formation, the Upper Miocene Davlos (Kaplıca) Formation, the Lower to Upper Miocene Mia Milia (Dağyolu) Formation, the Upper Miocene Yılmazköy Formation, the Upper Miocene Yazılıtepe Formation and the Upper Miocene Lapatza (Mermertepe) Gypsum (Fig. 2; Supplementary Figure S2-S3). The Yılmazköy and Yazılıtepe formations have been introduced to represent the lithological variation in the Upper Miocene succession (Hakyemez et al., 2000). Comprehensive descriptions and interpretations of all of these formations are given by Baroz (1979), Robertson and Woodcock (1986) and McCay and Robertson (2012). The dating is mainly based on a combination of planktonic foraminifera, calcareous nannofossils and strontium isotope stratigraphy (Baroz and Bizon, 1974; Baroz, 1979; Hakyemez et al., 2000; McCay et al., 2013). Facies evidence indicates that the Upper Eocene-Upper Miocene basin to the south of the Kyrenia Range was divided into northern and southern sub-basins by an E-W trending, inferred syn-sedimentary fault lineament (Kythrea Fault; Fig. 4) that was mainly active during the Middle to Late Miocene (McCay and Robertson, 2012, 2013).

Intense thrust imbrication affected the Kyrenia Range during the Late Miocene-Early Pliocene, with deformation locally continuing during the Pleistocene (Calon et al., 2005a, b; McCay and Robertson, 2012, 2013; Robertson and Kinnaird, 2016; McPhee and van Hinsbergen, 2019). Dominantly southward thrusting strongly affected the structure of the southern flank of the range and there is evidence of northward backthrusting along the northern flank of the range (Robertson and Kinnaird, 2016). The unconformity at the base of the Pliocene succession is likely to relate to the collision of the Tauride and North African (Arabian) continents in the eastern Mediterranean region (Robertson and Woodcock, 1986; McCay and Robertson, 2013; McPhee and van Hinsbergen, 2019).

2.4 Pliocene-Pleistocene

The Messinian Lapatza Gypsum is unconformably overlain by the Pliocene-Pleistocene shallow-marine Mesaoria (Mesarya) Group. Adjacent to the Kyrenia Range, the Mesaoria Group is mainly marls and siltstones with subordinate sandstones and conglomerates. There are three formations: the Myrtou (Çamlıbel) Formation, the Nicosia (Lefkosa) Formation and the Athalassa (Gürpınar) Formation (Baroz, 1979; Robertson and Woodcock, 1986; McCay and Robertson, 2012; Palamakumbura and Robertson, 2016). The youngest deposits exposed in the Kyrenia Range are mainly non-marine, and to lesser extent shallow-marine facies that document Pleistocene uplift and glacio-eustatic sea-level change (Palamakumbura and Robertson, 2016; Palamakumbura et al., 2016).

The collision of the Eratosthenes Seamount with the Cyprus trench to the south of Cyprus is interpreted to have strongly influenced the uplift of both the Troodos Massif and the Kyrenia Range (Fig. 1) (Robertson, 1998; Kempler, 1998; Reiche and Hübscher, 2015; Feld et al., 2017; Ring and Pantazides, 2019).

3. Sampling and Methods

New detrital U-Pb zircon isotopic data were obtained from 24 samples of Upper

Cretaceous to Upper Pliocene-Pleistocene sandstones, as exposed in four selected transects: i.e., western (n=7), central (n=6) and eastern (n=6) Kyrenia Range and the Karpas Peninsula (n=5) (Fig. 4). Rare Pleistocene sandstones were sampled only in the western range. Also, Upper Cretaceous sandstone is not exposed in the Karpas Peninsula. The sample locations, with GPS coordinates, are listed in Supplementary Tables 1-2. Comparative data are available from previous spot sampling (Chen et al., 2019) and for one transect in the eastern range (Fig. 4) (Shaanan et al., 2021; Glazer et al., 2021).

The methods used in this study are all tried and tested, as described in the supplementary publication, which includes all of the data for the Cyprus samples and for analytical standards (see Supplementary Table S1-S3). In outline, the U-Pb isotopic and trace element analysis of the zircons were carried out synchronously by laser ablation-inductively coupled plasma-mass spectrometry (LA-ICP-MS) at the Institute of Geology and Geophysics, Chinese Academy of Sciences, following the methods of Xie et al. (2008) and Wu et al. (2020). *In situ* Hf isotope ratio analysis was carried out on the same zircon grains, using the MC (Multicollector)-ICP-MS at Wuhan Sample Solution Analytical Technology Co., Ltd, using the operating conditions and analytical methods as described by Hu et al. (2012). The International Chronostratigraphic Chart of the International Commission on Stratigraphy (Cohen et al., 2021) was used for the timescale.

4. Results

Below, we summarize the U-Pb, Hf isotope and trace element data for the detrital zircons studied. We also note relevant textural features (e.g., roundness) and comment on the Th/U ratios that are indicative of igneous or metamorphic source rocks. Generally, zircons with Th/U <0.1 are attributed to a metamorphic origin, whereas those with Th/U >0.5 are of a magmatic origin (e.g., Rubatto, 2002; Corfu et al., 2003; Hoskin and Schaltegger, 2003; Teipel et al., 2004; Linnemann et al., 2011; Xiang et al., 2011). In addition, we summarize the petrography of the samples from each formation within the four transects studied. We also summarise the main paleontological age data for each formation, in relation to the minimum ages of the analysed detrital zircons. The full data base is recorded in Supplementary Tables 1-5.

4.1. Kiparisso Vouno Member

Two samples of medium- to coarse-grained sandstones were analysed from the Upper Cretaceous Kiparisso Vouno Member. Sample GC19-09 was collected from 2.5 km southeast of Karşıyaka, western Kyrenia Range (Fig. 4; Supplementary Figure S1a). Sample GC19-66 is from 600 m north of Beylerbeyi, central Kyrenia Range. Both sandstones are poorly sorted and contain angular to sub-angular grains of quartz (mainly monocrystalline) and plagioclase, together with abundant metamorphic rock fragments (mainly muscovite schist), with trace amounts of basalt, radiolarian chert and mudstone (Table S4) (Fig. 5a).

Sample GC19-09 has predominantly Precambrian (61%; Table S5), especially Neoproterozoic U-Pb ages (35%). This age group is dominantly Tonian (17%) with peaks at ca. 930 Ma, followed by Ediacaran (9%) and Cryogenian (8%) (Fig. 6; Table S5). Only a small number of zircons (4%) lie between 1.0 Ga and 1.6 Ga.

Paleoproterozoic and Archean zircons (mostly rounded; Supplementary Figure S4) are common (ca. 10%). There are also a significant number of Phanerozoic zircons (39%); i.e., Early Permian (8%; peaking at 297 Ma) and Late Cretaceous (5%; peaking at 85 Ma). The youngest zircon has an age of 63 ± 2 Ma (Table S5), slightly younger than the Late Campanian-Maastrichtian biostratigraphic age of the Kiparisso Vouno Member (Robertson et al., 2012b).

Sample GC19-66 similarly contains abundant Precambrian zircons (69%), mainly Ediacaran (22%), Cryogenian (10%) and Tonian (22%). The Neoproterozoic ages peak at 606 Ma and 916 Ma, slightly diifferent from those of sample GC19-09. A smaller number of zircons (3-8%) are older than 1.0 Ga. The Phanerozoic zircons (31%), which are mostly euhedral (Supplementary Figure S4), have similar age peaks to sample GC19-09 for the Early Permian, at 295 Ma (n=7) and also for the Late Cretaceous, at 89 Ma (n=7). Late Carboniferous zircons peak at 301 Ma (n=7). The youngest concordant zircon, which is subhedral (Supplementary Figure S4), yielded an age of 80 ± 9 Ma (Campanian) (Table S5), consistent with the Late Campanian-Maastrichtian biostratigraphic age of the Kiparisso Vouno Member based on planktic foraminifera within associated pelagic carbonates, including *Rugoglobigerina* sp., *R. scotti, Globotruncana falsostuarti, Gansserina gansseri, Contusotruncana fornicata*, *C. contusa*, *Abatomphalus mayaroensis* (Bolli) and *Globotruncanita stuartiformi* (Robertson et al., 2012b).

In the two sandstones from the Kiparisso Vouno Member, only 3% of the zircon grains have Th/U <0.1 (Fig. 7; Supplementary Figure S5), representing metamorphic zircons. These grains are Late Devonian (n=1), Ediacaran (n=2), Cryogenian (n=2) and Tonian (n=1). Most of the zircon population (58%) has Th/U ratios > 0.5 that are typical of magmatic zircons. 97% of the zircons have Th/U <1.5, indicative of derivation from felsic and/or intermediate melts.

4.2. Kalograia-Ardana Formation

One sample (GC19-11) was analysed from a normal-graded sandstone turbidite, 3 km NW of Kayalar, western Kyrenia Range (Fig. 4). In addition, a coarse-grained sandstone (debris-flow deposit; GC19-05) was sampled from 1 km NW of Ardahan, eastern Kyrenia Range (Supplementary Figure S1c). Both sandstones include abundant grains of ophiolite-related rock (serpentinite, chert and basalt) (Fig. 5b), terrigenous material (quartz, muscovite and sedimentary lithic fragments) (Table S4) and there are also calcareous bioclasts including the planktonic foraminifera *Acarinina bullbrooki*, *A. praetopilensis, Turborotalia frontosa, Igorina broedermanni, Morozovelloides crassatus* and *M. coronatus*, and also the large foraminifera, *Orbitoclypeus ramaraoi, Alveolina* cf. *A. ellipsoidalis, Chapmanina* sp. and *Sphaerogypsina globulus* that together date the maximum age range of the formation as Eocene (Ypresian-Bartonian). Nannofossil dating yielded mainly similar ages (Robertson et al., 2014).

Sample GC19-11 contains detrital zircons with mainly Precambrian ages (85%, Table S5). Neoproterozoic zircons dominate (61%) (Fig. 6), with major Ediacaran (596 Ma; n=13) and Tonian (909 Ma; n=9) age peaks. Paleoproterozoic zircons (14%) have an age peak at 1824 Ma (n=7). Archean zircons are scarce (3%). For the Paleozoic, the main age peak is Early Cambrian (522 Ma, n=6). The youngest zircon is 85 Ma (Santonian), much older than the planktonic foraminiferal age of Middle Eocene (Baroz, 1979; Robertson et al., 2014).

Sample GC19-05 contains less abundant Precambrian zircons (64%, Table S5) (Fig. 8). The dominant Neoproterozoic age group (48%) includes 18% Ediacaran, 13% Cryogenian and 17% Tonian grains. Trace-to-minor amounts of Mesoproterozoic-Archean zircons (3-9%) are present, with an age peak at 1857 Ma (n=7). Phanerozoic zircons (34%) have peaks of Early Cambrian (535 Ma; n=9), Early Permian (295 Ma; n=7) and Late Cretaceous (85 Ma; n=6) ages. The youngest detrital zircon, which is subhedral (Supplementary Figure S4), yielded an age of 80 Ma (Campanian) (Table S5), older than the paleontologically dated age (Robertson et al., 2014).

Overall, 52% of the analysed zircons have Th/U ratios >0.5, suggesting a magmatic origin (see Supplementary Figure S5); 96% of the zircons have Th/U <1.5, suggesting felsic and/or intermediate-composition igneous source rocks. Only 4% of the analysed grains with Th/U <0.1 have Devonian (n=1), Silurian (n=1), Cambrian (n=1) and Precambrian (n=6) ages, indicative of a metamorphic origin.

4.3. Kythrea Conglomerate

Three sandstones were sampled from the Kythrea Conglomerate Member at the base of the Kythrea Group. Sample GC19-13 is from Geçitköy Gorge, western Kyrenia Range (Fig. 4). Sample GC19-29 was collected 1.5 km NE of Değirmenlik, central Kyrenia Range. Sample GC19-04 is from 1 km south of Mersinlik, eastern Kyrenia Range (Supplementary Figure S2b). These sandstones are poorly sorted, with angular to sub-rounded grains, largely serpentinite and carbonate, cemented by calcite spar (see Fig. 5c) (Table S4). Interestingly, the sandstone matrix of the conglomerate contains more serpentinite than the conglomerate itself, which is rich in limestone and basic igneous clasts. This probably reflects the soft, friable nature of the serpentinite. The mostly non-marine Kythrea Conglomerate, lacks diagnostic fossils although its age is inferred to be Late Eocene-Oligocene from its position between the unconformably underlying Eocene (Ypresian-Bartonian) Kalograia-Ardana Formation and the overlying Upper Eocene-Oligocene Bellapais Formation (Baroz and Bizon, 1974; Hakyemez et al., 2000; McCay et al., 2013). In addition, a Late Eocene age has been obtained from planktonic foraminifera in two samples of marl near the top of the unit in the western Kyrenia Range (Baroz and Bizon, 1974; Baroz, 1979).

Sample GC19-13 contains abundant Precambrian detrital zircons (93%), characterised by Ediacaran (606 Ma; n=13) and Tonian (920 Ma; n=7) ages. Stenian (9%), Paleoproterozoic and Archean zircons are scarcer (9% and 8%, respectively), with ages peaking at 2486 Ma (n=6). Paleozoic zircons (7%) peak in the Early Cambrian (519 Ma; n=8) (Fig. 6). Two grains yielded Devonian and Silurian ages. The youngest zircon age is Late Devonian (372 Ma) (Table S5), much older than the inferred Late Eocene-Oligocene age (Baroz and Bizon, 1974; Hakyemez et al., 2000; McCay et al., 2013).

A restricted number (n=70) of detrital zircons analysed in sample GC19-29 yielded 58% Precambrian ages, with peaks in the Ediacaran (617 Ma; 15%) and Tonian (966 Ma; 13%). 8% of the zircons have a Stenian age. A few of the zircons of >1.6 Ga (n=7) are well rounded. The dominant Paleozoic age peak is late Carboniferous (310 Ma; n=7) (Fig. 6). The youngest age is Maastrichtian (72 Ma) (Table S5), compared to the paleontologically dated Late Eocene age (Baroz and Bizon, 1974; Hakyemez et al., 2000; McCay et al., 2013).

Sample GC19-04 has abundant Precambrian detrital zircons (75%) with dominant age peaks at 578 Ma (n=12) and 743 Ma (n=8), together with 8% Cryogenian, 7% Paleoproterozoic and 6% Archean grains, whereas Stenian grains are scarce (n=3). For the Paleozoic (19%), the main age peaks are Cambrian (538 Ma; n=7) and Early Ordovician (483 Ma; n=5) (Fig. 8). One subhedral zircon grain (see Supplementary Figure S4) yielded an age of 39 ± 1 Ma (Late Eocene) (Table S5), which is compatible with the inferred Late Eocene-Oligocene paleontological and strontium isotope ages (Baroz and Bizon, 1974; McCay et al., 2013).

For the three Kythrea Conglomerate samples, the Th/U ratios are >0.5 in 48% of the analysed zircons, <1.5 in 97% of the zircons, and <0.1 in 5% of the zircons (see Supplementary Figure S5). Zircons with Th/U <0.1 have Early Devonian (n=1), Neoproterozoic (n=9), Stenian (n=1), Paleoproterozoic (n=1) and Archean (n=3) ages.

4.4. Bellapais Formation

Two sandstones were sampled from the transitionally overlying marine Bellapais Formation, one from the western Kyrenia Range (GC19-12) and the other from the Karpas Peninsula (GC19-35) (Fig. 4). These sandstones have moderately to well sorted, angular to rounded grains. They are compositionally similar to the sandstone matrix of the Kythrea Conglomerate, with abundant igneous and sedimentary lithic fragments (see Fig. 5d). However, quartz is more abundant (5-15%; Table S4) whereas feldspar is rare. The Bellapais Formation is dated as Late Eocene-Oligocene based on a combination of planktonic foraminifera (e.g., *Globorotalia opima opima, Paragloborotalia opima*, *Globoquadrina venezuelana* and *Globigerina ouachitaensis), calcareous* nannofossils (e.g., *Cyclicargolithus abisectus*) and strontium isotope data (Baroz and Bizon, 1974; Hakyemez et al., 2000; McCay et al., 2013).

Sample GC19-12 contains mainly Precambrian zircons (64%), grouping in the Neoproterozoic (45%) (Table S5); i.e., Ediacaran (19%) and Tonian (19%) peaking at 610 Ma (n=13). The dominant Mesoproterozoic zircons are Stenian (4%); 15% of these >1.6 Ga ages (mostly rounded grains) peak at 2619 Ma (n=6). Paleozoic zircons (27%) mainly cluster in the Early Permian (282 Ma peak; n=5), late Carboniferous (321-301 Ma; n=10) and Early Cambrian (528 Ma peak; n=6) (Fig. 6). The youngest age is 86 Ma (Santonian), in contrast to the Late Eocene-Oligocene depositional age (Baroz and Bizon, 1974; Hakyemez et al., 2000; McCay et al., 2013).

For sample GC19-35, zircon populations group in the Ediacaran (19%), Cryogenian (9%), Tonian (19%), Stenian (8%) and Mesoproterozoic (6%), together with significant Carboniferous (9%), Triassic (8%) and Cretaceous (14%) age groups (Fig. 8). The youngest zircon is Campanian (80 ± 1 Ma) (Table S5), much older than the previously reported Late Eocene-Oligocene strontium isotopic and paleontological ages (Baroz and Bizon, 1974; McCay et al., 2013).

Only 3% of the zircon grains have Th/U ratios <0.1 (i.e., of metamorphic origin) (see Supplementary Figure S5); these are mainly Neoproterozoic (n=5), together with a few Late Devonian (n=1), Paleoproterozoic (n=1) and Archean (n=1) grains. 57% of the zircons have Th/U >0.5 (i.e., of magmatic origin); 96% of these grains have Th/U <1.5, indicative of felsic and/or intermediate-composition magmatic rocks.

4.5. Klepini Formation

One sample of coarse-grained sandstone (GC19-22) was sampled from a rare interval of mainly medium to thick-bedded, lenticular sandstones and mudstones within the mainly fine-grained Klepini Formation in the central Kyrenia Range, 200 m south of Arapköy (Fig. 4; Supplementary Figure S2d-e). Angular to well-rounded quartz grains and lithic clasts, mainly carbonates, occur in a micritic matrix (see Fig. 5e) (Table S4). Other lithic fragments are mainly serpentinite, with lesser amounts of muscovite schist. The depositional age of the Klepini Formation is Late Oligocene based on nannofossils indicative of biozones MNP25-MNN1 (Late Oligocene), strontium isotope stratigraphy (McCay et al., 2013) and planktonic foraminifera (e.g., *Globigerina ciperoensis* and *Paragloborotalia opima*) (Baroz and Bizon, 1974; Baroz, 1979).

The zircon populations mainly cluster in the Neoproterozoic (66%), with Ediacaran (19%), Cryogenian (12%) and Tonian (36%) components. Subordinate age groups occur in the Paleoproterozoic (17%) and Archean (7%). Paleozoic (8%) zircons are rare, mainly Cambrian (n=7) and Devonian (n=2) (Fig. 6). The youngest age is Late Devonian (373 Ma) (Table S5).

Th/U ratios are typically >0.1 (99%) (see Supplementary Figure S5); of these, 69% of the zircons have Th/U ratios >0.5 (i.e., of magmatic origin). Th/U <0.1 occurs in one grain (no. 86; 2249 Ma) (i.e., of metamorphic origin).

4.6. Flamoudi Formation

One sample of thick-bedded sandstone turbidite (GC19-31) was collected from the Flamoudi Formation, 1.8 km NE of Değirmenlik, central Kyrenia Range (Fig. 4). The Flamoudi Formation is mainly medium to fine-grained calcareous sandstone and marl (Supplementary Figure S2f). The sample collected has a mixed assemblage of planktic and benthic foraminifera, together with subordinate sub-angular, to rounded quartz and carbonate grains, with a sparite cement (Fig. 5f) (Table S4). The age of the Flamoudi Formation is Late Oligocene-Burdigalian, based on the occurrence of nannofossil biozones MNP25-MNN1 (Chattian-Aquitanian) and strontium isotope data. However, one sample contained *Catapsydrax dissimilis*, *Paragloborotalia mayeri*, '*Paragloborotalia*' *kugleri* and *Globigerina ciperoensis*, indicating a Langhian age (McCay et al., 2013).

Neoproterozoic (54%) zircons dominate, with age peaks in the Ediacaran (18%) (613 Ma; n=9) and Tonian (27%) (812 Ma; n=9). Minor fractions occur in the Stenian (10%), Paleoproterozoic (10%) and Archean (9%). Trace to minor populations cluster in the Cambrian (7%), Devonian (2%), Carboniferous (3%), Permian (1%) and Triassic (2%) (Fig. 6). A minor Neogene zircon fraction, mostly euhedral (Supplementary Figure S4), ranges from 19 to 15 Ma (Burdigalian-

Langhian). The youngest age is 15 Ma (Langhian) (Table S5), in agreement with one sample that was dated using planktonic foraminifera (McCay et al., 2013; see above); this Langhian age is considerably younger than the Aquitanian-Burdigalian age range suggested by some earlier work (Baroz, 1979; Hakyemez et al., 2000).

Th/U ratios of <0.1 occur in six zircons, either Ediacaran (n=5) or Paleoproterozoic (n=1) (see Supplementary Figure S5). 67% of the zircon grains have Th/U >0.5 (i.e., of magmatic origin). 25% of zircons have Th/U >1.5, indicative of a mafic igneous origin, with ages of Miocene (n=2), Carboniferous (n=2), Cambrian (n=3) and Precambrian (n=21).

4.7. Panagra Formation

Two samples of medium-grained sandstone turbidites were collected from the Panagra Formation, which is dominated by pale grey hemipelagic marl, with distinctive reddish-coloured intervals (Supplementary Figure S3a). The first sample (GC19-30) is from 1.5 km NE of Değirmenlik, central Kyrenia Range, and the second (GC19-38) from 200 m N of Balalan, Karpas Peninsula (Fig. 4). These sandstones have angular to rounded grains, mainly composed of monocrystalline quartz and redeposited micritic fragments (see Fig. 5g) (Table S4). The Panagra Formation is dated as mainly Burdigalian-Langhian based on strontium isotope stratigraphy and planktonic foraminifera (e.g., *Globigerinoides trilobus*, *Praeorbulina* sp., *Praegloborotalia siakensis* and *Globorotalia mayeri*) (McCay et al., 2013), longer ranging than the initially inferred Langhian age (Baroz and Bizon, 1974).

Sample GC19-30 contains abundant Neoproterozoic zircons (68%) with Ediacaran (25%) (606 Ma; n=18) and Tonian (27%) (954 Ma; n=13) age peaks. Cryogenian zircons are less abundant (16%). Minor zircon fractions occur in the Mesoproterozoic (5%), Paleoproterozoic (8%) and Archean (6%) (Fig. 6). There are also minor zircon fractions with Cambrian (n=5), Ordovician (n=1), Devonian (n=3), Carboniferous (n=2), Permian (n=1) and Triassic (n=1) ages. The youngest is 219 Ma (Table S5), much older than the inferred Burdigalian-Langhian depositional age.

Sample GC19-38 contains relatively less abundant Precambrian zircons (64%) that are dominantly Neoproterozoic (43%); i.e., Ediacaran (17%), Cryogenian (11%) and Tonian (18%). Minor zircon fractions of Mesoproterozoic (mainly Stenian, 4%), Paleoproterozoic (9%) and Archean (8%) ages are also present. Concordant Phanerozoic zircons are Cambrian (n=6), Ordovician (n=2), Silurian (n=2), Devonian (n=2), Carboniferous (n=5), Permian (n=1), Triassic (n=2) and Cretaceous (n=2) (Fig. 8). There is also a significant Neogene zircon fraction, mostly euhedral grains (Supplementary Figure S4), with a major age peak at 20 Ma (Burdigalian; n=18). The 17 Ma (Burdigalian) age of the youngest zircon (Table S5) is consistent with preferred Sr isotopic and planktonic foraminifera age data (see above).

The zircons typically have relatively high Th/U ratios (see Supplementary Figure S5); >0.1 in 96% and >0.5 in 59% (i.e., of magmatic origin). Only 4% of these zircons have Th/U <0.1; i.e., Late Cretaceous (n=1), Ediacaran-Cryogenian (n=8) and Archean (n=1). 5% of the Permian (n=1), Carboniferous (n=1), Ordovician (n=1) and Neoproterozoic (n=8) grains have Th/U >1.5, indicative of a mafic origin.

4.8. Trapeza Formation

Three sandstone turbidites were collected from the Trapeza Formation, which is interbedded with cream-coloured marls (Supplementary Figure S3b); i.e., 2.0 km NW of Beşparmak, central Kyrenia Range (GC19-26); 600 m W of Ardahan, eastern Kyrenia Range (GC19-06); and 800 m E of Balalan in the Karpas Peninsula (GC19-40) (Fig. 4). These sandstones are well-sorted, medium-grained and contain sub-rounded to rounded grains, mainly quartz, calcite and serpentinite (see Fig. 5h) (Table S4). The Trapeza Formation is dated as Langhian-Tortonian, based on strontium isotopes, planktonic foraminifera (e.g., *Paragloborotalia mayeri* and *Globorotalia menardii*) and the occurrence of nannofossil biozones MNN7a-MNN11a (McCay et al., 2013), in part slightly older than the initially inferred Serravallian-Tortonian age based on planktonic foraminifera (Baroz and Bizon, 1974; Baroz, 1979).

Sample GC19-26 includes a major Neoproterozoic age group; i.e., Ediacaran (15%), Cryogenian (11%) and Tonian (23%). Other zircons are >1.0 Ga (n=13), together with Mesoproterozoic (2%), Paleoproterozoic (5%) and Archean (4%) ages. The younger zircon fractions group in the Cretaceous, with peaks at 70 and 82 Ma (Campanian-Maastrichtian). Zircons of Cambrian (n=3), Carboniferous (n=1), Triassic (n=1) and Jurassic (n=1) ages are rare. There are also minor Paleogene (n=7) and Neogene (n=3) age groups (Fig. 6). The youngest concordant age is 9 Ma (Tortonian) (Table S5).

Sample GC19-06 has Ediacaran (18%), Tonian (12%), Mesoproterozoic (6%) and Paleoproterozoic (7%) age groupings. Phanerozoic ages are relatively abundant (54%), with major Campanian (75 Ma) and Burdigalian (16 Ma) age groups. There are also subordinate Cambrian (5%) and Ordovician zircons (4%). A few grains (typically n=<4) fall within other age ranges (Fig. 8). The youngest zircon is Tortonian (11 Ma) (Table S5).

Sample GC19-40 contains abundant Precambrian detrital zircons, with major age peaks at Ediacaran (615 Ma, 19%), Tonian (954 Ma, 22%), Paleoproterozoic (1946 Ma, 11%) and Archean (2495 Ma, 6%). Trace to minor zircon fractions include Cambrian (n=4), Devonian (n=2), Late Cretaceous (n=8) and Neogene (n=5). The youngest zircon is Tortonian (9 Ma) (Table S5). The Tortonian ages of the three samples analysed are consistent with the maximum age range (11-9 Ma), as inferred from Sr isotopic and planktonic foraminiferal dating (see above).

In the three Trapeza Formation samples, only 2% of the zircons have Th/U <0.1, (i.e., of metamorphic origin), namely Late Cretaceous (n=1), Neoproterozoic (n=5) and Mesoproterozoic (n=1) (see Supplementary Figure S5). 56% of the zircon population has Th/U >0.5 (i.e., of magmatic origin). 96% of the zircons have Th/U <1.5, consistent with derivation from felsic and/or intermediate-composition magmas.

4.9. Davlos Formation

Three samples were collected from very thick-bedded, massive sandstones of the

Davlos Formation (Supplementary Figure S3c-d). Sample GC19-59 is from 500 m SW of Geçitköy, sample GC19-33 from a coastal exposure, 2.0 km NW of Kaplıca (Supplementary Figure S3c) and sample GC19-39 from 800 m E of Balalan (Fig. 4). These sandstones contain abundant poorly sorted grains of quartz and redeposited micritic fragments, together with igneous and metamorphic lithics, mostly serpentinite and muscovite schist (see Fig. 5i) (Table S4). The Davlos Formation contains few dateable microfossils. However, a Tortonian age has been inferred, based on planktonic foraminifera (e.g., *Globorotalia acostaensis* and *Orbulina universa*) (Baroz, 1979; McCay et al., 2013).

Sample GC19-59 is dominated by detrital zircon clusters of Late Cretaceous (n=37) and Paleogene (n=14) ages, with major peaks at 72 Ma (Maastrichtian) and 53 Ma (Early Eocene) (Fig. 6). Older grains are largely Neoproterozoic (31%), with age peaks at ca. 622 Ma (n=10) and 942 Ma (n=6). Paleoproterozoic and Archean ages are sparse; i.e., 6% and 2%, respectively. The youngest age peak (which is also the minimum age) is ca. 9 Ma (Tortonian; n=5) (Table S5), consistent with the Tortonian age based on planktonic foraminifera.

Sample GC19-33 is dominated by Phanerozoic ages (69%), the majority of the zircon grains (64%) yield Late Cretaceous (47%) or younger ages (17%). Upper Cretaceous grains, which are generally subhedral to euhedral (Supplementary Figure S4), include three age peaks: 72 Ma (n=32), 79 Ma (n=19) and 84 Ma (n=14). Paleogene zircons are subordinate, mainly dated as 53-47 Ma, and there are a few Miocene grains (16-12 Ma; n=3). Scattered Paleozoic grains (3%) include Cambrian (n=1), Ordovician (n=1) and Carboniferous (n=1) ages. A single Triassic cluster (n=2) peaks at 211 Ma (n=2) (Fig. 8). There is also a Neoproterozoic age cluster, with the main age groups being Ediacaran (n=10) and Tonian (n=14). The youngest zircon age is 12 Ma (Serravallian; n=2) (Table S5), slightly older than the depositional age (preferred Tortonian) based on planktonic foraminifera (Baroz, 1979; McCay et al., 2013).

Sample GC19-39 is dominated by Neoproterozoic zircons (18%), whereas Mesoproterozoic and Archean grains are rare. Phanerozoic ages (80%) are broadly scattered, with Late Cretaceous (83-69 Ma; n=46) dominating. Minor Paleogene grains range from 58-31 Ma (n=9) (Fig. 8). The youngest 14 ages overlap with statistical uncertainties but imply a Tortonian youngest age cluster (ca. 10 Ma), which is consistent with the paleontologically determined age (Baroz, 1979; McCay et al., 2013).

Zircons from the western Kyrenia Range (GC19-59) have Th/U >0.1 (see Supplementary Figure S5). In contrast, some of the grains from the eastern Kyrenia Range (GC19-33; n=3) and the Karpas Peninsula (GC19-39; n=2), of Late Cretaceous (82-74 Ma; n=3), Ordovician (n=1) and Ediacaran (n=1) ages, have Th/U <0.1. 46% of the zircons have Th/U >0.5 (i.e., of magmatic origin). Only 1% of the grains, with ages of 46 Ma, 524 Ma and 791 Ma, have Th/U >1.5, suggesting a mafic origin.

4.10. Mia Milia Formation

Two sandstones were sampled from the Mia Milia Formation in the Mesaoria Basin, dominated by folded and imbricated sandstone turbidites and mudstones

(Supplementary Figure S3e-g). Sample GC19-57, a thin to medium-bedded sandstone turbidite, was collected from a roadcut 700 m S of Gürpınar, western Kyrenia Range. Sample GC19-41, also a sandstone turbidite, came from 1.5 km E of Balalan in the Karpas Peninsula (Fig. 4). These sandstones are mainly composed of igneous rock fragments (e.g., serpentinite), sedimentary rock fragments (e.g., redeposited micritic grains), together with biogenic material (e.g., foraminifera) (see Fig. 5j) (Table S4). Quartz grains are relatively common, whereas felspar is rare. The Mia Milia Formation is dated as Burdigalian-Tortonian based on planktonic foraminifera (e.g., *Globoturborotalita nepenthes*), calcareous nannofossils and Sr isotopic analyses (McCay et al., 2013), more long-ranging than the previously inferred Serravallian-Tortonian age range (Baroz and Bizon, 1974; Baroz, 1979; Hakyemez et al., 2000).

Zircons in sample GC19-57 are mainly Neoproterozoic; i.e., Ediacaran (29%), Cryogenian (14%) and Tonian (23%), together with minor fractions of Paleoproterozoic (9%) and Archean (8%) ages. Paleozoic zircons mainly cluster in the Cambrian (n=3), Ordovician (n=1), Devonian (n=2) and Carboniferous (n=1) (Fig. 6). There is a minor Late Cretaceous fraction (6%). The youngest zircon, which is euhedral (Supplementary Figure S4), yielded an age of 10 Ma (Tortonian; n=2) (Table S5).

In contrast, sample GC19-41 is dominated by Mesozoic zircons (75%), with Triassic (7%), Cretaceous (46%), Paleogene (10%) and Neogene (10%) age peaks. There is a relatively continuous scatter of Ordovician to Permian ages (n=<3, generally) (Fig. 8). There are also minor Neoproterozoic zircon fractions of

Ediacaran (4%), Cryogenian (3%) and Tonian (7%) ages. The youngest zircon is 9 Ma (Tortonian; n=6). The minimum Tortonian ages of the two samples analysed (Table S5) are consistent with the previously reported depositional age range (Baroz and Bizon, 1974; Baroz, 1979; Hakyemez et al., 2000).

52% of the zircons analysed have Th/U >0.5, while 97% are <1.5, suggestive of derivation from felsic and/or intermediate magmas. 4% of the zircons, of Late Cretaceous (73 Ma; n=1), Silurian (n=1), Cambrian (n=1), Neoproterozoic (n=6) and Paleoproterozoic (n=1) ages, have Th/U <0.1 (i.e., of metamorphic origin) (see Supplementary Figure S5).

4.11. Yılmazköy and Yazılıtepe Formations

The Yılmazköy Formation, which is equivalent to the upper marl unit of the previously defined Davlos Formation (Baroz, 1979), is mainly marl, mudstone and sandstone (Supplementary Figure S3h). The overlying Yazılıtepe Formation, which is equivalent to the lower marl unit of the traditional Lapatza Formation (e.g., Necdet and Anıl, 2006) comprises marl, limestone and sandstone, overlain by Messinian evaporite. Two thin-bedded, medium-grained gypsiferous sandstones with common small quartz, metamorphic lithic and biogenic grains (see Fig. 5k) were collected from 1.8 km NW of Altınova, eastern Kyrenia Range (Fig. 4; Supplementary Figure S3h). The Yılmazköy Formation has been dated as Tortonian using planktonic foraminifera (e.g., *Orbulina universa* and *Globoturborotalita nepenthes*), calcareous nannofossils and Sr isotopes (Hakyemez et al., 2000; McCay et al., 2013). The Yazılıtepe Formation is dated as

Tortonian-Messinian based on planktonic foraminifera, calcareous nannofossils and Sr isotopes (McCay et al., 2013), a longer age range than previously inferred for this interval based on the planktonic foraminifera, *Neogloboquadrina acostaensis* and *Neogloboquadrina humerosa* (Baroz, 1979).

In sample GC19-53, from the Yılmazköy Formation, Precambrian ages cluster in Ediacaran (17%), Cryogenian (6%) and Tonian (8%), together with rare Paleoproterozoic to Archean ages (<2%). Cambrian zircons form a significant age population (n=9). Ordovician to Jurassic grains are scattered (15%). Prominent age groups occur at 78-71 Ma (Campanian-Maastrichtian) and 16 Ma (Burdigalian) (Fig. 8). Minor Paleogene grains (n=10), peak at 48 Ma (n=4). The youngest zircon age is ca. 9 Ma (Tortonian; n=2) (Table S5), consistent with the Tortonian depositional age data (Hakyemez et al., 2000; McCay et al., 2013).

Sample GC19-54, from the overlying Yazılıtepe Formation, has a bimodal cluster of Neoproterozoic (39%) ages, mainly Ediacaran (n=9), Tonian (n=7) and also Neogene (55%), especially Messinian (n=27). Archean (n=1), Silurian (n=1) and Devonian (n=1) zircon grains are rare (Fig. 8). The weighted age mean of the youngest zircon cluster (mostly euhedral grains; see Supplementary Figure S4) is Messinian (5.4 ± 0.1 Ma; n=10) (Table S5), consistent with the Tortonian-Messinian depositional age data (McCay et al., 2013).

The zircons from the Yılmazköy Formation (sample GC19-53) typically have high Th/U ratios (>0.1; 92%). Eight grains have Th/U <0.1, characteristic of metamorphic zircons (see Supplementary Figure S5). These zircons are Early Paleocene (n=1), Late Cretaceous (83-69 Ma; n=4) and Ediacaran-Cryogenian (n=3). Four grains, with either Late Cretaceous (89-66; n=3) or Ediacaran (n=1) ages, have Th/U>1.5, indicative of a mafic magmatic origin. Th/U ratios are >0.1 in the zircons from the Yazılıtepe Formation (sample GC19-54) (see Supplementary Figure S5); of these, 80% have Th/U >0.5, indicative of magmatic zircons. Five grains of Messinian (n=4) and Ediacaran (n=1) ages have Th/U >1.5, characteristic of mafic melts.

4.12. Athalassa Formation

The overlying Pliocene marine marls and mudrocks (Myrtou and Nicosia formations) were not sampled for zircon dating in view of their relatively fine grain size. The Athalassa Formation, which depositionally overlies these units, is mainly carbonate rocks with very few sandstones suitable for zircon dating, although one sandstone (GC19-17) ca. 400 m W of Akdeniz, western Kyrenia Range (Fig. 4). This sandstone is mainly quartz and sedimentary lithics (e.g., carbonates and sandstones), together with biogenic material, mostly in the form of benthic foraminifera and calcareous algae (see Fig. 5l) (Table S4). The Athalassa Formation in the Mesaoria Basin is not well dated because the shallow-marine biota present are mainly long-ranging, although the occurrence of the planktonic foraminifera, *Globorotalia crassaformis* (Baroz, 1979; Hakyemez et al., 2000) and magnetostratigraphic data (Palamakumbura, 2016; Palamakumbura and Robertson, 2018) indicate a partly Pliocene age. Correlative shallow-marine carbonates in west Cyprus (Polis graben) are more precisely dated as Late Pliocene-Early Pleistocene (2.76-1.6 Ma) based on nannofossil and Sr isotope dating (Balmer et al., 2019).

Precambrian zircons in the Athalassa Formation sample have Ediacaran (28%), Cryogenian (9%), Tonian (20%) and Paleoproterozoic (9%) ages (Fig. 6). Mesoproterozoic (3%) and Archean (3%) grains are scarce. There are minor fractions of Cambrian (n=2), Ordovician (n=2) and Carboniferous (n=1) ages. Mostely euhedral zircons (see Supplementary Figure S4) dominate the Upper Cretaceous (n=15) and Eocene (54-39 Ma; n=9) fractions. One Lower Miocene grain is present (18 Ma). The youngest zircon age is ca. 9 Ma (Tortonian; n=2) (Table S5), much older than the inferred Late Pliocene- Early Pleistocene depositional age (see above).

Only 3% of the analysed zircons have Th/U <0.1 (i.e., of metamorphic origin), all of which are Precambrian (see Supplementary Figure S5). 50% of the zircons have Th/U ratios of 0.5-1.5, typical of zircons from felsic and/or intermediate melts. Three grains of Ediacaran (n=3), and one grain of Eocene age (48 Ma; n=1) have Th/U >1.5, indicative of a mafic magmatic origin.

4.13. Zircon trace element geochemistry

The concentrations of trace elements in the zircons analysed are as follows: U, 9-2994 ppm; Th, 0.8-3102 ppm; Y, 43-15335 ppm; Nb, 0.5-133.2 ppm; Yb, 3.8-3325.6 ppm; Hf, 5515-17840 ppm; Ta, 0.1-130.1 ppm (Table S2). All of the zircons are characterised by strong heavy REE enrichment (Ce/Yb<0.5) and have positive Ce and negative Eu anomalies (Supplementary Figure S6).

For the Ediacaran-Early Cambrian (570-520 Ma), the trace element data are compatible with a continental magmatic arc origin. For the Carboniferous, most of the zircon grains (76%) fall within the continental, arc-related orogenic field on the basis of their relatively high U/Yb, Hf/Th but low Th/U ratios (Fig. 9; Supplementary Figure S4). A smaller number of zircons (24%) are compositionally consistent with a within-plate setting (e.g., rift-related). The scattered Permian and Triassic grains indicate a range of continental margin arc to intra-plate settings. The trace element ratios (e.g., U/Yb, Nb/Yb) of the Upper Cretaceous grains are highly variable, consistent with a mixed derivation from both continental arc and ophiolite-related settings (Grimes et al., 2015) (Fig. 9). Specifically, the ophiolite-related zircons (89-82 Ma) have relatively high Y concentrations (>2000 ppm), high Nb/Hf (>0.001) but low U/Yb (<0.1) ratios (Supplementary Figure S7). The continental arc-related grains (85-67 Ma) are characterised by relatively low Y values (<2000 ppm), low Nb/Hf (<0.0004) but high U/Yb (>1) ratios (Supplementary Figure S7). The Eocene and Miocene zircons have mainly continental arc-type trace element compositions.

4.14. Detrital zircon Hf isotope signatures

Representative zircons (n=684) from 17 samples dated during this study yielded a total of 684 Lu-Hf isotopic analyses (Table S3). Paleoproterozoic and Archean zircons (n=53) are characterised by a relatively small spread of $\varepsilon Hf_{(t)}$ values, ranging from -20 to +5 (Fig. 10). The smaller Mesoproterozoic zircon fraction (n=22) shows a bimodal cluster of $\varepsilon Hf_{(t)}$ values, 50% of which are moderately to strongly juvenile (+2.7 to +13.7), whereas the remainder are relatively evolved (-3.4 to -13.5). In contrast, Neoproterozoic zircon populations (n=189) have a greater range of $\varepsilon Hf_{(t)}$ values (-30 to +11.2).

The Lower Cambrian zircons (540-519 Ma) exhibit highly evolved to strongly juvenile $\varepsilon Hf_{(t)}$ (-24.4 to +9.0), whereas the younger grains are dominated by evolved $\varepsilon Hf_{(t)}$ (-2.4 to -18.8), together with two positive outliers (+4.1, +7.1) (Fig. 10). 83% of the Ordovician to Silurian grains have evolved $\varepsilon Hf_{(t)}$, ranging from near-chondritic to strongly negative (-35.0). Six grains yield super-chondritic $\varepsilon Hf_{(t)}$ (+0.8, +7.0). In contrast, Devonian (417-360 Ma) grains have relatively restricted $\varepsilon Hf_{(t)}$ (-5, +5), with 2 negative and 2 positive outliers. Carboniferous zircons overlap, with mainly negative $\varepsilon Hf_{(t)}$ (-8, -3), together with 9 positive outliers ranging from +1.4 to +5.4. Permian (298-254 Ma) zircons have dominantly negative $\varepsilon Hf_{(t)}$ (ca. -6), together with subordinate juvenile $\varepsilon Hf_{(t)}$ (+1.9 to +11.1).

The Lower Triassic to the lower Upper Triassic (250-232 Ma) zircons have dominantly juvenile $\varepsilon Hf_{(t)}$, decreasing through time from +10.3 to +2.5 (Fig. 10). The Upper Triassic zircons mainly have evolved $\varepsilon Hf_{(t)}$ (ca. -5), together with three positive outliers. Jurassic grains (n=5) are sparce, with scattered $\varepsilon Hf_{(t)}$ from -8.3 to +12.1. Three Lower Cretaceous (111-102 Ma) zircons have strongly juvenile $\varepsilon Hf_{(t)}$ (+8.2 to +13.1). Cenomanian-Turonian (96-91 Ma) zircons mainly exhibit strongly positive $\varepsilon Hf_{(t)}$ ranging from +11.4 to +18.7, together with one strongly negative outlier (-13.8). Coniacian-lower Campanian (90-80 Ma) zircons have $\varepsilon Hf_{(t)}$ values ranging from around approximately -13 to +12 (spread vertically in Fig. 10). Lower to mid-Campanian (79-75 Ma) zircons have a smaller spread of $\varepsilon Hf_{(t)}$ values (-9.3 to +7.0). Upper Campanian-lower Maastrichtian (75-70 Ma) zircons are characterised by dominantly evolved $\varepsilon Hf_{(t)}$ values (ca. -7; 61%), together with three positive outliers. Upper Maastrichtian (70-66 Ma) grains are all strongly evolved (-6 to -10).

Lower Paleocene zircons (n=5), ranging from 65-62 Ma, have moderately to strongly negative $\varepsilon Hf_{(t)}$ (-9.0 to -3.7), followed in progressively younger zircons by an increase in $\varepsilon Hf_{(t)}$ to -0.9 (60 Ma), and then to +1.0 (58 Ma) (Fig. 10). Lower Ypresian (54-50 Ma) zircons have mostly evolved $\varepsilon Hf_{(t)}$ (-8 to -0.8) with one positive outlier (+1.2), whereas all of the middle to upper Eocene (49-39 Ma) grains have positive, juvenile $\varepsilon Hf_{(t)}$ (+1.9, +5.5). One Oligocene grain has strongly juvenile $\varepsilon Hf_{(t)}$ (+7.0). Aquitanian-Burdigalian (21-16 Ma) grains exhibit moderately evolved $\varepsilon Hf_{(t)}$ (ca. -5). Langhian (15 Ma) zircons have near chondritic to slightly juvenile $\varepsilon Hf_{(t)}$ (-1 to +2.7). Serravallian-Tortonian (12-9 Ma) zircons have dominantly juvenile $\varepsilon Hf_{(t)}$ (+2 to +9.2), together with two negative outliers. Messinian (6-5 Ma) zircons are characterised by $\varepsilon Hf_{(t)}$ ranging from -1 to +2 (spread vertically in Fig. 10).

5. Previous U-Pb and Lu-Hf zircon data

Interpretation of our new U-Pb and Hf isotopic data is aided by taking account of published data (Chen et al., 2019), in particular, from a transect in the eastern Kyrenia Range (Shaanan et al., 2021; Glazer et al., 2021) (see Fig. 4) (Table S1).

5.1. Previous detrital zircon U-Pb ages

The oldest sample, namely a calcschist intercalation within the Sikhari Formation (Trypa Group), of inferred a Triassic age, is characterised by abundant Ediacaran (15%), Cryogenian (10%) and Tonian (26%) zircons, together with subordinate Mesoproterozoic (5%), Paleoproterozoic (10%) and Archean (7%) fractions (Fig.

11). Upper Carboniferous zircons (11%) dominate the Paleozoic fraction. There is also a minor Triassic zircon fraction (5%) of inferred magmatic origin (Glazer et al., 2021). The Triassic radiometric age is consistent with the inferred depositional age (Ducloz, 1972; Baroz, 1979; Robertson and Woodcock, 1986).

Samples from the upper Campanian-Maastrichtian Kiparisso Vouno Member (n=2) exhibit predominantly Neoproterozoic ages (34-42%), with major contributions from the Ediacaran (13-15%) and Tonian (13-22%). Paleoproterozoic and Archean fractions are subordinate: 11-20% and 3-11%, respectively. Carboniferous (9-11%), Permian (15%), Triassic (7%) and Cenomanian-Maastrichtian (3-6%) age groups are also present (Fig. 11). Jurassic zircons are rare (5%) (Chen et al., 2019; Glazer et al., 2021).

Samples from the Lower-Middle Eocene Kalograia-Ardana Formation (n=2) are characterised by significant zircon populations of Neoproterozoic age (37-46%), together with subordinate Mesoproterozoic (7-9%), Paleoproterozoic (6-7%) and Archean (3-5%) fractions. There are also Carboniferous (7-13%), Triassic (4-7%) and Cretaceous (12-16%) fractions, whereas Permian and Paleogene grains are rare (ca. 4-5%) (Chen et al., 2019; Glazer et al., 2021) (Fig. 11). One sandstone sample (013-CY of Glazer et al., 2021) that was collected from near a large, detached block (olistolith) of Upper Paleozoic limestone (Kantara Limestone) in the eastern range has relatively abundant Carboniferous grains (17%). Some of the detached blocks are dated as Permian based on large foraminifera (Ducloz et al., 1972), although a Carboniferous age for some of the blocks may be possible (see Robertson et al., 2014).

One sample from the Upper Eocene-Oligocene Bellapais Formation is dominated by Precambrian zircons (90%), with major peaks of Ediacaran (15%), Cryogenian (14%), Tonian (33%) and Paleoproterozoic (17%) ages. Additional pronounced age clusters occur in the Mesoproterozoic at 1846 Ma (n=5) and the Cambrian at 531 Ma (Shaanan et al., 2021) (Fig. 11).

One sample from the Upper Oligocene-Burdigalian Flamoudi Formation has Precambrian zircons of 677 Ma, 805 Ma and 1043 Ma. Dominant Paleoproterozoic zircons peak at 1836 Ma and 2442 Ma. Minor fractions occur in the Cambrian (3%), Ordovician (1%) and Devonian (3%) (Shaanan et al., 2021) (Fig. 11).

One sample from the Tortonian Davlos Formation has Upper Cretaceous zircon grains (84-74 Ma; 83%), together with minor Neoproterozoic (7%), Eocene (2%) and Miocene (2%) fractions (Chen et al., 2019).

One sample from the Burdigalian-Tortonian Mia Milia Formation has mainly Cretaceous (52%), Ediacaran (13%) and Cryogenian (9%) zircons, together with minor fractions of Paleoproterozoic (4%) and Archean (3%) ages. Paleozoic zircons mainly cluster in the Cambrian (2%), Devonian (2%) and Carboniferous (5%) and there are also minor Paleogene (4%) and Neogene (3%) fractions (Shaanan et al., 2021).

The one sample previously analysed from the Tortonian Yılmazköy Formation has prominent Neoproterozoic (45%) and Paleoproterozoic (12%) zircons. Phanerozoic ages (32%) are scattered, with early Carboniferous (6%), Late Triassic (9%) and Late Cretaceous (4%) maximum probabilities (Shaanan et al., 2021) (Fig. 11).

5.2. Previous detrital zircon Lu-Hf isotopic data

Previous zircon analysis of 8 samples yielded a total of 319 Lu-Hf isotope analyses (Table S3): Triassic Sikhari Formation (n=9), Upper Cretaceous rhyolite block (n=13), Lower-Middle Eocene Kalogaria-Ardana Formation (n=187), Upper Eocene-Oligocene Bellapais Formation (n=44), Upper Oligocene-Burdigalian Flamoudi Formation (n=49) and the Burdigalian-Tortonian Mia Milia Formation (n=17) (Shaanan et al., 2021; Glazer et al., 2021) (Fig. 12).

Most of the Paleoproterozoic and Archean zircons exhibit negative $\varepsilon Hf_{(t)}$ (-16.8 to -0.2). A few zircons (n=8) have slightly positive (near chondritic) $\varepsilon Hf_{(t)}$ (+0.1 to +1.7). The Neoproterozoic zircons (n=140) have both negative (-44.7 to -0.2) and positive (+0.5 to +14.6) $\varepsilon Hf_{(t)}$.

Most of the Cambrian (535-502 Ma) zircons (6 out of 8) exhibit negative $\varepsilon Hf_{(t)}$ (-27.0 to -2.0) with the remainder being positive $\varepsilon Hf_{(t)}$ (+0.9 to +5.6). The Ordovician detrital zircons (476-453 Ma) have mainly negative $\varepsilon Hf_{(t)}$ (-19.2 to -1.6). A few Devonian zircons (n=3) have $\varepsilon Hf_{(t)}$ ranging from -11.7 to +6.2. Carboniferous (347-300 Ma, n=32) zircons mainly exhibit negative $\varepsilon Hf_{(t)}$ (-11.8 to -1.3), together with three positive outliers (+2.7 to +5.5). Permian zircons (n=4) have $\varepsilon Hf_{(t)}$ between -13.7 and +6.5. Triassic zircons are dominated by negative $\varepsilon Hf_{(t)}$ (-5.7 to -3.7), together with three positive outliers (+1.8 to +5.7). Two Lower Cretaceous zircons, dated at 101 Ma, yielded both negative and positive $\varepsilon Hf_{(t)}$ (-17.7, +8.4). Upper Cretaceous zircons (n=30) have highly variable $\varepsilon Hf_{(t)}$, ranging from strongly negative to strongly positive (-22.9 to +14.1). The youngest zircon fraction from the

Upper Cretaceous (77-72 Ma) rhyolite block yielded predominantly near-chondritic $\varepsilon Hf_{(t)}$ (-0.6, +4.2).

6. Discussion

6.1. Constraints on depositional age

Below, we compare the minimum detrital zircon ages, as obtained in this and previous studies (Table S5), with the ages of the stratigraphic units as determined paleontologically and by strontium isotopes.

The Sikhari Formation is dated as 240-233 Ma (Ladinian-Carnian) based on the youngest zircon ages (Table S5) (Glazer et al., 2021). This is similar to the Middle to Late Triassic age range utilizing large bivalves (megalodontids) and ostracods (Ducloz, 1972). The U-Pb detrital zircon data also point to a source of nearly-contemporaneous magmatic detritus, probably related to continental rifting (see Section 6.3).

The weighted mean ages of the youngest cluster of two or more grains in the Kiparisso Vouno Member (of magmatic origin) mainly range from 86-79 Ma (Santonian-Late Campanian) (Table S5), compared with the Late Campanian-Maastrichtian depositional age based on planktonic foraminifera and calcareous nannoplankton (Baroz, et al., 1979; Robertson et al., 2012b). The formation might therefore have begun to accumulate ca. 3 Ma earlier than as suggested by the biostratigraphic age.

Six samples analysed from the Eocene (Ypresian-Bartonian) Kalograia-Ardana Formation yielded the youngest, magmatic zircon U-Pb ages of 88-80 Ma

(Coniacian-Campanian) (Table S5). However, Middle Eocene (Lutetian), magmatic zircons (45 Ma; n=1) do rarely occur (Chen et al., 2019), in agreement with the Middle Eocene biostratigraphic age. Maastrichtian-Paleogene igneous or metamorphic lithologies were apparently absent from the source area. Whole-rock chemical analyses of clasts of fine to medium-grained basic igneous rocks from the Kalograia-Ardana Formation (mainly altered) range in composition from island arc tholeiite to boninitic, and are interpreted to have an ophiolitic provenance (Robertson et al., 2014). This is dissimilar to the more ‘enriched’ chemical composition of the fine to medium-grained basic igneous rocks within the underlying Maastrichtian-Lower Eocene Melounda and Ayios Nikolaos formations (Robertson and Woodcock, 1986; Huang et al., 2007; Chen and Robertson, 2021b). The provenance of the samples analysed from the Kalograia-Ardana Formation is therefore unlikely to have included a significant contribution from the underlying Maastrichtian-Paleogene succession.

The youngest zircon age obtained from the Kythrea Conglomerate sample (of magmatic origin) in this study is 39 Ma; i.e., Bartonian (late Middle Eocene) (Table S5), compared to the oldest reported Late Eocene paleontological age (from the western range). This suggests that the unconformity between the Kalograia-Ardana Formation and the Kythrea Conglomerate represent a relatively short time interval (several Ma at most) (see Section 2.2 for significance of the unconformity).

The youngest zircons from the Bellapais Formation (of magmatic origin) range from 95-80 Ma (Cenomanian-Campanian) (Table S5), compared to the Late Eocene-Oligocene paleontological age. This suggests that Paleogene zircons were absent from the source lithologies. Whole-rock chemical analyses of clasts of fine to medium-grained basic igneous rocks from the Bellapais Formation are mainly of near-MORB composition, but with a negative Nb anomaly which suggests a subduction influence (Robertson et al., 2014); this contrast with the more ‘enriched’ composition of the basalts within the underlying succession (see above). The source of the Bellapais Formation igneous clasts was probably ophiolitic, similar to those within the Kalograia-Ardana Formation (McCay and Robertson, 2012; Robertson et al., 2014).

The youngest detrital zircon age of the overlying Upper Oligocene Klepini Formation is 373 Ma (Late Devonian), suggesting that the inferred absence of zircon-bearing igneous or metamorphic source rocks of Paleocene age extended into the early Neogene. The youngest detrital zircon grains of magmatic origin (this study) in the Chattian-Langhian Flamoudi Formation are dated as 15 ± 1 M (Langhian). This points to a nearby contemporaneous magmatic source, in contrast to the underlying Upper Eocene-Oligocene formations. The youngest zircon age of the overlying Panagra Formation (of magmatic origin) is 17 Ma (Burdigalian) (Table S5), consistent with its paleontologically inferred Burdigalian-Langhian age range. Above this, the youngest zircon ages in the Trapeza Formation are 10.6-9.2 Ma (Tortonian), consistent with the inferred Langhian-Tortonian paleontological age.

The youngest zircons (of magmatic origin) within the overlying Davlos Formation are dated as 9 Ma (Tortonian) (Table S5), in agreement with the inferred Tortonian paleontological age. The Mia Milia Formation has youngest magmatic zircon ages of 15-9 Ma (Langhian-Tortonian), which is consistent with its paleontologically inferred Burdigalian-Tortonian age. The youngest zircons (of magmatic origin) in the overlying Yılmazköy Formation are 9 Ma (Tortonian), in agreement with its paleontologically inferred Tortonian age. The youngest zircon age (of magmatic origin) in the overlying Yazılıtepe Formation is 5.4 ± 1.0 Ma (Late Messinian) (Table S5). This contrasts with its Tortonian-Messinian age based on calcareous nannofossils, planktonic foraminifera and strontium isotopes. The overlying evaporites (Baroz, 1979; Necdet and Anıl, 2006; McCay et al., 2013) are assumed to have accumulated during the Messinian Salinity Crisis (ca. 5.96-5.33 Ma) (e.g., Roveri et al., 2014; Artiaga et al., 2021). Taking account of the 1.0 Ma total calculated error, the youngest zircon age could be as old as 6.4 Ma, consistent with the sample's position beneath (rather than within) the evaporites. The Upper Pliocene-Pleistocene Athalassa Formation has a youngest, magmatic zircon age of 9 Ma (Tortonian) (Table S5), pointing to an absence of contemporaneous, igneous or metamorphic detritus.

In summary, the main points from the above discussion of age relations are:

(1) There is a nearly-contemporaneous source of Triassic detritus in the Sikhari Formation sample (n=1);

(2) There is also a nearly-contemporaneous source of Upper Cretaceous detritus in the Kipasisso Vouno Member samples (n=5);

(3) There is an absence of Maastrichtian-Paleogene detritus in the samples from the Middle Eocene Kalograia-Ardana Formation and the Upper Eocene-Oligocene Bellapais Formation;

(4) Approximately coeval igneous sources existed for all of the samples from the overlying pre-Pliocene formations, except for the Upper Oligocene Klepini Formation. However, sandstones are rare in the Klepini Formation and the available detrital zircon age data could be unrepresentative or relate to local erosional effects or different depositional pathways.

(5) Upper Pliocene-Pleistocene igneous or metamorphic sources did not supply the sample analysed from the western Kyrenia Range.

6.2. Age variations along and across the range and through time

An understanding of the above detrital zircon variation can help with interpretation of provenance and depositional pathways, in relation to the potential source areas.

For the Upper Campanian-Maastrichtian Kiparisso Vouno Member (Fig. 11), the western range samples are relatively enriched in >1.5 Ga grains (22% and 11%, respectively), whereas the central range sample has relatively more (27%) Pan-African-aged grains (ca. 750-500 Ma). All of the samples contain abundant Permian zircons (up to 8%), whereas Carboniferous grains are instead present (up to 11%) in the central range.

There are no Carboniferous or Permian grains in the overlying Eocene Kalograia-Ardana Formation sample from the western range, whereas grains of this age range commonly occur in the eastern range sample (up to 8%). Cretaceous zircon grains (86-80 Ma) are additionally present in the eastern range samples (up to 12%). Rare Paleocene-Eocene (61-45 Ma; n=2) zircons also occur in the eastern range sample (Chen et al., 2019) (Fig. 11).

The Upper Eocene-Oligocene Kythrea Conglomerate sample from the western range contains abundant Precambrian grains (93%), compared to the samples from the central and eastern ranges (58% and 75%, respectively). For the central and eastern ranges, the zircon abundances are similar to the underlying Kiparisso Vouno Member and the Kalograia-Ardana Formation. Rare Eocene (47-39 Ma; n=2) zircon grains are only present in the eastern range sample (GC19-04) (Fig. 11).

The Upper Eocene-Oligocene Bellapais Formation samples from the western range and the Karpas Peninsula have abundant Carboniferous and/or Permian grains (up to 9%), compared to the sample from the eastern range (Fig. 11). Triassic and Upper Cretaceous grains are additionally present in the Karpas Peninsula sample (GC19-35), i.e., 8% and 14%, respectively.

The Upper Oligocene-Burdigalian Flamoudi Formation from the eastern range is characterised by a dominance of Precambrian zircons (93%), whereas the sample from the central range contains scattered Carboniferous to Triassic zircons, and also a Lower Miocene (19-15 Ma; 4%) age population.

For the Panagra Formation, Cretaceous grains occur rarely, only in the Karpas Peninsula sample, together with a Burdigalian age peak (20 Ma; 17%).

For the Trapeza Formation, the sample from the northern sub-basin (Fig. 4) in the central range includes minor Miocene grains (n=3), whereas the samples from the southern sub-basin in the eastern range and the Karpas Peninsula (Fig. 11) have a larger Miocene fraction.

For the Davlos Formation, the samples from the southern sub-basin in the western range and the northern sub-basin in the eastern range have similar aged populations, whereas the Karpas Peninsula sample has an additional Tortonian peak (13%).

The Mia Milia Formation samples, both from the southern sub-basin, are dominated by Precambrian grains (84%) in the western range, whereas there are prominent Upper Cretaceous and Tortonian grains, 46% and 10%, respectively, in the Karpas Peninsula (Fig. 11).

In summary, for units with more than one sample from different areas the main differences along and across the range are:

(1) The samples from the western and central ranges include more Precambrian grains (average 72% and 75%, respectively) than those from the eastern range and the Karpas Peninsula (average 54% and 48%, respectively). Of the total zircons analysed, the Neoproterozoic zircon fraction is consistently dominant, averaging, from west to east along the range: ca. 51%, 55%, 39% and 35%, respectively. The variation in Precambrian zircons is likely to represent differences in detrital input from the basement or cover of microcontinents located in southern Anatolia, generally to the north of Cyprus (see section 6.4 for discussion);

(2) Younger zircons, although generally present, only represent major age populations in the more easterly samples. For example, Upper Cretaceous and Miocene grains are more abundant in the eastern range (average 21% and 7%) and the Karpas Peninsula (22% and 9%) than the western range (8% and 1%) and the central range (6% and 1%). This probably relates to the occurrence of available

source rocks within Anatolia generally to the north and northeast of Cyprus (see section 6.4);

(3) Samples collected from the southern sub-basin (e.g., Trapeza Formation) include more Miocene zircons than those from the northern sub-basin. This is likely to represent differences in sediment supply via two distinct drainage systems (see section 6.4).

In addition to the above variation in zircon ages along the range, there are significant changes in zircon populations through time (Fig. 11):

(1) Precambrian zircons predominate all of the sandstones analysed, ranging from 15%-93%. The consistently relatively large Precambrian input indicates that source rocks of this age, or their erosional products, both located in southern Anatolia, continued to reach the Kyrenia Range from Triassic to Pleistocene time (see sections 6.3 and 6.4);

(2) Carboniferous to Permian zircons form significant age populations (up to 22%) in some samples during the Middle Triassic to Oligocene, but are relatively sparse after the Late Oligocene. This significant change is a key to evaluating the alternative tectonic hypotheses for the Kyrenia Range (see sections 6.4 and 6.5);

(3) Neogene (21-17 Ma) zircons become more abundant during the Early Miocene, representing magmatic or metamorphic detrital input from Anatolia during this time period (see section 6.3);

(4) Upper Cretaceous grains dominate the populations (up to 52%; Shaanan et al., 2021) during the Middle Miocene, whereas Miocene grains dominate those of Upper Miocene and younger formations (up to 55% for the Yazılıtepe Formation).

The differences in the Upper Cretaceous and Miocene zircon populations prompt a search for suitable paleo-river systems that could have supplied the Upper Miocene and Pleistocene sediments (see section 6.4).

6.3. Ages of potential zircon sources

6.3.1. Precambrian

The Precambrian zircon age spectra (>540 Ma) is strikingly like that of northeast Africa and Arabia (e.g., Chen et al., 2019; Shaanan et al., 2021). The Upper Ediacaran-Lower Cambrian (570-520 Ma) zircon grains can be correlated with the Andean-type Cadomian magmatism bordering the northern margin of Gondwana in the Eastern Mediterranean region (Ustaömer et al., 2009, 2012, 2016, 2020; Zlatkin et al., 2013; Abbo et al., 2015; Gürsu et al., 2017; see below). These zircons are unlikely to have been derived directly from Gondwana because the marine Levant basin existed to the southeast of the Kyrenia Range (Fig. 1), at least from the Late Triassic-Early Jurassic (Gardosh et al., 2010). Also, the deep-marine Herodotus Basin to the southwest of Cyprus (Fig. 1) possibly originated as early as the Carboniferous (e.g., Granot, 2016; Golan et al., 2018). Much more likely sources are from one, or several, microcontinents that are now located within Turkey to the north (see Ustaömer et al., 2009; Zlatkin et al., 2013; Abbo et al., 2015; Chen et al., 2019). Cadomian fragments began to rift by the Late Permian and then spread away from Gondwana towards Eurasia, beginning during the Late Triassic, thereby opening the Southern Neotethys (e.g., Şengör and Yılmaz, 1981; Robertson and Dixon, 1984; Garfunkel, 1998; Stampfli and Borel, 2002;

Göncüoğlu et al., 2004). Consistent with this interpretation, Gondwana-related zircons occur extensively in the Taurides to the north of the Kyrenia Range. Examples include the Neoproterozoic basement and Lower Paleozoic siliciclastic cover of the Menderes Massif, W Turkey (Zlatkin et al., 2013) and the Cadomian basement and Paleozoic to Triassic cover of the Karacahisar dome, central Turkey (Abbo et al., 2015) (Fig. 1). Detritus of north Gondwana origin (i.e., NE Africa/Arabian–Nubian Shield) (Chen et al., 2019) could have been recycled from Cadomian-aged primary lithologies into Paleozoic cover units throughout the Taurides. Both primary and secondary (recycled) material could later have been recycled, for example into the Triassic Sikhari Formation in the Kyrenia Range and the Mamonia Complex, SW Cyprus (Chen et al., 2019).

A few of the Proterozoic and Archean zircons (Th/U <0.1) are indicative of a metamorphic origin, especially in samples from the western transects (see Section 4). Suitable sources include the Neoproterozoic high-grade metamorphic basement in the eastern and central Taurides (Ustaömer et al., 2012; Abbo et al., 2015; Gürsu et al., 2017), the Precambrian high-grade metamorphic basement of Menderes Massif in western Anatolia (e.g., Okay, 2001; Özer et al., 2001; Candan et al., 2011) and/or the Precambrian basement of the Alanya Massif north of Cyprus (Fig. 1) (Çetinkaplan et al., 2016; Çetinkaplan, 2018; Robertson and Parlak, 2020). The relatively high U/Yb but low Nb/Hf ratios of the Upper Ediacaran-Lower Cambrian zircons (Fig. 9) are compatible with derivation from the Cadomian continental magmatic arc that is inferred from outcrops in southern Turkey (Gürsu and Göncüoğlu, 2005, 2008; Gürsu et al., 2015).

6.3.2. Paleozoic

Paleozoic zircons form minor, to subordinate age populations in all of the sandstones analysed, with major peaks in the Cambrian, Carboniferous and Permian. Compositionally appropriate Lower Cambrian crystalline basement rocks are represented by Cadomian active margin granitoids along the north-Gondwana margin (e.g., Bitlis Massif; Ustaömer et al., 2009). Related Cadomian 'back-arc' magmatism, of late-stage extensional or post-collisional origin, could also have supplied zircons (Gürsu and Göncüoğlu, 2005, 2008; Gürsu et al., 2015; Beyarslan et al., 2016).

Ordovician to Devonian zircons are relatively rare, with Th/U ratios >0.1 and zonal structures, signifying an igneous origin (Rubatto, 2002). A dominantly continental arc origin of the zircons analysed is inferred, based on their relatively high U/Yb, Th/Nb but low Nb/Hf ratios (see Figure S6). Volcanism of this age range, albeit volumetrically minor, is known in several areas of the Taurides, including the Orhaneli area, NW Turkey (Okay, 2002; Okay et al., 2008a, b; Özbey et al. 2013), the Antalya area, SW Turkey and the Feke area, central E Turkey (Göncüoğlu and Kozlu, 2000; Robertson et al., 2021a) (Fig. 1). However, these volcanics are mainly basaltic and unlikely to have supplied many zircons (e.g., Watson and Harrison, 1983; Keller et al., 2017).

Carboniferous and Permian zircon populations are well represented in the Middle Triassic to Oligocene of the Kyrenia Range (Fig. 11). Zircon trace element compositions are suggestive of mixed continental arc and within-plate (e.g., rift-related) settings (see Section 4.13). Potential sources are exposed in both the Taurides and the Anatolides. Carboniferous granites locally intrude older lithologies in the Afyon zone of the Anatolides, central W Turkey (Candan et al., 2016; Ustaömer et al., 2020), although these appear to be volumetrically minor. Basaltic-intermediate composition volcanics and volcaniclastic sediments are widely distributed across Tauride-related units in central and eastern Anatolia, extending at least from the Sultan Dağı in the western central Anatolia to the Malatya Massif in central eastern Anatolia (Göncüoğlu et al., 2007; Robertson et al., 2021a) (Fig. 1). Carboniferous magmatism affected the north margin of Gondwana following the opening of Paleotethys during Late Silurian-Devonian time (Stampfli and Borel, 2002; Cocks and Torsvik, 2006; Özbey et al., 2013; Robertson et al., 2021a).

Alternative explanations of the Carboniferous magmatism involve either rifting of the north-Gondwana continental margin or southward subduction of Paleotethys (see Robertson et al., 2021a). Carboniferous magmatic rocks also occur in the Konya Complex of the Anatolides (Afyon zone) (Fig. 1), although being volumetrically minor and mainly basaltic these are unlikely to have provided many zircons. In addition, voluminous sandstone turbidites within the Konya Complex include abundant Precambrian, Carboniferous, and locally also, Devonian zircons (Löwen et al., 2020; Ustaömer et al., 2020). The Carboniferous zircons are interpreted by Löwen et al. (2020) to have been derived from the Sakarya zone of the NW Pontides (Fig. 1). However, Lu-Hf isotopic ratios of the Carboniferous detrital zircons are dissimilar to those of the zircons of similar age in the NW

Pontides (Fig. 12), and alternative sources have been suggested farther west; i.e., within the north-Aegean region or beyond (Ustaömer et al., 2020).

Small volumes of Permian alkaline volcanic rocks are known in the Taurides, specifically within the Antalya Complex in the Güzelsu area (N of Cyprus) (Şahin et al., 2012) and within the Mersin Melange further east (Tekin et al., 2019) (Fig. 1). Also, Permian detrital grains occur in some Triassic Tauride sandstones, although their source is unclear (Ustaömer et al., 2020). The Permian volcanism is attributed to rifting of Neotethys (Tekin et al., 2019; Ustaömer et al., 2020; Robertson et al., 2021b), which is compatible with the relatively high Nb/Hf ratios of the detrital zircons (see Section 4.13).

6.3.3. Mesozoic

The Kyrenia Range Triassic zircons show a range of continental margin arc to intra-plate settings (see Section 4.13), consistent with a mixed derivation. Triassic zircons, generally n<4, were potentially derived from the widespread Triassic volcanics of the Tauride allochthons, including the Lycian nappes to the NW (Collins and Robertson, 1998; Sayit et al., 2015), the Antalya Complex directly to the NW (Robertson and Waldron, 1990; Maury et al., 2008; Robertson and Parlak, 2020; Robertson et al., 2020), the Beyşehir-Hoyran-Hadim (Bözkır) nappes to the north (Özgül, 1997; Andrew and Robertson, 2002), the Mersin Melange directly to the north (Parlak and Robertson, 2004; Sayit et al., 2017, 2020), the Andırın region to the NE (Uzuncimen et al., 2011; Robertson et al., 2016) and the Baer-Bassit region (N Syria) to the east (Al-Riyami and Robertson, 2002) (Fig. 1). The Triassic magmatic rocks of the Antalya, Andırın and Baer-Bassit units relate to rifting of the Southern Neotethys (e.g., Robertson et al., 2012a). In contrast, the Triassic magmatic rocks within the Lycian nappes, the Beyşehir-Hoyran-Hadim nappes and probably also the Mersin Melange relate to rifting of the İzmir-Ankara-Erzincan ocean (Northern Neotethys) farther north (Özgül, 1984a; Andrew and Robertson, 2002; Göncüoğlu et al., 2003; Parlak and Robertson, 2004). These allochthonous units were emplaced generally southwards over the Mesozoic Tauride carbonate platform during latest Cretaceous and Eocene (Özgül, 1997; Mackintosh and Robertson, 2009). Triassic meta-volcanic rocks (subduction-influenced) occur further north, within the Afyon zone of the Anatolides (Akal et al., 2012). As a whole, the Triassic volcanics are basaltic and so are unlikely to have supplied many zircons.

Jurassic zircons are rarely present in the Upper Cretaceous Kiparisso Vouno Member, the Middle Eocene Kalograia-Ardana Formation, the Upper Eocene-Oligocene Bellapais Formation and the Miocene Trapeza, Davlos and Yılmazköy formations (Fig. 11). The rare zircons analysed (n=3) with low Nb/Hf but high U/Yb ratios are consistent with a continental arc origin (Fig. 9). Jurassic igneous rocks are virtually absent from the Mesozoic carbonate platform units of the Taurides and Anatolides. Jurassic seamount-type volcanics do, however, characterise the Northern Neotethyan suture zone (İzmir-Ankara-Erzincan suture zone) (e.g., Rojay et al., 2004; Bortolotti et al., 2018). Middle-Upper Jurassic ophiolites and rare associated granitoid arc intrusives of the Ankara-Erzincan suture zone further east are potentially a source of Jurassic zircons (Dilek and Thy, 2006; Rolland et al., 2011; Çelik et al., 2013; Sarıfakıoğlu et al., 2017). In Eastern Anatolia, basaltic rocks are interbedded with Lower to Middle Jurassic deep-marine radiolarites that were emplaced southwards onto Tauride platform units during the Late Cretaceous (Robertson et al., 2016, 2021b); these basaltic rocks could also have provided a southward supply of zircon.

Elsewhere, alkaline/per-alkaline volcanics are interbedded with Middle Jurassic-Lower Cretaceous radiolarites in Baer-Bassit, N Syria (Al-Riyami and Robertson, 2002; Al-Riyami et al., 2002) (Fig. 1). Tiny intrusive bodies of this age range are also present in the Mamonia Complex, SW Cyprus (Fig. 1) (Chan et al., 2008). In addition, either plume-related (Garfunkel, 1998), or rift-related (Gardosh et al., 2010), Lower Jurassic volcanics occur in the northern margin of the Levant platform. Jurassic volcanics are also well represented in the Pontides, northern Turkey (Altıner et al., 1991; Genç and Tüysüz, 2010; Ustaömer et al., 2013; Okay et al., 2015; Akdoğan et al., 2018) (Fig. 1). Dismembered Jurassic ophiolites within the Intra-Pontide suture zone include basaltic extrusive and intrusive rocks (e.g., Marroni et al., 2020).

The only Lower Cretaceous zircon analysed, which is characterised by an enrichment of Y (2288 ppm) and a relatively low U/Yb ratio (0.012), could have an oceanic crust origin (see Table S2). Lower Cretaceous volcanism is documented, both within the Inner Tauride suture zone (Robertson et al., 2016) and the Northern Neotethyan suture zone (farther north), based on paleontological dating of interbedded deep-sea sediments (e.g., Rojay et al., 2004). However, these magmatic rocks are unlikely to have contributed many zircons as they are again mainly basaltic.

Upper Cretaceous detrital zircon grains dominate the Mesozoic populations of the Kyrenia Range (see section 6.2). Of these, a few Upper Cretaceous (83-69 Ma) grains from the Yılmazköy Formation, with Th/U ratios (<0.1) (see Supplementary Figure S5), are of metamorphic origin. Metamorphic zircons form under a wide range of greenschist, to amphibolite, to blueschist-facies conditions (e.g., Rubatto, 2002; Dempster et al., 2004; Hay and Dempster, 2009). Cretaceous greenschist to blueschist facies metamorphic rocks generally to the north of the Kyrenia Range that might have supplied zircons include the Alanya Massif of S Turkey (Campanian; 84-75 Ma) (Çetinkaplan et al., 2016), the Upper Paleozoic to Upper Cretaceous Malatya Metamorphics of E Turkey (Perinçek and Kozlu, 1984; Robertson et al., 2006, 2021b), the Afyon zone (Maastrichtian, 97-62 Ma) (Pourteau et al., 2010, 2016) and the Tavşanlı zone (Turonian-Selandian; 92-60 Ma) (Okay et al., 1998, 2020; Sherlock et al., 1999) (Fig. 1).

In addition, the few Upper Cretaceous grains (89-66 Ma) analysed from the Yılmazköy Formation, with Th/U >1.5 (Supplementary Figure S5), are inferred to be of mafic origin. Source candidates include numerous Cretaceous basaltic units, mainly associated with ophiolites and volcanic arc units throughout SE Anatolia (e.g., Schleiffarth et al., 2018), specifically, Upper Cretaceous ophiolites (92-84 Ma) and arc-related granitoids (ca. 88-70 Ma) (Parlak, 2006; Karaoğlan et al., 2012, 2013, 2016; Nurlu et al., 2016). The highly variable U/Yb and Nb/Yb zircon ratios suggest a mixed derivation from both continental arc and ophiolite-related source (see Section 4.13). In contrast, the Troodos ophiolite to the south is an unlikely source of Upper Cretaceous ophiolitic detritus as it remained covered by Upper Cretaceous to Upper Pliocene marine sediments, as exposed along the southern margin of the Mesaoria Basin and in deep wells to the south of the Kyrenia Range (Fig. 4) (e.g., Robertson and Hudson, 1974; Lord et al., 2000; Harrison et al., 2004; Morag et al., 2016). Uplift and deep erosion of the Troodos Massif did not take place until the Pleistocene (e.g., Poole and Robertson, 1991; Kinnaird and Robertson, 2013; Ring and Pantazides, 2019) and, therefore, a supply of detritus from the Troodos ophiolite or its sedimentary cover to the Kyrenia Range is unlikely. As a caveat, it should be noted however that the composition of any crust beneath the Kyrenia Range remains unknown.

6.3.4. Cenozoic

A minor Eocene zircon population in the Kyrenia Range peaks at ca. 53-47 Ma (Fig. 11). Continental arc-type trace element compositions dominated the zircons analysed, together with a minor within-plate-type fraction (see Section 4.13). Eocene volcanic rocks and small related intrusives are present in the Maden Complex (Fig. 1), as widely exposed across Eastern Anatolia (Aktaş and Robertson, 1984, 1990, Elmas and Yılmaz, 2003; Erturk et al., 2018). These rocks are mainly basaltic-andesitic and therefore may not be an important zircon source. Localised, Lower-Mid Eocene magmatisic rocks of alkaline, within-plate type (both extrusives and intrusives), occur farther north, e.g., in the Hekimhan Basin of central E Turkey (Fig. 1) (Booth et al., 2014). Other possible sources include calc-alkaline magmatic rocks, mainly granitoids (e.g., Doğanşehir area; Fig. 1), in SE

Turkey (Karaoğlan et al., 2013; Parlak et al., 2013). Zircons are abundant in these rocks, although the Eocene granitoids are much less extensive than the Upper Cretaceous granitoids in the same region (see above).

A few Oligocene grains are present in the Middle-Upper Miocene Trapeza and Yılmazköy formations of the eastern and central Kyrenia Range (Table S1). Post-collisional Oligocene volcanism is well documented in W Turkey (Yılmaz, 1989; Altunkaynak and Genç, 2008; Ersoy et al., 2012) but is rare in central and E Turkey (Oyan, 2018), closer to the Kyrenia Range.

Miocene zircons, peaking at ca. 20 Ma, 16 Ma and 9 Ma, constitute up to 17% of the grains analysed in the Middle to Upper Miocene sediments (Table S1) (see section 6.2). Available zircon trace element compositions are suggestive of mixed continental arc and within-plate settings (see Section 4.13). Possible sources include the Neogene, post-collisional volcanic rocks in the southern Kırşehir Block (Fig. 1), central Anatolia (e.g., Innocenti et al., 1975). Volcanic rocks in this region range from Early Miocene (21 Ma) to Quaternary (Innocenti et al., 1975; Platzman et al., 1998; Asan and Kurt, 2011; Schleiffarth et al., 2018). Generally younger (ca. 13 Ma-Holocene) post-collisional magmatic rocks occur farther east, within the Eastern Anatolia Volcanic Province of E Turkey, Armenia and NE Iran (Innocenti et al., 1975; Pearce et al., 1990; Keskin et al., 1998), although this is >900 km northeast of Cyprus. Felsic ignimbrites of the İzmir-Afyon-Isparta volcanic zone in the Western Anatolian Volcanic Province also have similar radiometric ages; i.e., ca. 21-10 Ma (Aquitanian-Tortonian) (e.g., Bingöl, 1977; Aydar, 1998; Dilek and Altunkaynak, 2010). Lower to Middle Miocene (ca. 19-15 Ma) basaltic magmatic rocks are widespread in central and eastern Anatolia (e.g., Sivas-Elazığ-Malatya regions; Fig. 1) (e.g., Arger et al., 2000; Önal et al., 2008; Gürsoy et al., 2011), mainly as basanites to basaltic andesites, with subordinate rhyolite, rhyolitic dykes, trachyandesite and basaltic-trachyandesitic dykes (e.g., Arger et al., 2000; Önal et al., 2008). Much closer sources are mainly restricted to basaltic and andesitic rocks in the Türkoğlu-Pazarcık area of the Kahramanmaraş region (Fig. 1), which are dated as 18.6-16.5 Ma (Burdigalian) by the K-Ar method (Arger et al., 2000). Lower Miocene basaltic extrusive rocks and minor associated dykes occur extensively in the central and northern Amanos Mountain area (Fig. 1), to the northeast of Cyprus (Duman et al., 2017). In addition, zircons could have been locally reworked from tuffaceous intercalations in the underlying Panagra Formation, which have a U-Pb age of ca. 16.6 Ma (Burdigalian) (Chen and Robertson, 2021a).

Messinian (6-5 Ma) zircon grains are very abundant (55%) in the Yazılıtepe Formation (Table S5). A relatively proximal source could be airfall tuffs and silicic extrusives, which are dated as 5.8 Ma by the Ar-Ar method in the Erciyes Basin, central Turkey (Fig. 1) (Jaffey et al., 2004). Messinian rhyolites and airfall tuffs are present in the Kırşehir Block, central Anatolia (Aydar et al., 2012). 6.2-5.2 Ma-aged lavas occur in coastal areas of western Syria (Banias-Mt Saphita; Fig. 1) (Sharkov et al., 1994, 1998; Trifonov et al., 2011). In addition, Messinian ash layers (5.53 Ma) are reported from the central-northern Mediterranean Basin (Cosentino et al., 2013).

6.3.5. Major zircon sources

Bearing in mind that felsic rocks, especially intrusives, are the most likely to have supplied zircons (Watson and Harrison, 1983; Keller et al., 2017), the following units seem most likely to have contributed large number of zircons to the Kyrenia Range:

(1) The Precambrian grains were likely recycled from the rifted Cadomian microcontinental blocks and, or their Paleozoic sedimentary cover in southern Turkey. The sources were therefore generally to the north rather than from the Arabian-Nubian Shield directly;

(2) The Upper Ediacaran-Lower Cambrian grains relate to erosion of Cadomian active margin granitoids (e.g., Bitlis Massif, SE Turkey) that were intruded along the north-Gondwana margin. After Triassic rifting, these Caromian zircons were derived generally from the north, in Turkey, possibly following significant recycling;

(3) Devonian-Carboniferous zircons are likely to have been derived from Devonian-earliest Permian sandstone turbidites of the Konya Complex (or equivalents), as located along the northern margin of the Anatolide-Tauride Block (Afyon zone) in central Anatolia. Another, local source could be from the upper Carboniferous granitoids in the same area, although, as currently known, these are volumetrically minor and may not have been exhumed by late Carboniferous time. Direct derivation from the Upper Paleozoic, S Eurasian active continental margin is unlikely because in many interpretations Paleotethys intervened (see discussion in section 6.6);

(4) Upper Cretaceous zircons were derived from coeval arc-related granitoids,

as widely exposed in SE Turkey;

(5) Eocene zircons came from the arc/back-arc magmatic rocks of the Maden Complex in SE Turkey;

(6) Neogene zircons were derived from evolved, post-collisional volcanic products in SE Turkey.

6.4. Sediment pathways

The interpretation of zircon provenance and deposition needs to take account of available sedimentological evidence, especially paleocurrent data from the Eocene-Miocene clastic sediments. Northern Cyprus was characterised by southerly paleocurrents during the Late Eocene-Early Oligocene (Fig. 2), as indicated by variably developed clast imbrication within the Kythrea Conglomerate (McCay and Robertson, 2012) (see Supplementary Figure S2). As summarized above, the combined zircon data indicate that suitable-aged source lithologies exist generally to the north of Cyprus, including within the Precambrian basement of the Alanya Massif (Çetinkaplan et al., 2016; Çetinkaplan, 2018), the Antalya Complex (e.g., Güzelsu area) (Monod, 1977; Robertson et al., 2020), the Mersin Melange (Parlak and Robertson, 2004; Sayit et al., 2017, 2020) and the Beyşehir-Hoyran-Hadim (Bözkır) nappes that were emplaced southwards over the Mesozoic Tauride carbonate platform finally during the Eocene (Özgül, 1997; Andrew and Robertson, 2002; Mackintosh and Robertson, 2012) (Fig. 1). The clast composition (including ophiolitic rocks) and the paleocurrent data suggest that the non-marine Kythrea Conglomerate was supplied generally from the north; i.e., from southern

Turkey or from the now-submerged crust beneath the Cilicia Basin, rather than locally from the Kyrenia Range. A further implication is that the deep-water Cilicia basin post-dates the Kythrea Conglomerate (Robertson and Woodcock, 1986; McCay and Robertson, 2012).

Our new results also indicate that Precambrian grains have more significant age populations in the western and central ranges compared to the eastern range and the Karpas Peninsula (Table S5; see section 6.2). A possible explanation is that the Precambrian grains were preferentially derived from the basement of the Alanya Massif generally to the northwest of Cyprus (Fig. 1), whereas Precambrian basement is absent to the north of the eastern range and the Karpas Peninsula (MTA, 2011). Consistent with their outcrop distribution, the Alanya Massif and the equivalent Bitlis and Pütürge massifs (Fig. 1) of SE Turkey have been interpreted as separate Mesozoic microcontinental blocks rather than as a continuous crustal unit (e.g., Şengör and Yılmaz, 1981; Robertson and Dixon, 1984; Robertson et al., 2012a).

The Upper Cretaceous Kiparisso Vouno Member and the Middle Eocene Kalograia-Ardana Formation include significant populations of Carboniferous-Permian detrital zircons (see section 6.2) for which there is no obvious source in Cyprus or the adjacent E Mediterranean region (Chen et al., 2019; Glazer et al., 2021). One possible explanation, mentioned above (section 6.3), is that the Carboniferous-Permian zircons were ultimately derived from the Paleotethyan suture zone to the west of Turkey, where Paleotethys sutured prior to Early Permian in some interpretations (e.g., Zanchi et al., 2003; Robertson and

Ustaömer, 2009b; Okay and Topuz, 2017; Robertson, 2022).

Whatever their magmatic source(s), Carboniferous zircons accumulated along the northern margin of Gondwana (Anatolides) during the late Carboniferous-earliest Permian, within the Konya Complex and its Mesozoic cover (Halıcı and Ardıçlı formations), or equivalent units (e.g., Löwen et al., 2020). Once deposited there, southward recycling became possible, independently of their original source. Carboniferous-Permian zircons also occur within Middle-Upper Triassic sandstones of the Taurides, including the Anamas-Akseki platform (Kasımlar Formation) (Ustaömer et al., 2020) and the Karaburun Peninsula of Aegean Turkey (Güvercinlik Formation) (Löwen et al., 2017; Ustaömer et al., 2020) (Fig. 1). The Carboniferous zircons from the Tauride and the Karaburun Peninsula samples, with characteristic εHf(t) values <-5, are compatible with a source within Carboniferous arc-type granites of the Anatolides (Ustaömer et al., 2020), although other sources are possible. The Carboniferous Kyrenia Range zircons have a continental arc affinity (see Section 4.13), together with a likely felsic/intermediate-related magmatic origin (i.e., Th/U=0.22-0.85; median 0.47), also mainly negative εHf(t) ranging from -8 to -3 (see section 4.14), which together suggest granitic/andesitic source(s), either from Eurasia or from the Anatolides (although known outcrops there are small).

Relatively common (3-7%) Carboniferous zircons, together with a few Permian zircons, occur farther south, within the Middle-Upper Triassic sandstones of the Antalya Complex (Güzelsu area) and reach ca. 18% in some Cretaceous sandstones in the same area (Chen et al., 2022). Black chert grains are present in

Middle-Upper Triassic sandstone turbidites in many areas (Gutnic et al., 1979), including the NE Antalya Complex (Waldron, 1984), the SW Antalya Complex (Robertson and Woodcock, 1984) and the E Antalya Complex (Alanya window) (Robertson et al., 2020). In the absence of any stratigraphically underlying (older) source of black chert (mid-Triassic cherts are reddish coloured), the black chert is likely to have been derived from Paleotethys to the north. In support, paleocurrents, measured in mainly Upper Triassic successions (Çayır Formation) exposed in both the regional autochthon (Geyik Dağı) and the over-riding thrust sheets (Bolkar and Hadim nappes) (Fig. 1) are southerly directed (Mackintosh and Robertson, 2009).

Upper Paleozoic detrital zircons are unlikely to have been transported far southwards during the Jurassic-Eocene because developing carbonate platforms, notably the Bey Dağları, Geyik Dağı and Akseki-Anamas platforms (e.g., Özgül, 1997) (Fig. 1) are likely to have blocked this transport route. Northerly sources were potentially re-established during the Eocene following the southward over-thrusting of the Tauride thrust sheets (Beyşehir-Hoyran-Hadim nappes) that include Triassic sandstones (e.g., Hadim and Bolkar nappes) (Özgül, 1997; Mackintosh and Robertson, 2013; McPhee et al., 2018). Any additional clastic sediment supply from northwest of the Bey Dağları carbonate platform (Fig. 1) was delayed until the Miocene (Hayward and Robertson, 1982).

Of the Kyrenia Range zircons analysed, Devonian grains are relatively rare (generally <4), similar to the abundance in the Middle-Upper Triassic sandstones of the Tauride Anamas-Akseki platform (Kasımlar Formation) (Ustaömer et al., 2020). In contrast, the upper Carboniferous and Triassic sandstones of the

Karaburun Peninsula contain abundant Devonian zircons that, however, occur only locally in the Konya Complex (Löwen et al., 2017, 2020). The paucity of Devonian zircons in the Tauride Triassic and in the Kyrenia Range sandstones is at odds with the Kyrenia Range being located along the Eurasian continental margin during the Late Paleozoic-Paleocene (see section 6.6).

In summary, we infer that the Upper Paleozoic detrital zircons of the Kyrenia Range were mainly derived from Paleotethyan active margin magmatic rocks, with the ultimate source being located in the N Aegean region or farther west. Zircons of this age range were eroded and deposited in upper Carboniferous-earliest Permian sandstone turbidites along the northern margin of Gondwana (Afyon zone, Anatolides). After Triassic uplift and erosion in the north Upper Paleozoic zircons were transported southwards within non-marine, shallow-marine and deep-marine siliciclastic sediments, mainly during Mid-Late Triassic time. After having reached a southerly position bordering the Southern Neotethys, Carboniferous-Permian zircon-bearing facies were strongly deformed during the Late Cretaceous (Campanian-Maastrichtian) and again during the Late Paleocene-Middle Eocene related to Neotethyan closure. The zircons were then supplied to the relict S Neotethys (Eastern Mediterranean Sea), including the future Kyrenia Range.

The Oligocene was characterised by a fundamental shift from southward to westward deep-water gravity flows persisted at least until the Messinian (Fig. 2). This switch is inferred from abundant paleocurrent data (e.g., flutes, grooves) in sandstone turbidites from both the northern and the southern flanks of the Kyrenia Range (Weiler, 1970; McCay and Robertson, 2012) (see Supplementary Figures

S2-S3). Lithologies of the appropriate ages to supply zircons to the Kyrenia Range are present throughout the Misis-Andırın-Engizek suture zone (Kelling et al., 1987; Robertson et al., 2004, 2006) and its eastward extension, the Bitlis suture zone in SE Turkey (Fig. 1). The suturing resulted from Eocene-Lower Miocene closure of the Southern Neotethys (e.g., Perinçek and Kozlu, 1984; Aktaş and Robertson, 1984; Yılmaz, 1993; Robertson et al., 2004; Darin et al., 2018).

The Upper Eocene-Oligocene Bellapais Formation was sourced locally, mainly from the north (Fig. 2), until subsidence of the Cilicia Basin (Fig. 1) between the Kyrenia Range and Turkey ended this southerly sediment supply, including the Upper Paleozoic zircons.

Conversely, zircons of Late Cretaceous, Eocene and Miocene ages became more abundant in progressively younger sediments (see section 6.2). The prevailing westward paleocurrents (Fig. 2) point to sources in SE Turkey, as noted above. In eastern Anatolia, metamorphic and volcanic arc rocks were partially exhumed by the latest Cretaceous based on stratigraphic evidence (Perinçek and Kozlu, 1984; Robertson et al., 2016, 2021b). There is also evidence of thrusting, uplift and erosion during the Eocene (e.g., Hekimhan area). Southward thrusting during the Early-Middle Miocene (related to collision) and then again during the Late Miocene (related to suture tightening), resulted in uplift and erosion (Okay et al., 2010; Karaoğlan et al., 2016; Cavazza et al., 2018). The uplift accelerated erosion into deeper levels of the thrust stack, resulting in longer and deeper fluvial incision into Upper Cretaceous and Eocene lithologies (e.g., granitoids), coupled with supply from post-collisional Miocene magmatic rocks, for example, in the

Sivas-Elazığ-Malatya-Kahramanmaraş region (Fig. 1) (e.g., Arger et al., 2000; Önal et al., 2008; Gürsoy et al., 2011).

The northeasternmost corner of the Arabian platform was uplifted, related to continental collision during the Oligocene-Miocene (Boulton, 2009; Duman et al., 2017), potentially providing an additional source of Precambrian to Miocene zircons. However, the Precambrian outcrop area is minimal, suggesting that the Amanos Mountains were not a significant source. The Upper Cretaceous ophiolites in this area (e.g., Hatay ophiolite) are unlikely to have supplied many zircons as these are basic-ultrabasic igneous rocks with very few zircons.

Detrital zircon sources from within the uplifted Arabian continent to the east or southeast of Cyprus are questionable because of the development of several intervening topographic lineaments (e.g., the Tartus and Amanos-Larnaca ridges) (Fig. 1) that are likely to have blocked northwestward turbidity current flow (Ben-Avraham et al., 1995; Robertson, 1998; Calon et al., 2005a; Hardenberg and Robertson, 2007). Sediments from the onshore Arabian plate areas are likely to have accumulated mainly within the Outer Latakia Basin, the Cyprus Basin and the deeper Levant Basin to the SW (Fig. 1).

Given the dominantly westward paleocurrents, the most likely controls of zircon provenance during the Miocene-Pleistocene are: (1) uplift of SE Anatolia beginning during Middle-Late Miocene (Jaffey and Robertson, 2005; Okay et al., 2010; Meijers et al., 2020); (2) development of the Seyhan, Ceyhan and other regional river catchments as major sediment suppliers to the NE Mediterranean basin (e.g., Robertson et al., 2019); and (3) development of ca. SW-NE trending topographic ridges (e.g., Kyrenia-Misis, Tartus and Amanos-Larnaca ridges) (see above; Fig. 1) that channelled turbidite distribution towards Cyprus from specific fluvial inputs.

A recent reconstruction during the Messinian sea-level drawdown (Aksu et al., 2021) suggests that the Seyhan and Göksu paleorivers could have contributed much sediment to the Cilicia Basin and the future Kyrenia Range, whereas the paleo-Ceyhan and Orontes (Asi) river systems carried sediment to the Latakia and Mesaoria basins (Fig. 1) (e.g., Calon et al., 2005a) farther southwest. A clue to the Miocene sediment provenance is provided by the contrasting zircon age profiles of the southern versus northern sub-basins of the Kyrenia Range (see section 6.2). For the Upper Miocene and Pleistocene sandstones, especially the Middle-Upper Miocene Trapeza Formation, the southern sub-basin samples are characterised by a relatively high Cretaceous-Miocene zircon contribution. On the other hand, the samples from the northerly sub-basin have relatively small Miocene fractions (see section 6.2). Preliminary zircon geochronological data from Oligocene-Miocene turbidites in the adjacent Miocene Adana Basin indicate similarities with the Kyrenia Range northern sub-basin; e.g., relatively sparse Miocene detritus (Chen et al., 2021). The Adana Basin is transected by the Seyhan River (Fig. 1), which may have contributed zircons to both of these areas during the Late Miocene. Conversely, the Misis Basin farther southeast (Fig. 1) shows similarities with the Kyrenia Range southern sub-basin; e.g., relatively abundant (and constant) Upper Cretaceous to Miocene detrital input (Chen et al., 2021). The Ceyhan River runs through the Misis Basin (Fig. 1) and could have contributed zircons to both the

Misis Basin and the Kyrenia Range southern sub-basin.

Clastic sediment supply to the easternmost Mediterranean Sea was strongly influenced by the surface uplift of central and southeast Anatolia. Paleogeographic reconstruction based on leaf, pollen and phytolith data suggests that highlands existed by the Middle to Late Miocene, for example in the central east region (Sivas-Adana) of SE Anatolia (e.g., Huang et al., 2019; Meijers et al., 2020). The uplift triggered a switch from inward-drainage basins to incision and outflow to the eastmost Mediterranean Sea, for example along the srike-slip controlled Ecemiş corridor (Fig. 1) (Jaffey and Robertson, 2005). Major drainage catchments became established (e.g., Seyhan and Göksu paleorivers) and were entrenched during the Messinian low-stand (Aksu et al., 2021). Further uplift focussed on the Taurus Mountains took place during the Late Miocene-Pleistocene steepening the southern margin of the Anatolian plateau (e.g., Cosentino et al., 2012; Schildgen et al., 2012; Meijers et al., 2020; Racano et al., 2020) and exposing deeper structural levels to erosion (Chen et al., 2021). Climate and climate change also affected erosion and fluvial run-off to the ocean (e.g., Harris and Mix, 2002; Molnar, 2004) although more research is needed before the effects of tectonism versus ‘climate’ can be distinguished in the study region.

In addition, 6-5 Ma grains commonly occur in the eastern range samples, which contrasts with an absence of Messinian grains in the western range samples (see section 6.2). The Upper Miocene succession shows a gradual decrease in sandstone turbidites (still with westerly paleo-flow), whereas mudrocks become much more abundant, followed by Messinian gypsum. Likely zircon sources include airfall tuffs and ignimbrites of central Turkey (Akin et al., 2021). The absence of airfall zircon grains in the western range samples might represent localised fallout or sediment reworking by currents or gravity flows.

The Kyrenia Range itself is not likely to have provided many zircons. Only minor Triassic siliciclastic rocks are present, overlain by the Mesozoic platform carbonates (mainly marble and dolomite). The Maastrichtian-Middle Eocene felsic and basic igneous rocks of the Kyrenia Range also contain few zircons (Chen and Robertson, 2021b) and thus were not a significant zircon source. The structural and stratigraphical break between the Middle Eocene Kalograia-Ardana Formation and the transgressive Upper Eocene-Oligocene (Kythrea Conglomerate) was short-lived (several Ma), without evidence of deep erosion that could have supplied much siliciclastic sediment. In addition, the geochemistry of igneous blocks and clasts in both the Middle Eocene Kalograia-Ardana Formation and the Upper Eocene-Oligocene Bellapais Formation suggests an ophiolitic source, including boninites that are not present in the Kyrenia Range (Eyüboğlu et al., 2010; Robertson et al., 2014). As noted above (see section 6.3), the Troodos Massif to the south is unlikely to have contributed detritus to the Kyrenia Range because it retained its sedimentary cover until the Pleistocene.

6.5. Differentiation of crustal type using Lu-Hf isotope data

Crustal sources can be specified more clearly when the Lu-Hf isotope data are taken into account. The dominant strongly negative $\varepsilon Hf_{(t)}$ values of Paleoproterozoic and Archean detrital zircons from the Kyrenia Range consistently suggest a recycled crustal origin. The Mesoproterozoic is characterised by igneous quiescence in the inferred ultimate provenance area (North Africa/Levant). Igneous activity resumed towards the end of Stenian time related to the Tonian-Stenian orogeny, consistent with the occurrence of occasional Stenian-aged detrital zircons (1193-1031 Ma). In contrast, Neoproterozoic detrital zircons are characterised by a wide spread of $\varepsilon Hf_{(t)}$ ratios; half of these (52%) show negative $\varepsilon Hf_{(t)}$ values, which suggests the involvement of ancient crust. The remainder of the zircon grains are juvenile, with positive $\varepsilon Hf_{(t)}$ (+0.1, +14.6), consistent with juvenile sources like the Arabian-Nubian Shield (e.g., Ustaömer et al., 2016, 2020).

The Cambrian detrital zircons mainly exhibit negative $\varepsilon Hf_{(t)}$, which suggests the involvement of ancient crust. The Ordovician and Devonian detrital zircons with negative $\varepsilon Hf_{(t)}$ values suggest recycled crust formation, together with probable reworking of juvenile Tonian-Stenian (arc) crust (0.8-1.2 Ga).

Zircon grains of Carboniferous, Permian and Triassic ages suggest a dominant involvement of melts related to Mesoproterozoic crust, as well as some grains derived from young juvenile Ediacaran-Tonian crust. However, specific sources are difficult to identify because the isotopic data for the Carboniferous zircons overlaps for the Taurides (Aladağ)-Anatolides (e.g., Afyon zone) and the Pontides (Sakarya zone) (Fig. 12) (Ustaömer et al., 2020).

The Upper Cretaceous (96-91 Ma) zircons with dominantly super-chondritic $\varepsilon Hf_{(t)}$ (+11.4, +18.7) indicate juvenile magmatic additions, compatible with the radiometrically dated ophiolites (e.g., Parlak et al., 2013). Subordinate contemporaneous (Upper Cretaceous) zircons with negative $\varepsilon Hf_{(t)}$ values (-22.9 to

-14.6) mainly occur in the Kalograia-Ardana Formation (e.g., Glazer et al., 2021). The analysed samples from the Kalograia-Ardana Formation are rich in detrital serpentinite of ultramafic ophiolitic origin (Fig. 5b). In contrast, the Upper Cretaceous (90-66 Ma) detrital zircons, with vertically arrays of $\varepsilon Hf_{(t)}$ values, point to mixture of juvenile and reworked materials. Upper Cretaceous ophiolites, other related basaltic rocks (e.g., accretionary melange) and younger volcanic arc units are possible sources (see section 6.3), all with positive $\varepsilon Hf_{(t)}$ values (Bingöl et al., 2018; Xin et al., 2021) and highly variable U/Yb and Nb/Yb ratios (see section 4.13). The strongly negative $\varepsilon Hf_{(t)}$ values could be explained in several different ways: (1) the involvement of subducted sediments during late-stage ophiolite formation (Bingöl et al., 2018); (2) the involvement of sub-continental mantle lithosphere related to an intra-continental rift or narrow ocean (Arenas et al., 2014; Tsikouras et al., 2021); or (3) the influence of ancient recycled oceanic crust (e.g., Gregory and Taylor, 1981; Eiler, 2001).

Paleocene-Lower Miocene zircons have increasing $\varepsilon Hf_{(t)}$ values, involving juvenile materials (e.g., remnant Neotethys) and recycled crustal additions. A possible decreasing $\varepsilon Hf_{(t)}$ trend during ca. 40-20 Ma could indicate a contribution related to crustal assimilation in the source magmatic system. A small number of the 21-16 Ma grains from the Panagra Formation can be attributed to post-collisional volcanism in western Anatolia (Chen and Robertson, 2021a). The Upper Miocene grains (Tortonian-Messinian) with near-chondritic to juvenile εHf(t), -5 to 5, are comparable to those of the widespread ignimbrites of Central Anatolia (e.g., Akin et al., 2021).

6.6. Testing alternative models

Three contrasting tectonic models for the tectonic development of the Kyrenia Range can be tested and developed using the assembled detrital zircon geochronological data and relevant geological evidence for the Middle Triassic to Pleistocene siliciclastic sediments.

In model 1 (Fig. 13a), the Kyrenia Range is restored to the northern margin of the Southern Neotethys, adjacent to southern Turkey. A passive margin setting existed from Triassic to Cretaceous (Fig. 13a1-a2), followed by a switch to an active margin or collisional setting related to northward plate convergence from the Late Cretaceous onwards (Robertson and Woodcock, 1986; McCay and Robertson, 2012; Robertson et al., 2012a, 2014; Chen et al., 2019). The Cilicia Basin between Cyprus and Turkey is interpreted as continental crust that subsided to form a deep sea during accumulation of the Upper Eocene-Oligocene Bellapais Formation. This model assumes that the Southern Neotethys existed as a southerly oceanic basin, separated from more northerly Tethyan oceanic basins by the Tauride microcontinents, which are likely to have been important sediment contributors to the Kyrenia Range.

In model 1, two distinct provenances existed. The first was characterised by a general north to south sediment transport during Late Cretaceous-Early Oligocene (Fig. 13a2-a3). The dominantly Pan-African and Grenvillian zircon populations were derived from the rifted Cadomian basement (rifted microcontinents) within Anatolia (e.g., Zlatkin et al., 2013; Abbo et al., 2015; Chen et al., 2019). The Upper Cretaceous zircons were derived from continental margin arc and/or ophiolite-related magmatism within Anatolia (Fig. 13a2). Eocene zircons associated with serpentinite-derived detritus came from the supra-subduction zone ophiolites in S Turkey including boninites (e.g., Mersin ophiolite, or equivalent) (Robertson et al., 2014) (Fig. 13a3). After the Middle Eocene, coarse clastic transport, associated with similar supra-subduction zone ophiolitic rocks, remained generally from N to S, as indicated by paleocurrent data (Fig. 2) (McCay and Robertson, 2012). From Late Oligocene onwards, the major supply of detritus was from the east (Fig. 2), from the developing Tauride-Arabia collision zone in SE Turkey. The Eocene and Neogene zircon grains were mainly derived from late-stage subduction-related magmatism (e.g., Eocene granitoids) and, or evolved collision-related magmatism in SE Turkey (see Fig. 13a4).

In model 2, the Kyrenia Range is restored as part of the distal, N Africa continental margin (e.g., Maffione et al., 2017; McPhee and van Hinsbergen, 2019) (Fig. 13b). The Mesozoic carbonate platform (Trypa Group) represents part of the North African passive margin, with oceanic crust to the north. The Kyrenia Range, together with the Mamonia Complex of SW Cyprus, and the Bitlis and Pütürge continental units of SE Turkey formed parts of the North Africa/Arabia continental margin (Fig. 13b1). During the Late Cretaceous, supra-subduction zone ophiolites formed within Neotethys far to the northeast (Maffione et al., 2017). The supra-subduction zone slab rolled back into pre-existing oceanic gap between North Africa/Arabia and the Tauride continent. Ophiolites were emplaced by ‘radial invasion’, generally northwards onto the Tauride continent and also southwards onto the opposing Arabian continent (Maffione et al., 2017). The Troodos ophiolite, part of the ‘invaded’ supra-subduction zone oceanic crust, underwent southward emplacement over the N African continental margin during the Late Cretaceous. Passive margin-type deposition persisted in the Kyrenia Range during the Paleogene when the Kyrenia Range remained as part of the North Africa/Arabia continental margin. Down-margin sliding of olistoliths, took place during the Eocene (without compressional tectonics) to form the Kalograia-Ardana Formation (Fig. 13b2). Northward subduction was then activated in the south and this consumed remaining oceanic crust (Misis ocean) between North Africa/Arabia and Turkey (Eurasian plate) during the Oligocene-Miocene, culminating in Late Miocene continental collision (Fig. 13b3) (McPhee and van Hinsbergen, 2019). Van Hinsbergen et al. (2020) retained the above model of Upper Cretaceous ophiolite emplacement (Maffione et al., 2017) but re-assigned the Bitlis and Pütürge continental units to the Taurides rather than to Arabia. This would imply the existence of a Mesozoic oceanic basin to the south of the Bitlis and Pütürge continental units.

Some aspects of the detrital zircon provenance are compatible with Model 2, including the ultimate North Africa-Arabia provenance of the Precambrian zircons and the presence of Upper Cretaceous ophiolite-derived zircons. Also, the provenance from Oligocene-Recent is similar in both models because northward subduction/collision and Miocene collision are common to both models.

Several aspects of the detrital zircon provenance are, however, incompatible with model 2: (1) There is no known source of Carboniferous-Permian zircons related to magmatism or metamorphism in the North Africa-Arabia region, which remained passive during the Late Paleozoic (e.g., Cocks and Torsvik, 2006; Rolland et al., 2011); (2) The Upper Cretaceous (82-74 Ma) continental arc-type zircons, with relatively high U/Yb ratios but low Y concentrations (Fig. 9; Supplementary Figure S7), are explicable by derivation from the continental margin arc rocks of eastern Anatolia (e.g., Baskil Intrusives) (Chen and Robertson, 2021b). However, there is no known source of such arc-derived zircons within the North African-Arabia region which remained passive during this time. Eocene zircons similarly have a ready source in the continental margin arc rocks in eastern Anatolia (e.g., Doğanşehir area, see above) but are again absent from North Africa/Arabia.

Some other geological evidence is also incompatible with model 2 including: (1) The deep Herodotus Basin (Fig. 1) to the SW of Cyprus has been interpreted as oceanic crust (e.g., Woodside, 1977; Granot, 2016) that separated the North Africa passive margin from Cyprus, including the Kyrenia Range and the Mamonia Complex of W Cyprus (Fig. 1). Because this deep-water basin still exists, it is difficult to interpret the Kyrenia Range as a carbonate platform along the North Africa/Arabia continental margin, which was instead characterised by carbonate-evaporite facies (e.g., Sharief, 1986; Davies and Simmons, 2018). Similarly, the Levant basin farther east was deeply submerged from the Early Jurassic onwards, with the rifted North African continental margin to the south (Gardosh et al., 2010); (2) The Mamonia Complex includes Triassic-Cretaceous passive margin-type sedimentary rocks (e.g., debris-flow deposits) that were derived from a nearby continental block and carbonate platform, which is unlikely to correlate with the rifted North African margin far to the south (Robertson and Woodcock, 1979). The Mamonia Complex is instead lithologically and temporally similar to the Antalya Complex (=Antalya nappes) of the Taurides in adjacent SW Turkey (Torley and Robertson, 2018). The Antalya Complex is widely interpreted as rift/passive margin lithologies that bordered the southern margin of the Tauride continental block (e.g., Woodcock and Robertson, 1977; Poisson, 1977; Şengör and Yılmaz, 1981); (3) Arc magmatism of Upper Cretaceous and Eocene age in SE Turkey implies northward subduction, which is incompatible with eastward subduction, as indicated by the westward oceanic crust 'invasion' hypothesis (see Robertson and Parlak, 2020). Also, arc magmatism of Oligocene-Miocene age is absent from southern Turkey but would be expected if significant northward subduction took place during the Eocene, as in model 2.

In Model 3 (Fig. 13c), the entire Kyrenia Range is allochthonous and was emplaced from far to the north during the Eocene. The model implies that the entire Triassic to Eocene of the Kyrenia Range developed along the southern margin of Eurasia (Fig. 13c1-2) (Glazer et al., 2021). The lithologies making up the Triassic to Paleogene of Kyrenia Range were thrust southwards over the Anatolides/Taurides to near their present position during the Mid-Eocene, coeval with the widely reported southward thrusting in the Kyrenia Range (Fig. 13c3) (although not accepted in model 2). Carboniferous zircons that are common within the units ranging from the Middle Triassic Sikhari Formation to Middle Eocene Kalograia-Ardana Formation (Chen et al., 2019; Glazer et al., 2021) were derived directly from the Eurasian active continental margin in the NW Pontides (Meinhold et al., 2008; Löwen et al., 2017, 2020). An alternative considered by Glazer et al. (2021) is that the Kyrenia Range originated between the Kırşehir continental block and the Anatolides/Taurides (Fig. 13c1-c2), still far to the north of its present location. In both options, Carboniferous zircons became rare in Upper Oligocene and younger lithologies because they were structurally removed from the dominant Upper Paleozoic zircon source(s) following southward emplacement of the Kyrenia Range during the Eocene to near its present position in the eastern Mediterranean (Glazer et al., 2021).

The combined detrital zircon data also question model 3, especially the preferred Eurasian (Pontide) origin of the Kyrenia Range. Although there are similarities in the ages of geological units in the Pontides and Anatolides/Taurides (e.g., Upper Cretaceous ophiolites and continental margin arc units), there are also significant differences, as follows. Triassic sandstones of the Tauride autochthon have Carboniferous zircon populations (ca. 7%) that are comparable to those of the Middle Triassic to Oligocene sandstones of the Kyrenia Range (7-13%), in contrast to the Triassic to Jurassic-aged sediments of the Pontides (14-25%) (Akdoğan et al., 2018). Specially, Jurassic granitoids are widespread in the eastern and central Pontides (e.g., Genç and Tüysüz, 2010; Ustaömer et al., 2013, 2020; Okay et al., 2015). Upper Triassic-Lower Jurassic (210-190 Ma) detrital zircons dominate (40-67%) the Jurassic sandstones of the E Pontides (Akdoğan et al., 2018), but are very rare in the Kyrenia Range samples (Fig. 11). Post-Carboniferous clastic sediments in the Pontides are not always greatly enriched in

Carboniferous zircons (8-25%) (Akdoğan et al., 2018), suggesting that source and distribution were localised.

The Pontides were located along the northern margin of Tethys as a whole during the Upper Paleozoic to the Upper Cretaceous or the Paleogene when collision occurred in different interpretations (e.g., Barrier et al., 2018; Okay et al., 2018). On the other hand, some authors restore the Upper Paleozoic Sakarya arc close to, or directly along the northern margin of Gondwana (e.g., Göncüoğlu et al., 2007; Şengör et al., 2019), which, if correct, could have provided zircons directly to the north-Gondwana margin (Anatolides) (see Robertson, 2022 for discussion).

In line with the known regional geology, possible timings of southward emplacement of the Kyrenia Range over the Taurides would be Late Cretaceous (Campanian-Maastrichtian) or Eocene, together with ophiolitic and continental margin units (e.g., Özgül, 1984a; Mackintosh and Robertson, 2009; McPhee and van Hinsbergen, 2019).

The highest and most southerly travelled of the Tauride thrust sheets is the Hadim nappe, which reaches the Mediterranean coast (near Silifke) (MTA, 2011). However, there are no counterparts of the Kyrenia Range tectonostratigraphy within the Tauride units emplaced during the Late Cretaceous or the Eocene, or any indications of the former existence of km-thick thrust stack above the Hadim nappe (e.g., low-grade metamorphism). In addition, structural and facies evidence indicate that both the Antalya Complex and the Alanya metamorphic massif were emplaced northwards over the southern margin of the Tauride carbonate platforms during the Paleocene to Middle Eocene (Monod, 1977; Özgül, 1984b; Robertson and Parlak, 2020; Robertson et al., 2020). The Hadim nappe locally overrode the Antalya Complex and the Alanya Massif due to slightly later Eocene emplacement (Özgül, 1984b; MTA, 2011). The Eocene emplaced Alanya Massif would have constituted a barrier to overthrusting by the Kyrenia Range.

Rather than an isolated structural unit (klippen), the Kyrenia Range is instead part of a pile of thrust sheets that extends eastward through SE Turkey into Iran. The Kyrenia Range runs under the sea and comes on land as the Misis Mountains, that in turn links northeastwards with the Andırın Range, then with the Engizek Mountains and the Bilits suture zone of SE Turkey (e.g., Perinçek and Kozlu, 1984; Robertson and Woodcock, 1986; Kempler and Garfunkel, 1994; Robertson et al., 2006). Mesozoic carbonate platform units (‘Andırın limestones’), similar to those of the Kyrenia Range, are located at a low level in the regional tectonic pile, overlain by Upper Cretaceous ophiolitic, metamorphic and arc-type magmatic rocks in SE Turkey (Perinçek and Kozlu, 1984; Robertson et al., 2006; Nurlu et al., 2016). Deriving the Kyrenia Range from far to the north in a high structural position and then having it emplaced in a low structural position far to the south would require major, regional out-of-sequence thrusting for which field evidence is currently lacking (e.g., Robertson et al., 2021b).

In addition, southward emplacement of the Kyrenia Range as a whole (pre-Late Eocene) would imply the presence of a major foreland basin including abundant detritus beneath and to the south of the Kyrenia Range. This crust is unfortunately hidden because of Upper Miocene southward thrusting (accepted in all three models). However, it is notable that the ophiolitic and continental margin detritus occurs within the Middle Eocene Kaolgrai-Ardana Formation (i.e., part of the range stratigraphy) suggesting that only this material rather than the entire pre-Late Eocene stratigraphy of Kyrenia Range was derived from the north.

6.7 Zircon texture/recycling and wider implications

We propose that the combined zircon data presented here are more consistent with model 1 than with the alternative models 2 and 3. A possible objection is that the Carboniferous zircon grains are relatively angular (Chen et al., 2019; Glazer et al., 2021; this study) (Fig. 11). However, evidence from elsewhere increasingly suggests that angular to subangular zircon grains can survive multiple cycles of erosion. Variable-distance transport by fluvial or gravity-flow processes may not result in significant rounding, even during multiple sediment cycling (e.g., Mange and Maurer, 1992; Garzanti et al., 2015; Zoleikhaei et al., 2015). Phanerozoic zircons throughout Turkey are mainly euhedral/subhedral, with well-rounded zircons being generally restricted to the older Precambrian (T. Ustaömer, personal communication, 2021). The degree of rounding is therefore not a reliable indicator of the proximity of zircon sources.

As summarized above (sections 4 and 6.2), the Middle Triassic, Upper Cretaceous and Eocene samples from throughout the Kyrenia Range contain subordinate, but pronounced, fractions of euhedral/subhedral zircons of Carboniferous and Permian ages (Fig. 11). Similar-aged zircons are also present in Middle-Upper Triassic Tauride samples in some units (Ustaömer et al., 2020). In contrast, Carboniferous and Permian zircons are relatively rare in the Oligocene-Upper Miocene sediments (Fig. 11). Contemporaneous subsidence of the Cilicia Basin terminated the input of Upper Paleozoic zircons from the north. Provenance then switched to the east (Fig. 2), mainly from SE Turkey. Zircons from the Taurides of SE Turkey are mainly Precambrian, without Carboniferous-Devonian zircons (Ustaömer et al., 2020), explaining their sparsity in the Oligocene-Miocene sediments of the Kyrenia Range. Interestingly, where present, Carboniferous-Permian zircons are mainly rounded/subrounded in the Oligocene-Miocene sediments (Fig. 11). A possible explanation is that the angular/subangular zircons were ultimately derived from the north, including the Konya Complex in central Anatolia, involving relatively rapid transport and redepositional events (Middle-Late Triassic and Late Cretaceous). In contrast, the rare, but better-rounded Carboniferous-Permian grains in the Oligocene-Upper Miocene samples were derived from the E Taurides. Lithologies of these ages in this area (e.g., Malatya Metamorphics) (Perinçek and Kozlu, 1984; Robertson et al., 2021a, b) were ultimately sourced from the Precambrian of the Arabian-Nubian Shield rather than Paleotethys, explaining the textural difference.

Eocene final suturing of the İzmir-Ankara-Erzincan ocean basin (Northern Neotethys) and the Inner Tauride ocean (controversial for some authors; e.g., van Hinsbergen et al., 2020), and related regional-scale thrusting (see Section 2) were followed by uplift, erosion and fluvial reworking, as indicated by the extensive accumulation of Oligocene red bed-type clastic sediments throughout Anatolia ('Kastel Formation'); e.g., Aktoprak Formation of the Ulukışla Basin (Fig. 1) (Clark and Robertson, 2002; Akgün et al., 2021). Some of the associated detrital zircons were redeposited into the eastern Mediterranean basin including the Kyrenia Range via near-coastal Miocene basins (Chen et al., 2021).

Our preferred development of the Kyrenia Range along the northern margin of the Southern Neotethys (Model 1) has additional implications:

(1) Ideally zircon geochronology allows unique sources to be identified. However, conjugate rifting places similar aged units on opposite sides of ocean basins that ultimately suture. A good example is the Triassic rifting of Precambrian fragments from the NE African/Arabian-Nubian Shield to form microcontinents to the north of the Southern Neotethys. The source of Precambrian zircons in Cyprus was Anatolia rather than North Africa-Levant (see section 6.3). If the Mediterranean basin had already completely closed, comparable with many suture zones, then the recognition of southerly versus northerly provenances could be more very difficult;

(2) Additional complications arise where multiple suture zones exist in areas that could have supplied detrital zircons. In the case of Turkey, there are similarities in the timing and setting of more than one sutured ocean basin (S vs. N Neotethys) and it is necessary to identify unique zircon-bearing units that could have supplied zircons (e.g., Upper Cretaceous and Eocene granitoids of SE Turkey);

(3) Interpretations need to take account of the propensity for zircons to be recycled multiple times through successive geological units without necessarily become texturally mature (i.e., well-rounded). During such recycling, zircons may either be concentrated or dispersed according to local sedimentological conditions.

Based on this study, recycling is likely to have taken place from Upper Paleozoic granitoid rocks to, successively upper Carboniferous-earliest Permian, Mid-Upper Triassic and post-Cretaceous formations;

(4) Interpretations of detrital zircons geochronology are critically dependent on a knowledge of paleo-drainage, which is commonly eroded in orogenic belts, together with sub-aqueous paleocurrents. A good example is the present evidence of Neogene generally westward sediment transport away from the Southern Neotethyan suture zone into the eastern Mediterranean basin, including the Kyrenia Range;

(5) Interpretation of detrital zircon data is enhanced when complementary analytical data are available, including from zircon trace elements and Lu-Hf isotopes. In the present study, the trace-element data allowed zircon sources during the latest Cretaceous and Eocene to be related to the availability of supra-subduction zone-type ophiolitic debris (including boninites) that was derived from outside the immediate area. Lu-Hf isotopic data particularly aid recognition of evolved versus juvenile crustal sources, such as the Upper Cretaceous and Eocene granitoids in SE Turkey.

(6) Finally, interpretation of the detrital zircon geochronology of any particular region is dependent on the overall geological knowledge, in this case the North Africa/Arabia-Eastern Mediterranean-Anatolia region.

7. Conclusions

A combination of new and existing detrital zircon geochronology, new and existing zircon Hf isotopic evidence and new zircon trace element data, together with published geological evidence (especially published paleocurrent data), allows systematic interpretation of the provenance and tectonic setting of the clastic sediments of Triassic to Neogene age throughout the Kyrenia Range of northern Cyprus. The new zircon data (24 samples) are mainly from four transects of the Kyrenia Range (over ca. 150 km laterally) and include previously unsampled time slices (e.g., Late Eocene-Early Oligocene, Pliocene). The new zircon trace element data for Carboniferous to Triassic grains also allow tectonic discrimination of continental margin arc versus intra-plate settings

Two stratigraphic ages are refined according to maximum depositional zircon age; i.e., the Kiparisso Vouno Member (Santonian-Late Campanian) is ca. 3 Ma older than previously inferred, and the Lapatza Gypsum is no older than 5.4 Ma.

In nearly all of the sandstones analysed, Precambrian-Cambrian zircons predominate, with major age peaks at ca. 930 Ma, 630 Ma and 530 Ma. These dominantly Pan-African and Grenvillian zircon populations were derived from Cadomian basement units in Anatolia, following Triassic rifting of microcontinents from North Africa (Gondwana) during opening of the Southern Neotethys.

Carboniferous-Permian zircons form significant age populations (up to 13%) in some of the samples, peaking at 320 Ma, 305 Ma and 295 Ma. Zircons in the pre-Oligocene sandstones are mainly euhedral. The Upper Paleozoic zircons were originally derived from Upper Paleozoic magmatic arc units, possibly following closure of Paleotethys farther west (Aegean-Balkan region). The provenance of the Upper Paleozoic zircons in the Kyrenia Range is preferentially explained by repeated recycling of siliciclastic sediments; i.e., during Carboniferous-earliest Permian, Mid-Upper Triassic and Upper Cretaceous-Paleogene. In suppot, there is much paleocurrent evidence of Mid-Upper Triassic southward reworking of Paleotethyan detritus within central Anatolia.

Upper Cretaceous zircons (up to 16%) have age peaks of 99-85 Ma and are characterised by highly variable U/Yb and Nb/Yb ratios. The clastic sediment supply included ophiolitic (92-84 Ma) and volcanic arc (ca. 88-70 Ma) units, together with relatively minor metamorphic rock-derived detritus, potentially from the Alanya Massif to the north.

Subordinate Paleogene zircons occur in the Upper Miocene sandstones (up to 14%) were potentially derived from localised Lower-Mid Eocene magmatic rocks in central or SE Turkey.

Oligocene-Pliocene sandstones contain sparse zircons of Carboniferous and Permian age (up to 6%), which are relatively well rounded. These zircons were recycled through non-marine continental environments before being finally redeposited within turbidites. The Oligocene-Pliocene sandstones also contain abundant Upper Cretaceous zircons (up to 52%), with age peaks at 84 Ma, 80 Ma, 75 Ma and 70 Ma. The main source of these zircons is likely to have been coeval continental arc granitoid rocks, as widely exposed in eastern Anatolia.

A significant Miocene zircon fraction (up to 17%), with major age peaks at ca. 20-17 Ma, was probably derived from evolved, calc-alkaline magmatic rocks in SE Turkey. The more common Messinian zircons in the eastern range samples (up to 55%) compared to the western range ones (<1%) could be explained by derivation from Messinian airfall tuffs and ignimbrites in central Turkey.

Paleocene-Lower Miocene zircons are characterised by highly variable $\varepsilon Hf_{(t)}$ values, with derivation from juvenile materials (e.g., remnant Neotethys) and/or reworked crust (e.g., exposed ‘microcontinental’ or metamorphic units).

The combined zircon geochronological, isotopic and zircon trace element evidence indicates a marked change in provenance between pre-Oligocene and post-Oligocene. The Southern Neotethys sutured in southeast Anatolia during Oligocene-Miocene, creating a dominant source from the Tauride thrust sheets in SE Turkey. Collision-related uplift in S and SE Turkey generated sediment that was transported into the easternmost deep-sea Mediterranean, including the future Kyrenia Range. Paleogene zircons were supplied continuously from the Middle Miocene-Pliocene, which is explicable by first, subduction and later, by collision-related magmatism in southeast Turkey. Upper Miocene grains with near chondritic to juvenile $\varepsilon Hf_{(t)}$ could have a tuff/ignimbrite origin in central Turkey. Also, Messinian zircons from post-collisional magmatic rocks were supplied to Tortonian-Messinian sediments in the eastern Kyrenia Range.

The combined evidence has also been used to test three different tectonic models: i.e., the Kyrenia Range developed along the northern margin of the Southern Neotethys; the range originated along the northern margin of North Africa; or the range represents a far-travelled allochthon emplaced from the southern margin of Eurasia, or possibly from theAnatolides (Afyon zone). In the light of the regional geological evidence, the combined zircon and other geochemical data assembled here, mainly supports the first hypothesis that the Kyrenia Range developed along the northern margin of the Southern Neotethys; this was passive during the Triassic, active during the Late Cretaceous-Paleogene and collision-related during the Miocene-Recent. The dominant sources during the pre-Oligocene were generally in southern Anatolia to the north and northeast, whereas from Oligocene onwards supply was largely from SE Anatolia related to the development of post-collisional river catchments.

Declaration of Competing Interest

The authors declare that they have no known competing financial interests or personal relationships that could have appeared to influence the work reported in this paper.

Acknowledgements

This work was financially supported by the National Natural Science Foundation of China (41888101, 91755000 and 42002126). Fieldwork by the second author was aided by the John Dixon Memorial Fund. Osman Parlak and Zhongyu Meng kindly assisted in the field. Shitou Wu and Shaohua Zhang are kindly thanked for analytical assistance. We are very grateful to Lin Ding, Xiumian Hu, Fangyang Hu, Timothy Kinnaird, Chuanzhou Liu, Tong Liu, Gillian McCay, Qingren Meng, Mehmet Necdet, Romesh Palamakumbura, Osman Parlak, Hongbing Tan, Timur Ustaömer, Bo Wan and Dicheng Zhu for beneficial discussion. The manuscript benefitted from comments by Alexandros Konstantinou, an anonymous reviewer and the editor, Carlo Doglioni.

References

Abbo, A., Avigad, D., Gerdes, A. and Güngör, T., 2015. Cadomian basement and Paleozoic to Triassic siliciclastics of the Taurides (Karacahisar dome, south-central Turkey): paleogeographic constraints from U–Pb–Hf in zircons. Lithos 227, 122-139. http://doi.org/10.1016/j.lithos.2015.03.023

Akal, C., Candan, O., Koralay, O.E., Oberhänsli, R., Chen, F. and Prelević, D., 2012. Early Triassic potassic volcanism in the Afyon Zone of the Anatolides/Turkey: implications for the rifting of the Neo-Tethys. Int. J. Earth Sci. 101, 177-194. http://doi.org/10.1007/s00531-011-0654-2

Akdoğan, R., Okay, A. and Dunkl, I., 2018. Triassic-Jurassic arc magmatism in the Pontides as revealed by the U-Pb detrital zircon ages in the Jurassic sandstones of northeastern Turkey. Turk. J. Earth Sci. 27, 89-109. http://doi.org/10.3906/yer-1706-19

Akgün, F., Kayseri‐Özer, M.S., Tekin, E., Varol, B., Şen, Ş., Herece, E., Gündoğan, İ., Sözeri, K. and Us, M.S., 2021. Late Eocene to Late Miocene palaeoecological and palaeoenvironmental dynamics of the Ereğli‐Ulukışla Basin (Southern Central Anatolia). Geol. J. 56, 673-703. http://doi.org/10.1002/gj.4021

Akin, L., Aydar, E., Schmitt, A.K., Çubukçu, H.E. and Gerdes, A., 2021. Zircon geochronology and O-Hf isotopes of Cappadocian ignimbrites: New insights into continental crustal architecture underneath the Central Anatolian Volcanic Province, Turkey. Gondwana Res. 91, 166-187. http://doi.org/10.1016/j.gr.2020.12.003

Aksu, A., Hall, J. and Yaltırak, C., 2021. Miocene–Quaternary tectonic, kinematic and sedimentary evolution of the eastern Mediterranean Sea: A regional synthesis. Earth-Sci. Rev. 220, 103719. http://doi.org/10.1016/j.earscirev.2021.103719

Aktaş, G. and Robertson, A.H.F., 1984. The Maden Complex, SE Turkey: evolution of a Neotethyan active margin. In: J.E. Dixon and A.H.F. Robertson (Editors), The Geological Evolution of the Eastern Mediterranean. Geological Society of London, Special Publications, pp. 375-402.

Aktaş, G. and Robertson, A.H.F., 1990. Tectonic evolution of the Tethys suture zone in SE Turkey: evidence from the petrology and geochemistry of Late Cretaceous and Middle Eocene extrusives. In: J. Malpas, E.M. Moores, A. Panayiotou and C. Xenophontos (Editors), Ophiolites-Oceanic Crustal Analogues. Proceedings of the International Symposium ‘Troodos 1987’. Cyprus Geological Survey Department, Nicosia, pp. 311-329.

Al-Riyami, K., Robertson, A., Dixon, J. and Xenophontos, C., 2002. Origin and emplacement of the Late Cretaceous Baer–Bassit ophiolite and its metamorphic sole in NW Syria. Lithos 65, 225-260. http://doi.org/10.1016/S0024-4937(02)00167-6

Al-Riyami, K. and Robertson, A.H.F., 2002. Mesozoic sedimentary and magmatic evolution of the Arabian continental margin, northern Syria: evidence from the Baer–Bassit Melange. Geol. Mag. 139, 395-420. http://doi.org/10.1017/s0016756802006660

Altıner, D., Koçyiğit, A., Farinacci, A., Nicosia, U. and Conti, M., 1991. Jurassic, Lower Cretaceous stratigraphy and paleogeographic evolution of the southern part of north-western Anatolia. Geol. Romana 27, 13-80.

Altunkaynak, Ş. and Genç, Ş.C., 2008. Petrogenesis and time-progressive evolution of the Cenozoic continental volcanism in the Biga Peninsula, NW Anatolia (Turkey). Lithos 102, 316-340. http://doi.org/10.1016/j.lithos.2007.06.003

Andersen, T., 2002. Correction of common lead in U–Pb analyses that do not report ^{204}Pb. Chem. Geol. 192, 59-79. http://doi.org/10.1016/S0009-2541(02)00195-X

Andrew, T. and Robertson, A.H.F., 2002. The Beyşehir–Hoyran–Hadim Nappes: genesis and emplacement of Mesozoic marginal and oceanic units of the northern Neotethys in southern Turkey. J. Geol. Soc. 159, 529-543. http://doi.org/10.1144/0016-764901-157

Arenas, R., Martínez, S.S., Gerdes, A., Albert, R., Fernández, R.D. and Andonaegui, P., 2014. Re-interpreting the Devonian ophiolites involved in the Variscan suture: U–Pb and Lu–Hf zircon data of the Moeche Ophiolite (Cabo Ortegal Complex, NW Iberia). Int. J. Earth Sci. 103, 1385-1402. http://doi.org/10.1007/s00531-013-0880-x

Arger, J., Mitchell, J., Westaway, R.W.C., Bozkurt, E., Winchester, J.A. and Piper, J.D.A., 2000. Neogene and Quaternary volcanism of southeastern Turkey. In: E. Bozkurt, J.A. Winchester and J.D.A. Piper (Editors), Tectonics and Magmatism in Turkey and the Surrounding Area. Geological Society, London, Special Publication, pp. 459-487.

Artiaga, D., García-Veigas, J., Cendón, D.I., Atalar, C. and Gibert, L., 2021. The Messinian evaporites of the Mesaoria basin (North Cyprus): A discrepancy with the current chronostratigraphic understanding. Palaeogeogr. Palaeoclimatol. Palaeoecol. 584. http://doi.org/10.1016/j.palaeo.2021.110681

Asan, K. and Kurt, H., 2011. Petrology and geochemistry of post‐collisional early miocene volcanism in the Karacadağ Area (Central Anatolia, Turkey). Acta Geol. Sin. Ed. 85, 1100-1117. http://doi.org/10.1111/j.1755-6724.2011.00543.x

Aydar, E., 1998. Early Miocene to Quaternary evolution of volcanism and the basin formation in western Anatolia: a review. J. Volcanol. Geotherm. Res. 85, 69-82. http://doi.org/10.1016/S0377-0273(98)00050-X

Aydar, E., Schmitt, A.K., Çubukçu, H.E., Akin, L., Ersoy, O., Sen, E., Duncan, R.A. and Atici, G., 2012. Correlation of ignimbrites in the central Anatolian volcanic province using zircon and plagioclase ages and zircon compositions. J. Volcanol. Geotherm. Res. 213, 83-97. http://doi.org/10.1016/j.jvolgeores.2011.11.005

Balmer, E.M., Robertson, A.H.F., Raffi, I. and Kroon, D., 2019. Pliocene–Pleistocene sedimentary development of the syntectonic Polis graben, NW Cyprus: evidence from facies analysis, nannofossil biochronology and strontium isotope dating. Geol. Mag. 156, 889-917. http://doi.org/10.1017/s0016756818000286

Baroz, F., 1979. Etude géologique dans le Pentadaktylos et la Mesaoria (Chypre Septentrionale). Doctor of Science Thesis (Published). Université de Nancy, France, 434 pp.

Baroz, F. and Bizon, G., 1974. Le néogène de la chaine du Pentadaktylos et de la partie nord de la Mésaoria (Chypre). Etude stratigraphique et micropaléontologique. Revue de l'Institut Français du Pétrole 29, 327-360. http://doi.org/10.2516/ogst:1974015

Barrier, E., Vrielynck, B., Brouillet, J.F. and Brunet, M.F., 2018. Paleotectonic Reconstruction of the Central Tethyan Realm. Tectono-Sedimentary-Palinspastic Maps from Late Permian to Pliocene. Atlas of 20 maps (scale 1/15000000). CCGM/CGMW, Paris.

Ben-Avraham, Z., Tibor, G., Limonov, A., Leybov, M., Ivanov, M., Tokarev, M.Y. and Woodside, J., 1995. Structure and tectonics of the eastern Cyprean Arc. Mar. Pet. Geol. 12, 263-271. http://doi.org/10.1016/0264-8172(95)98379-J

Beyarslan, M., Lın, Y.-C., Bingöl, A.F. and Chung, S.-L., 2016. Zircon U-Pb age and geochemical constraints on the origin and tectonic implication of Cadomian (Ediacaran-Early Cambrian) magmatism in SE Turkey. J. Asian Earth Sci. 130, 223-238. http://doi.org/10.1016/j.jseaes.2016.08.006

Bingöl, A.F., Beyarslan, M., Lin, Y.-C. and Lee, H.-Y., 2018. Geochronological and geochemical constraints on the origin of the Southeast Anatolian ophiolites, Turkey. Arab. J. Geosci. 11, 569. http://doi.org/10.1007/s12517-018-3880-0

Bingöl, E., 1977. The geology of Muratdagi on the petrology of the main rock units. Bull. Geol. Soc. Turk. 20, 13-66.

Booth, M.G., Robertson, A.H.F., Tasli, K. and İnan, N., 2014. Late Cretaceous to Late Eocene Hekimhan Basin (Central Eastern Turkey) as a supra-ophiolite sedimentary/magmatic basin related to the later stages of closure of Neotethys. Tectonophysics 635, 6-32. http://doi.org/10.1016/j.tecto.2014.05.039

Bortolotti, V., Chiari, M., Göncüoğlu, M.C., Principi, G., Saccani, E., Tekin, U.K. and Tassinari, R., 2018. The Jurassic–Early Cretaceous basalt–chert association in the ophiolites of the Ankara Mélange, east of Ankara, Turkey: age and geochemistry. Geol. Mag. 155, 451-478. http://doi.org/10.1017/s0016756817000401

Boulton, S.J., 2009. Record of Cenozoic sedimentation from the Amanos Mountains, Southern Turkey: implications for the inception and evolution of the Arabia–Eurasia continental collision. Sediment. Geol. 216, 29-47. http://doi.org/10.1016/j.sedgeo.2009.01.008

Boulton, S.J. and Robertson, A.H.F., 2008. The Neogene–Recent Hatay Graben, South Central Turkey: graben formation in a setting of oblique extension (transtension) related to post-collisional tectonic escape. Geol. Mag. 145, 800-821. http://doi.org/10.1017/S0016756808005013

Bouvier, A., Vervoort, J.D. and Patchett, P.J., 2008. The Lu–Hf and Sm–Nd isotopic composition of CHUR: Constraints from unequilibrated chondrites and implications for the bulk composition of terrestrial planets.Earth Planet. Sci. Lett. 273, 48-57. http://doi.org/10.1016/j.epsl.2008.06.010

Bretschneider, L., Hathorne, E.C., Huang, H., Lübbers, J., Kochhann, K.G., Holbourn, A., Kuhnt, W., Thiede, R., Gebregiorgis, D. and Giosan, L., 2021. Provenance and weathering of clays delivered to the Bay of Bengal during the middle Miocene: Linkages to tectonics and monsoonal climate. Paleoceanogr. Paleoclimatology 36, e2020PA003917. http://doi.org/10.1029/2020PA003917

Calon, T., Aksu, A. and Hall, J., 2005a. The Neogene evolution of the outer Latakia Basin and its extension into the eastern Mesaoria Basin (Cyprus), eastern Mediterranean. Mar. Geol. 221, 61-94. http://doi.org/10.1016/j.margeo.2005.03.013

Calon, T., Aksu, A. and Hall, J., 2005b. The Oligocene-Recent evolution of the Mesaoria Basin (Cyprus) and its western marine extension, Eastern Mediterranean. Mar. Geol. 221, 95-120. http://doi.org/10.1016/j.margeo.2005.03.012

Candan, O., Akal, C., Koralay, O.E., Okay, A.I., Oberhänsli, R., Prelević, D. and Mertz-Kraus, R., 2016. Carboniferous granites on the northern margin of Gondwana, Anatolide-Tauride Block, Turkey – Evidence for southward subduction of Paleotethys. Tectonophysics 683, 349-366. http://doi.org/10.1016/j.tecto.2016.06.030

Candan, O., Koralay, O.E., Akal, C., Kaya, O., Oberhänsli, R., Dora, O.Ö., Konak, N. and Chen, F., 2011. Supra-Pan-African unconformity between core and cover series of the Menderes Massif/Turkey and its geological implications. Precambrian Res. 184, 1-23. http://doi.org/10.1016/j.precamres.2010.09.010

Cavazza, W., Cattò, S., Zattin, M., Okay, A.I. and Reiners, P., 2018. Thermochronology of the Miocene Arabia-Eurasia collision zone of southeastern Turkey. Geosphere 14, 2277-2293. http://doi.org/10.1130/GES01637.1

Cawood, P.A., Hawkesworth, C.J. and Dhuime, B., 2012. Detrital zircon record and tectonic setting. Geology 40, 875-878. http://doi.org/10.1130/g32945.1

Çelik, Ö.F., Chiaradia, M., Marzoli, A., Billor, Z. and Marschik, R., 2013. The Eldivan ophiolite and volcanic rocks in the İzmir–Ankara–Erzincan suture zone, Northern Turkey: Geochronology, whole-rock geochemical and Nd–Sr–Pb isotope characteristics. Lithos 172, 31-46. http://doi.org/10.1016/j.lithos.2013.03.010

Çetinkaplan, M., 2018. Anamur (Alanya Masifi, Mersin) Bölgesinde yer alan Prekambriyen yaşlı kayaçların çok evreli P-T-t evrimi (Multi-Stage P-T-t evolution of Precambrian-aged rocks in Anamur (Alanya Massif, Mersin) Region). Geological Bulletin of Turkey 61, 91-130 (in Turkish with English abstract). http://doi.org/10.25288/tjb.358187

Çetinkaplan, M., Pourteau, A., Candan, O., Koralay, O.E., Oberhänsli, R., Okay, A.I., Chen, F., Kozlu, H. and Şengün, F., 2016. P–T–t evolution of eclogite/blueschist facies metamorphism in Alanya Massif: time and space relations with HP event in Bitlis Massif, Turkey. Int. J. Earth Sci. 105, 247-281. http://doi.org/10.1007/s00531-014-1092-8

Chan, G.H.-N., Malpas, J., Xenophontos, C. and Lo, C.-H., 2008. Magmatism associated with Gondwanaland rifting and Neo-Tethyan oceanic basin development: evidence from the Mamonia Complex, SW Cyprus. J. Geol. Soc. 165, 699-709. http://doi.org/10.1144/0016-76492007-050

Chauvel, C., Lewin, E., Carpentier, M., Arndt, N.T. and Marini, J.-C., 2008. Role of recycled oceanic basalt and sediment in generating the Hf–Nd mantle array. Nat. Geosci. 1, 64-67. http://doi.org/10.1038/ngeo.2007.51

Chen, G. and Robertson, A.H.F., 2021a. Early Miocene calc-alkaline felsic tuffs within deep-marine turbidites in the Kyrenia Range, north Cyprus, with a possible post-collisional eruptive centre in western Anatolia. Geol. Mag.1-13. http://doi.org/10.1017/S0016756820001399

Chen, G. and Robertson, A.H.F., 2021b. Evidence from Late Cretaceous-Paleogene volcanic rocks of the Kyrenia Range, northern Cyprus for the northern, active continental margin of the Southern Neotethys. Lithos 380, 105835. http://doi.org/10.1016/j.lithos.2020.105835

Chen, G., Robertson, A.H.F. and Ustaömer, T., 2019. U–Pb detrital zircon ages used to infer provenance and tectonic setting of Late Triassic–Miocene sandstones related to the Tethyan development of Cyprus. J. Geol. Soc. 176, 863-884. http://doi.org/10.1144/jgs2018-207

Chen, G., Robertson, A.H.F., Parlak, O. and Wu, F.-Y., 2021. Source to sink in the easternmost Mediterranean: insights from the provenance of Oligo-Miocene turbidites in the south Turkish basins, AGU 2021 Fall Meeting, New Orleans, LA and virtual, pp. 1.

Chen, G., Robertson, A.H.F., Parlak, O. and Wu, F.-Y., 2022. Provenance of sandstones related to pre, syn and post-rifting of N Gondwana: evidence from detrital zircon geochronology (Antalya Complex, E Mediterranean), 21st International Sedimentological Congress, Beijing, China, pp. 1-2.

Clark, M. and Robertson, A., 2002. The role of the Early Tertiary Ulukışla Basin, southern Turkey, in suturing of the Mesozoic Tethys ocean. J. Geol. Soc. 159, 673-690. http://doi.org/10.1144/0016-764902-015

Clift, P., Gaedicke, C., Edwards, R., Il Lee, J., Hildebrand, P., Amjad, S., White, R.S. and Schlüter, H.-U., 2002. The stratigraphic evolution of the Indus Fan and the history of sedimentation in the Arabian Sea. Mar. Geophys. Res. 23, 223-245. http://doi.org/10.1023/A:1023627123093

Clift, P.D., 2002. A brief history of the Indus River. In: P.D. Clift, D. Kroon, C. Gaedicke and J. Craig (Editors), The Tectonic and Climatic Evolution of the Arabian Sea Region. Geological Society of London, Special Publications, pp. 237-258.

Cocks, L.R.M. and Torsvik, T.H., 2006. European geography in a global context from the Vendian to the end of the Palaeozoic. In: D.G. Gee and R.A. Stephenson (Editors), European Lithosphere Dynamics. Geological Society, London, Memoirs, pp. 83-95.

Cohen, K.M., Finney, S.C., Gibbard, P.L. and Fan, J., 2021. The ICS international Chronostratigraphic Chart. Episodes 36, 199-204.

Collins, A.S. and Robertson, A.H.F., 1998. Processes of Late Cretaceous to Late Miocene episodic thrust-sheet translation in the Lycian Taurides, SW Turkey. J. Geol. Soc. 155, 759-772. http://doi.org/10.1144/gsjgs.155.5.0759

Corfu, F., Hanchar, J.M., Hoskin, P.W. and Kinny, P., 2003. Atlas of zircon textures. Rev. Mineral. Geochem. 53, 469-500. http://doi.org/10.2113/0530469

Cosentino, D., Buchwaldt, R., Sampalmieri, G., Iadanza, A., Cipollari, P., Schildgen, T.F., Hinnov, L.A., Ramezani, J. and Bowring, S.A., 2013. Refining the Mediterranean “Messinian gap” with high-precision U-Pb zircon geochronology, central and northern Italy. Geology 41, 323-326. http://doi.org/10.1130/G33820.1

Cosentino, D., Schildgen, T.F., Cipollari, P., Faranda, C., Gliozzi, E., Hudáčková, N., Lucifora, S. and Strecker, M.R., 2012. Late Miocene surface uplift of the southern margin of the Central Anatolian Plateau, Central Taurides, Turkey. Geol. Soc. Am. Bull. 124, 133-145. http://doi.org/10.1130/b30466.1

Darin, M.H., Umhoefer, P.J. and Thomson, S.N., 2018. Rapid Late Eocene exhumation of the Sivas Basin (central Anatolia) driven by initial Arabia ‐ Eurasia collision. Tectonics 37, 3805-3833. http://doi.org/10.1029/2017tc004954

Davies, R. and Simmons, M., 2018. Triassic sequence stratigraphy of the Arabian Plate. In: M. Poppelreiter (Editor), Lower Triassic to Middle Jurassic Sequence of the Arabian Plate. EAGE, pp. 101-162.

Dempster, T., Hay, D. and Bluck, B., 2004. Zircon growth in slate. Geology 32, 221-224. http://doi.org/10.1130/G20156.1

Dilek, Y. and Altunkaynak, Ş., 2010. Geochemistry of Neogene–Quaternary alkaline volcanism in western Anatolia, Turkey, and implications for the Aegean mantle. Int. Geol. Rev. 52, 631-655. http://doi.org/10.1080/00206810903495020

Dilek, Y. and Thy, P., 2006. Age and petrogenesis of plagiogranite intrusions in the Ankara melange, central Turkey. Isl. Arc 15, 44-57. http://doi.org/10.1111/j.1440-1738.2006.00522.x

Ducloz, C., 1972. The geology of the Bellapais-Kythrea area of the Central Kyrenia Range. Bulletin of the Geological Survey Department 6, Nicosia, Cyprus, 75 pp.

Duman, T.Y., Robertson, A.H.F., Elmacı, H. and Kara, M., 2017. Palaeozoic-Recent geological development and uplift of the Amanos Mountains (S Turkey) in the critically located northwesternmost corner of the Arabian continent. Geodin. Acta 29, 103-138. http://doi.org/10.1080/09853111.2017.1323428

Eiler, J.M., 2001. Oxygen isotope variations of basaltic lavas and upper mantle rocks. Rev. Mineral. Geochem. 43, 319-364. http://doi.org/10.2138/gsrmg.43.1.319

Elmas, A. and Yılmaz, Y., 2003. Development of an oblique subduction zone-tectonic evolution of the Tethys suture zone in southeast Turkey. Int. Geol. Rev. 45, 827-840. http://doi.org/10.2747/0020-6814.45.9.827

Ersoy, Y.E., Helvacı, C., Uysal, İ., Karaoğlu, Ö., Palmer, M.R. and Dindi, F., 2012. Petrogenesis of the Miocene volcanism along the İzmir-Balıkesir Transfer Zone in western Anatolia, Turkey: Implications for origin and evolution of potassic volcanism in post-collisional areas. J. Volcanol. Geotherm. Res. 241, 21-38. http://doi.org/10.1016/j.jvolgeores.2012.05.022

Erturk, M.A., Beyarslan, M., Chung, S.-L. and Lin, T.-H., 2018. Eocene magmatism (Maden Complex) in the Southeast Anatolian Orogenic Belt: Magma genesis and tectonic implications. Geosci. Front. 9, 1829-1847. http://doi.org/10.1016/j.gsf.2017.09.008

Eyüboğlu, Y., 2010. Late Cretaceous high‐K volcanism in the eastern Pontide orogenic belt: Implications for the geodynamic evolution of NE Turkey. Int. Geol. Rev. 52, 142-186. http://doi.org/10.1080/00206810902757164

Feld, C., Mechie, J., Hübscher, C., Hall, J., Nicolaides, S., Gurbuz, C., Bauer, K., Louden, K. and Weber, M., 2017. Crustal structure of the Eratosthenes Seamount, Cyprus and S. Turkey from an amphibian wide-angle seismic profile. Tectonophysics 700, 32-59. http://doi.org/10.1016/j.tecto.2017.02.003

Fu, B., Bröcker, M., Ireland, T., Holden, P. and Kinsley, L.P.J., 2015. Zircon U–Pb, O, and Hf isotopic constraints on Mesozoic magmatism in the Cyclades, Aegean Sea, Greece. Int. J. Earth Sci. 104, 75-87. http://doi.org/10.1007/s00531-014-1064-z

Gardosh, M.A., Garfunkel, Z., Druckman, Y. and Buchbinder, B., 2010. Tethyan rifting in the Levant Region and its role in Early Mesozoic crustal evolution. In: C. Homberg and M. Bachmann (Editors), Evolution of the Levant Margin and Western Arabia Platform since the Mesozoic. Geological Society, London, Special Publications, pp. 9-36.

Garfunkel, Z., 1998. Constrains on the origin and history of the Eastern Mediterranean basin. Tectonophysics 298, 5-35. http://doi.org/10.1016/S0040-1951(98)00176-0

Garzanti, E., Resentini, A., Andò, S., Vezzoli, G., Pereira, A. and Vermeesch, P., 2015. Physical controls on sand composition and relative durability of detrital minerals during ultra‐long distance littoral and aeolian transport (N amibia and southern A ngola). Sedimentology 62, 971-996. http://doi.org/10.1111/sed.12169

Gehrels, G., 2014. Detrital zircon U-Pb geochronology applied to tectonics. Annu. Rev. Earth Planet. Sci. 42, 127-149. http://doi.org/10.1146/annurev-earth-050212-124012

Genç, Ş.C. and Tüysüz, O., 2010. Tectonic setting of the Jurassic bimodal magmatism in the Sakarya Zone (Central and Western Pontides), Northern Turkey: a geochemical and isotopic approach. Lithos 118, 95-111. http://doi.org/10.1016/j.lithos.2010.03.017

Glazer, A., Avigad, D., Morag, N., Güngör, T. and Gerdes, A., 2021. The Kyrenia Terrane (Northern Cyprus): Detrital Zircon Evidence for Exotic Elements in the Southern Neotethys. Tectonics 40, e2021TC006763. http://doi.org/10.1029/2021TC006763

Golan, T., Katzir, Y. and Coble, M.A., 2018. Early Carboniferous anorogenic magmatism in the Levant: implications for rifting in northern Gondwana. Int. Geol. Rev. 60, 101-108. http://doi.org/10.1080/00206814.2017.1326089

Göncüoğlu, M.C., Çapkınoğlu, S., Gursu, S., Noble, P., Turhan, N., Tekin, U.K., Okuyucu, C. and Göncüoğlu, Y., 2007. The Mississippian in the Central and Eastern Taurides (Turkey): constraints on the tectonic setting of the Tauride-Anatolide Platform. Geol. Carpathica 58, 427.

Göncüoğlu, M.C., Göncüoğlu, Y., Kozur, H.W. and Kozlu, H., 2004. Paleozoic stratigraphy of the Geyikdag Unit in the Eastern Taurides (Turkey): New age data and implications for Gondwanan evolution. Geol. Carpath. 55, 433-447.

Göncüoğlu, M.C. and Kozlu, H., 2000. Early Paleozoic evolution of the NW Gondwanaland: data from southern Turkey and surrounding regions. Gondwana Res. 3, 315-324. http://doi.org/10.1016/S1342-937X(05)70290-2

Göncüoğlu, M.C., Turhan, N. and Tekin, U.K., 2003. Evidence for the Triassic rifting and opening of the Neotethyan Izmir-Ankara Ocean and discussion on the presence of Cimmerian events at the northern edge of the Tauride-Anatolide Platform, Turkey. Bolletino Soc. Geol. Ital. Spec. Vol. 2, 203-212.

Granot, R., 2016. Palaeozoic oceanic crust preserved beneath the eastern Mediterranean. Nat. Geosci. 9, 701-705. http://doi.org/10.1038/ngeo2784

Gregory, R.T. and Taylor Jr, H.P., 1981. An oxygen isotope profile in a section of Cretaceous oceanic crust, Samail Ophiolite, Oman: Evidence for δ18O buffering of the oceans by deep (> 5 km) seawater ‐ hydrothermal circulation at mid ‐ ocean ridges. J. Geophys. Res.: Solid Earth 86, 2737-2755. http://doi.org/10.1029/JB086iB04p02737

Griffin, W., 2008. GLITTER: data reduction software for laser ablation ICP-MS. Laser Ablation ICP-MS in the Earth Sciences: Current practices outstanding issues 40, 308-311.

Grimes, C.B., Wooden, J.L., Cheadle, M.J. and John, B.E., 2015. “Fingerprinting” tectono-magmatic provenance using trace elements in igneous zircon. Contrib. Mineral. Petrol. 170, 46. http://doi.org/10.1007/s00410-015-1199-3

Gürsoy, H., Tatar, O., Piper, J., Koçbulut, F., Akpınar, Z., Huang, B., Roberts, A. and Mesci, B., 2011. Palaeomagnetic study of the Kepezdağ and Yamadağ volcanic complexes, central Turkey: Neogene tectonic escape and block definition in the central-east Anatolides. J. Geodyn. 51, 308-326. http://doi.org/10.1016/j.jog.2010.07.004

Gürsu, S. and Göncüoğlu, M.C., 2005. Early Cambrian back-arc volcanism in the western Taurides, Turkey: implications for rifting along the northern Gondwanan margin. Geol. Mag. 142, 617-631. http://doi.org/10.1017/s0016756805000919

Gürsu, S. and Göncüoğlu, M.C., 2008. Petrogenesis and geodynamic evolution of the Late Neoproterozoic post-collisional felsic magmatism in NE Afyon area, western central Turkey. In: N. Ennih and J.-P. Liégeois (Editors), The Boundaries of the West African Craton. Geological Society of London, Special Publications, pp. 409-431.

Gürsu, S., Möller, A., Göncüoglu, M.C., Köksal, S., Demircan, H., Köksal, F.T., Kozlu, H. and Sunal, G., 2015. Neoproterozoic continental arc volcanism at the northern edge of the Arabian Plate, SE Turkey. Precambrian Res. 258, 208-233. http://doi.org/10.1016/j.precamres.2014.12.017

Gürsu, S., Möller, A., Usta, D., Köksal, S., Ateş, Ş., Sunkari, E.D. and Göncüoğlu, M.C., 2017. Laser Ablation Inductively Coupled Plasma Mass Spectrometry U-Pb Dating of Detrital and Magmatic Zircons of Glacial Diamictites and Pebbles in Late Ordovician Sediments of the Taurides and Southeast Anatolian Autochthon Belt, Turkey: Indications for Their Arabian-Nubian Provenance. J. Geol. 125, 165-202. http://doi.org/10.1086/690199

Gutnic, M.F., Monod, O., Poisson, A. and Dumont, J., 1979. Geologie des Taurides Occidentales (Turquie), 137. Société Géologique de France, Mémoire, 112 pp.

Hakyemez, A. and Özkan-Altıner, S., 2007. Beşparmak Dağları’ndaki (Kuzey Kıbrıs) Üst Maastrihtiyen-Eosen İstifinin Planktonik Foraminifer Biyostratigrafisi (Planktonic

Foraminiferal Biostratigraphy of the Upper Maastrichtian – Eocene Sequence in the Beşparmak Range, Northern Cyprus), 60th Geological Congress of Turkey. Abstract Book, Ankara, pp. 416-419.

Hakyemez, Y., Turhan, N., Sönmez, I. and Sümengen, M., 2000. Kuzey Kıbrıs Türk Cumhuriyeti'nin Jeolojisi (Geology of the Turkish Republic of Northern Cyprus). Genel Müdürlüğü Jeoloji Etütleri Diaresi, Maden Tektik ve Arama, Ankara, 44 pp.

Hardenberg, M.F. and Robertson, A.H.F., 2007. Sedimentology of the NW margin of the Arabian plate and the SW–NE trending Nahr El-Kabir half-graben in northern Syria during the latest Cretaceous and Cenozoic. Sediment. Geol. 201, 231-266. http://doi.org/10.1016/j.sedgeo.2007.02.009

Harris, S.E. and Mix, A.C., 2002. Climate and tectonic influences on continental erosion of tropical South America, 0–13 Ma. Geology 30, 447-450. http://doi.org/10.1130/0091-7613(2002)030<0447:CATIOC>2.0.CO;2

Harrison, R., Newell, W., Batıhanlı, H., Panayides, I., McGeehin, J., Mahan, S., Őzhűr, A., Tsiolakis, E. and Necdet, M., 2004. Tectonic framework and Late Cenozoic tectonic history of the northern part of Cyprus: implications for earthquake hazards and regional tectonics. J. Asian Earth Sci. 23, 191-210.

Hawkesworth, C. and Kemp, A., 2006. Using hafnium and oxygen isotopes in zircons to unravel the record of crustal evolution. Chem. Geol. 226, 144-162. http://doi.org/10.1016/j.chemgeo.2005.09.018

Hay, D. and Dempster, T., 2009. Zircon behaviour during low-temperature metamorphism. J. Petrol. 50, 571-589. http://doi.org/10.1093/petrology/egp011

Hayward, A. and Robertson, A., 1982. Direction of ophiolite emplacement inferred from Cretaceous and Tertiary sediments of an adjacent autochthon, the Bey Daglari, southwest Turkey. Geol. Soc. Am. Bull. 93, 68-75. http://doi.org/10.1130/0016-7606(1982)93<68:DOOEIF>2.0.CO;2

Henson, F.R.S., Browne, R.V. and McGinty, J., 1949. A synopsis of the stratigraphy and geological history of Cyprus. Quarterly Journal of the Geological Society, 105, 41 pp.

Hoskin, P.W. and Schaltegger, U., 2003. The composition of zircon and igneous and metamorphic petrogenesis. Rev. Mineral. Geochem. 53, 27-62. http://doi.org/10.2113/0530027

Hu, Z., Liu, Y., Gao, S., Liu, W., Zhang, W., Tong, X., Lin, L., Zong, K., Li, M. and Chen, H., 2012. Improved in situ Hf isotope ratio analysis of zircon using newly designed X skimmer cone and jet sample cone in combination with the addition of nitrogen by laser ablation multiple collector ICP-MS. J. Anal. At. Spectrom. 27, 1391-1399. http://doi.org/10.1039/C2JA30078H

Huang, K., Malpas, J. and Xenophontos, C., 2007. Geological studies of igneous rocks and their relationships along the Kyrenia Range. In: K. Moumani, K. Shawabkeh, A. Al-Malabeh and M. Abdelghafoor (Editors), 6th International Congress of Eastern Mediterranean Geology, Amman, Jordan, pp. 53.

Huang, S., Meijers, M.J.M., Eyres, A., Mulch, A. and Fritz, S.A., 2019. Unravelling the history of biodiversity in mountain ranges through integrating geology and biogeography. J. Biogeogr. 46, 1777-1791. http://doi.org/10.1111/jbi.13622

Innocenti, F., Mazzuoli, R., Pasquare, G., Di Brozolo, F.R. and Villari, L., 1975. The Neogene calcalkaline volcanism of Central Anatolia: geochronological data on Kayseri-Nigde area. Geol. Mag. 112, 349-360. http://doi.org/10.1017/S0016756800046744

Jaffey, N. and Robertson, A., 2005. Non-marine sedimentation associated with Oligocene-Recent exhumation and uplift of the Central Taurus Mountains, S Turkey. Sediment. Geol. 173, 53-89. http://doi.org/10.1016/j.sedgeo.2003.11.025

Jaffey, N., Robertson, A. and Pringle, M., 2004. Latest Miocene and Pleistocene ages of faulting, determined by 40Ar/39Ar single-crystal dating of airfall tuff and silicic extrusives of the Erciyes Basin, central Turkey: evidence for intraplate deformation related to the tectonic escape of Anatolia. Terra Nova 16, 45-53. http://doi.org/10.1111/j.1365-3121.2003.00526.x

Karaoğlan, F., Parlak, O., Hejl, E., Neubauer, F. and Kloetzli, U., 2016. The temporal evolution of the active margin along the Southeast Anatolian Orogenic Belt (SE Turkey): Evidence from U–Pb, Ar–Ar and fission track chronology. Gondwana Res. 33, 190-208. http://doi.org/10.1016/j.gr.2015.12.011

Karaoğlan, F., Parlak, O., Klötzli, U., Thöni, M. and Koller, F., 2012. U–Pb and Sm–Nd geochronology of the ophiolites from the SE Turkey: implications for the Neotethyan evolution. Geodin. Acta 25, 146-161. http://doi.org/10.1080/09853111.2013.858948

Karaoğlan, F., Parlak, O., Klötzli, U.R.S., Thöni, M. and Koller, F., 2013. U–Pb and Sm–Nd geochronology of the Kızıldağ (Hatay, Turkey) ophiolite: implications for the timing and duration of suprasubduction zone type oceanic crust formation in the southern Neotethys. Geol. Mag. 150, 283-299. http://doi.org/10.1017/s0016756812000477

Karsli, O., Dokuz, A. and Kandemir, R., 2016. Subduction-related Late Carboniferous to Early Permian Magmatism in the Eastern Pontides, the Camlik and Casurluk plutons: Insights from geochemistry, whole-rock Sr–Nd and in situ zircon Lu–Hf isotopes, and U–Pb geochronology. Lithos 266-267, 98-114. http://doi.org/10.1016/j.lithos.2016.10.007

Keller, C.B., Boehnke, P. and Schoene, B., 2017. Temporal variation in relative zircon abundance throughout Earth history. Geochem. Perspect. Lett. 3, 179-189. http://doi.org/10.7185/geochemlet.1721

Kelling, G., Gökçen, S.L., Floyd, P.A. and Gökçen, N., 1987. Neogene tectonics and plate convergence in the eastern Mediterranean: new data from southern Turkey. Geology 15, 425-429. http://doi.org/10.1130/0091-7613(1987)15<425:NTAPCI>2.0.CO;2

Kempler, D. and Garfunkel, Z., 1994. Structures and kinematics in the northeastern Mediterranean: a study of an irregular plate boundary. Tectonophysics 234, 19-32. http://doi.org/10.1016/0040-1951(94)90202-X

Kempler, D., 1998. Eratosthenes Seamount: The possible spearhead of incipient continental collision in the Eastern Mediterranean. In: A.H.F. Robertson, K.-C. Emeis, C. Richter and A. Camerlenghi (Editors), Proceedings of the Ocean Drilling Program, Scientific Results. Ocean Drilling Program, College Station, TX, pp. 709-721.

Keskin, M., Pearce, J.A. and Mitchell, J., 1998. Volcano-stratigraphy and geochemistry of collision-related volcanism on the Erzurum–Kars Plateau, northeastern Turkey. J. Volcanol. Geotherm. Res. 85, 355-404. http://doi.org/10.1016/S0377-0273(98)00063-8

Kinnaird, T. and Robertson, A., 2013. Tectonic and sedimentary response to subduction and incipient continental collision in southern Cyprus, easternmost Mediterranean region. In: A.H.F. Robertson, O. Parlak and U.C. Ünlügenç (Editors), Geological Development of Anatolia and the Easternmost Mediterranean Region. Geological Society of London, Special Publications, pp. 585-614.

Kumar, A., Dutt, S., Saraswat, R., Gupta, A.K., Clift, P.D., Pandey, D.K., Yu, Z. and Kulhanek, D.K., 2020. A late pleistocene sedimentation in the Indus fan, Arabian Sea, IODP site U1457. Geol. Mag. 157, 920-928. http://doi.org/10.1017/S0016756819000396

Lin, Y.-C., Chung, S.-L., Bingöl, A., Beyarslan, M., Lee, H. and Yang, J.-H., 2015. Petrogenesis of late Cretaceous Elazig magmatic rocks from SE Turkey: New age and geochemical and Sr-Nd-Hf isotopic constraints, Goldschmidt 2015 Abstracts, Prague, pp. 1869.

Linnemann, U., Ouzegane, K., Drareni, A., Hofmann, M., Becker, S., Gärtner, A. and Sagawe, A., 2011. Sands of West Gondwana: An archive of secular magmatism and plate interactions — A case study from the Cambro-Ordovician section of the Tassili Ouan Ahaggar (Algerian Sahara) using U–Pb–LA-ICP-MS detrital zircon ages. Lithos 123, 188-203. http://doi.org/10.1016/j.lithos.2011.01.010

Lord, A.R., Panayides, I., Urquhart, E. and Xenophontos, C., 2000. A biochronostratigraphical framework for the Late Cretaceous-Recent circum-Troodos sedimentary sequence, Cyprus. In: I. Panayides, C. Xenophontos and J. Malpas (Editors), Proceedings of the Third International Conference on the Geology of the Eastern Mediterranean. Cyprus Geological Survey Department, Nicosia, Cyprus, pp. 289-298.

Löwen, K., Meinhold, G., Arslan, A., Güngör, T. and Berndt, J., 2020. Evolution of the Palaeotethys in the Eastern Mediterranean: a multi-method approach to unravel the age, provenance and tectonic setting of the Upper Palaeozoic Konya Complex and its Mesozoic cover sequence (south-central Turkey). Int. Geol. Rev. 62, 389-414. http://doi.org/10.1080/00206814.2019.1616619

Löwen, K., Meinhold, G., Güngör, T. and Berndt, J., 2017. Palaeotethys-related sediments of the Karaburun Peninsula, western Turkey: constraints on provenance and stratigraphy from detrital zircon geochronology. Int. J. Earth Sci. 106, 2771-2796. http://doi.org/10.1007/s00531-017-1458-9

Mackintosh, P.W. and Robertson, A.H.F., 2009. Structural and sedimentary evidence from the northern margin of the Tauride platform: Testing models of Late Triassic

‘Cimmerian’uplift and deformation in southern Turkey. Tectonophysics 473, 203-215. http://doi.org/10.1016/j.tecto.2008.10.031

Mackintosh, P.W. and Robertson, A.H.F., 2012. Late Devonian–Late Triassic sedimentary development of the central Taurides, S Turkey: Implications for the northern margin of Gondwana. Gondwana Res. 21, 1089-1114. http://doi.org/10.1016/j.gr.2011.07.016

Mackintosh, P.W. and Robertson, A.H.F., 2013. Sedimentary and structural evidence for two-phase Upper Cretaceous and Eocene emplacement of the Tauride thrust sheets in central southern Turkey. In: A.H.F. Robertson, O. Parlak and Ü.C. Ünlügenç (Editors), Geological Development of Anatolia and the Easternmost Mediterranean Region. Geological Society of London, Special Publications, pp. 299-322.

Maffione, M., van Hinsbergen, D.J., de Gelder, G.I., van der Goes, F.C. and Morris, A., 2017. Kinematics of Late Cretaceous subduction initiation in the Neo‐Tethys Ocean reconstructed from ophiolites of Turkey, Cyprus, and Syria. J. Geophys. Res.: Solid Earth 122, 3953-3976. http://doi.org/10.1002/2016JB013821

Mange, M.A. and Maurer, H., 2012. Heavy minerals in colour. Chapman and Hall, London, 147 pp.

Marcoux, J., Ricou, L., Burg, J. and Brun, J., 1989. Shear-sense criteria in the Antalya and Alanya thrust system (southwestern Turkey): evidence for a southward emplacement. Tectonophysics 161, 81-91. http://doi.org/10.1016/0040-1951(89)90304-1

Marroni, M., Göncüoğlu, M.C., Frassi, C., Sayit, K., Pandolfi, L., Ellero, A. and Ottria, G., 2020. The Intra-Pontide ophiolites in Northern Turkey revisited: From birth to death of a Neotethyan oceanic domain. Geosci. Front. 11, 129-149. http://doi.org/10.1016/j.gsf.2019.05.010

Maury, R.C., Lapierre, H., Bosch, D., Marcoux, J., Krystyn, L., Cotten, J., Bussy, F., Brunet, P. and Senebier, F., 2008. The alkaline intraplate volcanism of the Antalya nappes (Turkey): a Late Triassic remnant of the Neotethys. Bull. Soc. Géol. Fr. 179, 397-410. http://doi.org/10.2113/gssgfbull.179.4.397

McCay, G.A., 2010. Tectonic-sedimentary evolution of the Girne (Kyrenia) Range and the Mesarya (Mesaoria) Basin, North Cyprus. Unpublished PhD thesis Thesis, University of Edinburgh, 586 pp.

McCay, G.A. and Robertson, A.H.F., 2012. Late Eocene–Neogene sedimentary geology of the Girne (Kyrenia) Range, northern Cyprus: A case history of sedimentation related to progressive and diachronous continental collision. Sediment. Geol. 265, 30-55. http://doi.org/10.1016/j.sedgeo.2012.03.001

McCay, G.A. and Robertson, A.H.F., 2013. Upper Miocene–Pleistocene deformation of the Girne (Kyrenia) Range and Dar Dere (Ovgos) lineaments, northern Cyprus: role in collision and tectonic escape in the easternmost Mediterranean region. In: A.H.F. Robertson, O. Parlak and U.C. Ünlügenç (Editors), Geological Development of Anatolia and the Easternmost Mediterranean Region. Geological Society of London, Special Publications, pp. 421-445.

McCay, G.A., Robertson, A.H.F., Kroon, D., Raffi, I., Ellam, R.M. and Necdet, M., 2013. Stratigraphy of Cretaceous to Lower Pliocene sediments in the northern part of Cyprus based on comparative $^{87}Sr/^{86}Sr$ isotopic, nannofossil and planktonic foraminiferal dating. Geol. Mag. 150, 333-359. http://doi.org/10.1017/s0016756812000465

McPhee, P.J. and van Hinsbergen, D.J., 2019. Tectonic reconstruction of Cyprus reveals Late Miocene continental collision of Africa and Anatolia. Gondwana Res. 68, 158-173. http://doi.org/10.1016/j.gr.2018.10.015

McPhee, P.J., Altıner, D. and Van Hinsbergen, D.J., 2018. First balanced cross section across the Taurides fold‐thrust belt: geological constraints on the subduction history of the Antalya slab in southern Anatolia. Tectonics 37, 3738-3759. http://doi.org/10.1029/2017TC004893

Meijers, M.J.M., Brocard, G.Y., Whitney, D.L. and Mulch, A., 2020. Paleoenvironmental conditions and drainage evolution of the central Anatolian lake system (Turkey) during late Miocene to Pliocene surface uplift. Geosphere 16, 490-509. http://doi.org/10.1130/ges02135.1

Meinhold, G. and Frei, D., 2008. Detrital zircon ages from the islands of Inousses and Psara, Aegean Sea, Greece: constraints on depositional age and provenance. Geol. Mag. 145, 886-891. http://doi.org/10.1017/S0016756808005505

Molnar, P., 2004. Late Cenozoic increase in accumulation rates of terrestrial sediment: How might climate change have affected erosion rates? Annu. Rev. Earth Planet. Sci. 32, 67-89. http://doi.org/10.1146/annurev.earth.32.091003.143456

Monod, O., 1977. Récherches Géologique dans les Taurus occidental au sud de Beyşehir (Turquie), Université de Paris-Sud, Orsay, France.

Moore, T.A., 1960. The geology and mineral resources of the Astromeritis-Kormakiti area. Geological Survey Department, Memoir 6, Nicosia, Cyprus, 96 pp.

Morag, N., Haviv, I. and Katzir, Y., 2016. From ocean depths to mountain tops: uplift of the Troodos ophiolite (Cyprus) constrained by low-temperature thermochronology and geomorphic analysis. Tectonics 35, 622-637. http://doi.org/10.1002/2015tc004069

MTA, 2011. Geological map of Turkey 1:250,000 (General Directorate of Mineral Research and Exploration). Maden Tektik ve Arama Genel Müdürlüğü (MTA), Ankara.

Mukasa, S.B. and Ludden, J.N., 1987. Uranium-lead isotopic ages of plagiogranites from the Troodos ophiolite, Cyprus, and their tectonic significance. Geology 15, 825-828. http://doi.org/10.1130/0091-7613(1987)15<825:UIAOPF>2.0.CO;2

Necdet, M. and Anıl, M., 2006. The Geology and Geochemistry of the Gypsum Deposits in Northern Cyprus. Geosound 48, 11-50.

Nurlu, N., Parlak, O., Robertson, A.H.F. and von Quadt, A., 2016. Implications of Late Cretaceous U–Pb zircon ages of granitic intrusions cutting ophiolitic and volcanogenic rocks for the assembly of the Tauride allochthon in SE Anatolia (Helete area, Kahramanmaraş Region, SE Turkey). Int. J. Earth Sci. 105, 283-314. http://doi.org/10.1007/s00531-015-1211-1

Okay, A.I. and Topuz, G., 2017. Variscan orogeny in the Black Sea region. Int. J. Earth Sci. 106, 569-592. http://doi.org/10.1007/s00531-016-1395-z

Okay, A.I., 2001. Stratigraphic and metamorphic inversions in the central Menderes Massif: a new structural model. Int. J. Earth Sci. 89, 709-727. http://doi.org/10.1007/s005310000098

Okay, A.I., 2002. Jadeite–chloritoid–glaucophane–lawsonite blueschists in north‐west Turkey: unusually high P/T ratios in continental crust. J. Metamorph. Geol. 20, 757-768. http://doi.org/10.1046/j.1525-1314.2002.00402.x

Okay, A.I., Altiner, D. and Kilic, A.M., 2015. Triassic limestone, turbidites and serpentinite–the Cimmeride orogeny in the Central Pontides. Geol. Mag. 152, 460-479. http://doi.org/10.1017/S0016756814000429

Okay, A.I., Bozkurt, E., Satır, M., Yiğitbaş, E., Crowley, Q.G. and Shang, C.K., 2008a. Defining the southern margin of Avalonia in the Pontides: geochronological data from the Late Proterozoic and Ordovician granitoids from NW Turkey. Tectonophysics 461, 252-264. http://doi.org/10.1016/j.tecto.2008.02.004

Okay, A.I., Harris, N.B. and Kelley, S.P., 1998. Exhumation of blueschists along a Tethyan suture in northwest Turkey. Tectonophysics 285, 275-299. http://doi.org/10.1016/S0040-1951(97)00275-8

Okay, A.I., Satır, M. and Shang, C.K., 2008b. Ordovician metagranitoid from the Anatolide‐Tauride Block, northwest Turkey: geodynamic implications. Terra Nova 20, 280-288. http://doi.org/10.1111/j.1365-3121.2008.00818.x

Okay, A.I., Sunal, G., Sherlock, S., Kylander‐Clark, A.R.C. and Özcan, E., 2020. İzmir‐Ankara Suture as a Triassic to Cretaceous Plate Boundary—Data From Central Anatolia. Tectonics 39. http://doi.org/10.1029/2019tc005849

Okay, A.I., Zattin, M. and Cavazza, W., 2010. Apatite fission-track data for the Miocene Arabia-Eurasia collision. Geology 38, 35-38. http://doi.org/10.1130/G30234.1

Önal, A., Boztuğ, D., Arslan, M., Spell, T.L. and Kueruem, S., 2008. Petrology and ^{40}Ar-^{39}Ar Age of the Bimodal Orduzu Volcanics (Malatya) from the Western end of the Eastern Anatolian Neogene Volcanism, Turkey. Turk. J. Earth Sci. 17, 85-109.

Oyan, V., 2018. Ar-Ar dating and petrogenesis of the Early Miocene Taşkapı-Mecitli (Erciş-Van) granitoid, Eastern Anatolia Collisional Zone, Turkey. J. Asian Earth Sci. 158, 210-226. http://doi.org/10.1016/j.jseaes.2018.03.002

Özbey, Z., Ustaömer, T., Robertson, A.H.F. and Ustaömer, P.A., 2013. Tectonic significance of Late Ordovician granitic magmatism and clastic sedimentation on the northern margin of Gondwana (Tavşanlı Zone, NW Turkey). J. Geol. Soc. 170, 159-173. http://doi.org/10.1144/jgs2011-091

Özer, S., Sözbilir, H., Özkar, İ., Toker, V. and Sari, B., 2001. Stratigraphy of Upper Cretaceous–Palaeogene sequences in the southern and eastern Menderes Massif (western Turkey). Int. J. Earth Sci. 89, 852-866. http://doi.org/10.1007/s005310000142

Özgül, N., 1984a. Stratigraphy and tectonic evolution of the central Taurides. In: O. Tekeli and M.C. Göncüoğlu (Editors), Proceedings of the International Symposium on the Geology of the Taurus Belt. MTA, Ankara, pp. 77-90.

Özgül, N., 1984b. Alanya Tektonik Penceresi ve Bati Kesiminin Jeolojisi (Alanya tectonic window and geology of its western part). Geological Society of Turkey, Ketin Symposium, Ankara, pp. 97–120.

Özgül, N., 1997. Stratigraphy of the tectonostratigraphical units around Hadim–Bozkir–Taşkent region, northern part of the Central Taurides. Bull. Miner. Resour. Exloration (Turk.) 119, 113-174.

Palamakumbura, R., 2016. Sedimentary response to the tectonic uplift of the Kyrenia Range, northern Cyprus, in its Eastern Mediterranean tectonic setting. Unpublished PhD Thesis Thesis, University of Edinburgh, UK, 417 pp.

Palamakumbura, R.N. and Robertson, A.H.F., 2016. Pleistocene terrace deposition related to tectonically controlled surface uplift: An example of the Kyrenia Range lineament in the northern part of Cyprus. Sediment. Geol. 339, 46-67. http://doi.org/10.1016/j.sedgeo.2016.03.022

Palamakumbura, R.N. and Robertson, A.H.F., 2018. Pliocene–Pleistocene sedimentary–tectonic development of the Mesaoria (Mesarya) Basin in an incipient, diachronous collisional setting: facies evidence from the north of Cyprus. Geol. Mag. 155, 997-1022. http://doi.org/10.1017/S0016756816001072

Palamakumbura, R.N., Robertson, A.H.F., Kinnaird, T.C., van Calsteren, P., Kroon, D. and Tait, J.A., 2016. Quantitative dating of Pleistocene deposits of the Kyrenia

Range, northern Cyprus: implications for timing, rates of uplift and driving mechanisms. J. Geol. Soc. 173, 933-948. http://doi.org/10.1144/jgs2015-130

Parlak, O., 2006. Geodynamic significance of granitoid magmatism in the southeast Anatolian orogen: geochemical and geochronogical evidence from Göksun–Afşin (Kahramanmaraş, Turkey) region. Int. J. Earth Sci. 95, 609-627.

Parlak, O., Karaoğlan, F., Rızaoğlu, T., Klötzli, U., Koller, F. and Billor, Z., 2013. U–Pb and ^{40}Ar–^{39}Ar geochronology of the ophiolites and granitoids from the Tauride belt: implications for the evolution of the Inner Tauride suture. J. Geodyn. 65, 22-37.

Parlak, O. and Robertson, A.H.F., 2004. The ophiolite-related Mersin Melange, southern Turkey: its role in the tectonic–sedimentary setting of Tethys in the Eastern Mediterranean region. Geol. Mag. 141, 257-286. http://doi.org/10.1017/S0016756804009094

Pearce, J.A., Bender, J., De Long, S., Kidd, W., Low, P., Güner, Y., Saroglu, F., Yilmaz, Y., Moorbath, S. and Mitchell, J., 1990. Genesis of collision volcanism in Eastern Anatolia, Turkey. J. Volcanol. Geotherm. Res. 44, 189-229. http://doi.org/10.1016/0377-0273(90)90018-B

Perinçek, D. and Kozlu, H., 1984. Stratigraphy and structural relations of the units in the Afşin-Elbistan-Doğanşehir region (Eastern Taurus). In: O. Tekeli and M.C. Göncüoğlu (Editors), Geology of the Taurus Belt: Proceedings of the International Symposium. Maden Tetkik ve Arama Enstitüsü, Ankara, pp. 181-198.

Pickering, K.T., Pouderoux, H., McNeill, L.C., Backman, J., Chemale, F., Kutterolf, S., Milliken, K.L., Mukoyoshi, H., Henstock, T.J., Stevens, D.E., Parnell, C. and Dugan, B., 2020. Sedimentology, stratigraphy and architecture of the Nicobar Fan (Bengal–Nicobar Fan System), Indian Ocean: Results from International Ocean Discovery Program Expedition 362. Sedimentology 67, 2248-2281. http://doi.org/10.1111/sed.12701

Platzman, E., Tapirdamaz, C. and Sanver, M., 1998. Neogene anticlockwise rotation of central Anatolia (Turkey): preliminary palaeomagnetic and geochronological results. Tectonophysics 299, 175-189. http://doi.org/10.1016/S0040-1951(98)00204-2

Poisson, A., 1977. Recherches géologiques dans les Taurides occidentales (Turquie). Unpublished PhD thesis Thesis, Université de Paris-Sud Orsayde, 795 pp.

Poole, A. and Robertson, A., 1991. Quaternary uplift and sea-level change at an active plate boundary, Cyprus. J. Geol. Soc. 148, 909-921. http://doi.org/10.1144/gsjgs.148.5.0909

Pourteau, A., Candan, O. and Oberhänsli, R., 2010. High‐pressure metasediments in central Turkey: Constraints on the Neotethyan closure history. Tectonics 29. http://doi.org/10.1029/2009TC002650

Pourteau, A., Oberhänsli, R., Candan, O., Barrier, E. and Vrielynck, B., 2016. Neotethyan closure history of western Anatolia: a geodynamic discussion. Int. J. Earth Sci. 105, 203-224. http://doi.org/10.1007/s00531-015-1226-7

Racano, S., Jara‐Muñoz, J., Cosentino, D. and Melnick, D., 2020. Variable Quaternary Uplift Along the Southern Margin of the Central Anatolian Plateau Inferred From Modeling Marine Terrace Sequences. Tectonics 39. http://doi.org/10.1029/2019tc005921

Reiche, S. and Hübscher, C., 2015. The Hecataeus Rise, easternmost Mediterranean: A structural record of Miocene-Quaternary convergence and incipient continent-continent-collision at the African-Anatolian plate boundary. Mar. Pet. Geol. 67, 368-388. http://doi.org/10.1016/j.marpetgeo.2015.04.021

Ring, U. and Pantazides, H., 2019. The uplift of the Troodos massif, Cyprus. Tectonics 38, 3124-3139. http://doi.org/10.1029/2019TC005514

Robertson, A.H.F. and Dixon, J.E., 1984. Introduction: aspects of the geological evolution of the Eastern Mediterranean. In: J.E. Dixon and A.H.F. Robertson (Editors), The Geological Evolution of the Eastern Mediterranean. Geological Society of London, Special Publications, pp. 1-74.

Robertson, A.H.F. and Kinnaird, T.C., 2016. Structural development of the central Kyrenia Range (north Cyprus) in its regional setting in the eastern Mediterranean region. Int. J. Earth Sci. 105, 417-437. http://doi.org/10.1007/s00531-015-1215-x

Robertson, A.H.F. and Parlak, O., 2020. Late Cretaceous-Palaeocene subduction-collision-exhumation of a microcontinent along the northern, active margin of South Neotethys: evidence from the Alanya Massif and the adjacent Antalya Complex (S Turkey). J. Asian Earth Sci. 104467. http://doi.org/10.1016/j.jseaes.2020.104467

Robertson, A.H.F. and Ustaömer, T., 2009a. Formation of the Late Palaeozoic Konya Complex and comparable units in southern Turkey by subduction–accretion processes: Implications for the tectonic development of Tethys in the Eastern Mediterranean region. Tectonophysics 473, 113-148. http://doi.org/10.1016/j.tecto.2008.10.027

Robertson, A.H.F. and Ustaömer, T., 2009b. Upper Palaeozoic subduction/accretion processes in the closure of Palaeotethys: Evidence from the Chios Melange (E Greece), the Karaburun Melange (W Turkey) and the Teke Dere Unit (SW Turkey). Sediment. Geol. 220, 29-59. http://doi.org/10.1016/j.sedgeo.2009.06.005

Robertson, A.H.F. and Waldron, J., 1990. Geochemistry and tectonic setting of Late Triassic and late Jurassic–Early Cretaceous basaltic extrusives from the Antalya Complex, SW Turkey. In: M.Y. Savaşçin and A.H. Eronat (Editors), Proceedings of the International Earth Sciences Congress on Aegean Regions, Izmir, Turkey, pp. 279-299.

Robertson, A.H.F. and Woodcock, N.H., 1979. Mamonia Complex, southwest Cyprus: Evolution and emplacement of a Mesozoic continental margin. Geol. Soc. Am. Bull. 90, 651-665. http://doi.org/10.1130/0016-7606(1979)90<651:mcscea>2.0.co;2

Robertson, A.H.F. and Woodcock, N.H., 1984. The SW segment of the Antalya Complex, Turkey as a Mesozoic-Tertiary Tethyan continental margin. In: J.E. Dixon and A.H.F. Robertson (Editors), The Geological Evolution of the Eastern Mediterranean. Geological Society of London, Special Publications, pp. 251-271.

Robertson, A.H.F. and Woodcock, N.H., 1986. The role of the Kyrenia Range Lineament, Cyprus, in the geological evolution of the eastern Mediterranean area. Philos. Trans. R. Soc. Lond., Math. Phys. Sci. 317, 141-177. http://doi.org/10.1098/rsta.1986.0030

Robertson, A.H.F., 1990. Tectonic evolution of Cyprus. In: J. Malpas, E.M. Moores, A. Panayiotou and C. Xenophontos (Editors), Ophiolites-Oceanic Crustal Analogues: Proceedings of the International Symposium ‘Troodos 1987’. Cyprus Geological Survey Department, Nicosia, pp. 235-250.

Robertson, A.H.F., 1998. Mesozoic-Tertiary tectonic evolution of the easternmost Mediterranean area: integration of marine and land evidence. In: A.H.F. Robertson, K.-C. Emeis, C. Richter and A. Camerlenghi (Editors), Proceedings of the Ocean Drilling Program, Scientific Results. Ocean Drilling Program, College Station, TX, pp. 723-782.

Robertson, A.H.F., 2022. Palaeozoic-Early Mesozoic transition from Palaeotethys to Neotethys: Synthesis of data and interpretations from the northern periphery of Gondwana (central and western Anatolia, Aegean, Balkans and Sicily). Earth-Sci. Rev. 230, 104000. http://doi.org/10.1016/j.earscirev.2022.104000

Robertson, A.H.F., Boulton, S.J., Taslı, K., Yıldırım, N., İnan, N., Yıldız, A. and Parlak, O., 2016. Late Cretaceous-Miocene sedimentary development of the Arabian continental margin in SE Turkey (Adıyaman region): Implications for regional palaeogeography and the closure history of Southern Neotethys. J. Asian Earth Sci. 115, 571-616. http://doi.org/10.1016/j.jseaes.2015.01.025

Robertson, A.H.F., McCay, G.A., Tasli, K. and Yıldız, A., 2014. Eocene development of the northerly active continental margin of the Southern Neotethys in the Kyrenia Range, north Cyprus. Geol. Mag. 151, 692-731. http://doi.org/10.1017/s0016756813000563

Robertson, A.H.F., Necdet, M., Raffi, I. and Chen, G., 2019. Early Messinian manganese deposition in NE Cyprus related to cyclical redox changes in a silled hemipelagic basin prior to the Mediterranean salinity Crisis. Sediment. Geol. 385, 126-148. http://doi.org/10.1016/j.sedgeo.2019.03.009

Robertson, A.H.F., Parlak, O. and Ustaömer, T., 2012a. Overview of the Palaeozoic-Neogene evolution of Neotethys in the Eastern Mediterranean region (southern Turkey, Cyprus, Syria). Pet. Geosci. 18, 381-404. http://doi.org/10.1144/petgeo2011-091

Robertson, A.H.F., Parlak, O. and Ustaömer, T., 2021a. Late Palaeozoic extensional volcanism along the northern margin of Gondwana in southern Turkey: implications for Palaeotethyan development. Int. J. Earth Sci. 110, 1961-1994. http://doi.org/10.1007/s00531-021-02051-7

Robertson, A.H.F., Parlak, O., Kinnaird, T.C., Taslı, K. and Dumitrica, P., 2020. Cambrian-Eocene pre-rift, pulsed rift, passive margin and emplacement processes along the northern margin of the Southern Neotethys: evidence from the Antalya Complex in the Alanya Window (S Turkey). J. Asian Earth Sci.: X 3, 100026. http://doi.org/10.1016/j.jaesx.2020.100026

Robertson, A.H.F., Parlak, O., Ustaömer, T., Taslı, K. and Dumitrica, P., 2021b. Late Palaeozoic-Neogene sedimentary and tectonic development of the Tauride continent and adjacent Tethyan ocean basins in eastern Turkey: new data and integrated interpretation. J. Asian Earth Sci.104859. http://doi.org/10.1016/j.jseaes.2021.104859

Robertson, A.H.F., Parlak, O., Ustaömer, T., Taslı, K., İnan, N., Dumitrica, P. and Karaoğlan, F., 2013. Subduction, ophiolite genesis and collision history of Tethys adjacent to the Eurasian continental margin: new evidence from the Eastern Pontides, Turkey. Geodin. Acta 26, 230-293. http://doi.org/10.1080/09853111.2013.877240

Robertson, A.H.F., Tasli, K. and İnan, N., 2012b. Evidence from the Kyrenia Range, Cyprus, of the northerly active margin of the Southern Neotethys during Late Cretaceous–Early Cenozoic time. Geol. Mag. 149, 264-290. http://doi.org/10.1017/s0016756811000677

Robertson, A.H.F., Unlügenç, Ü.C., İnan, N. and Tasli, K., 2004. The Misis–Andırın Complex: a Mid-Tertiary melange related to late-stage subduction of the Southern Neotethys in S Turkey. J. Asian Earth Sci. 22, 413-453. http://doi.org/10.1016/s1367-9120(03)00062-2

Robertson, A.H.F., Ustaömer, T., Parlak, O., Ünlügenç, U.C., Taşlı, K. and İnan, N., 2006. The Berit transect of the Tauride thrust belt, S Turkey: Late Cretaceous-Early Cenozoic accretionary/collisional processes related to closure of the Southern Neotethys. J. Asian Earth Sci. 27, 108-145. http://doi.org/10.1016/j.jseaes.2005.02.004

Rojay, B., Altıner, D., Altıner, S.Ö., Pırıl Önen, A., James, S. and Thirlwall, M.F., 2004. Geodynamic significance of the Cretaceous pillow basalts from North Anatolian Ophiolitic Mélange Belt (Central Anatolia, Turkey): geochemical and paleontological constraints. Geodin. Acta 17, 349-361. http://doi.org/10.3166/ga.17.349-361

Rolland, Y., Sosson, M., Adamia, S. and Sadradze, N., 2011. Prolonged Variscan to Alpine history of an active Eurasian margin (Georgia, Armenia) revealed by $^{40}Ar/^{39}Ar$ dating. Gondwana Res. 20, 798-815. http://doi.org/10.1016/j.gr.2011.05.007

Roveri, M., Flecker, R., Krijgsman, W., Lofi, J., Lugli, S., Manzi, V., Sierro, F.J., Bertini, A., Camerlenghi, A., De Lange, G., Govers, R., Hilgen, F.J., Hübscher, C., Meijer, P.T. and Stoica, M., 2014. The Messinian Salinity Crisis: Past and future of a great challenge for marine sciences. Mar. Geol. 352, 25-58. http://doi.org/10.1016/j.margeo.2014.02.002

Rubatto, D., 2002. Zircon trace element geochemistry: partitioning with garnet and the link between U–Pb ages and metamorphism. Chem. Geol. 184, 123-138. http://doi.org/10.1016/S0009-2541(01)00355-2

Şahin, N., Altıner, D. and Bülent Ercengiz, M., 2012. Discovery of Middle Permian volcanism in the Antalya Nappes, southern Turkey: tectonic significance and global meaning. Geodin. Acta 25, 286-304. http://doi.org/10.1080/09853111.2013.858949

Sarıfakıoğlu, E., Dilek, Y., Sevin, M. and Sorkhabi, R., 2017. New synthesis of the Izmir-Ankara-Erzincan suture zone and the Ankara mélange in northern Anatolia based on new geochemical and geochronological constraints. In: R. Sorkhabi (Editor), Tectonic Evolution, Collision, and Seismicity of Southwest Asia: In Honor of Manuel Berberian's Forty-Five Years of Research Contributions. Geological Society of America, Special Papers, pp. 1-63.

Sayit, K., Bedi, Y., Tekin, U.K., Göncüoglu, M.C. and Okuyucu, C., 2017. Middle Triassic back-arc basalts from the blocks in the Mersin Melange, southern Turkey: Implications for the geodynamic evolution of the Northern Neotethys. Lithos 268, 102-113. http://doi.org/10.1016/j.lithos.2016.10.032

Sayit, K., Bedi, Y., Tekin, U.K. and Okuyucu, C., 2020. Carnian (Upper Triassic) Lavas and Tuffites from the Mersin Mélange: Evidence for Intraoceanic Arc Rifting in the Northern Neotethys. J. Geol. 128, 445-464. http://doi.org/10.1086/711000

Sayit, K., Göncüoglu, M.C. and Tekin, U.K., 2015. Middle Carnian arc-type basalts from the Lycian nappes, southwestern Anatolia: Early Late Triassic subduction in the northern branch of Neotethys. J. Geol. 123, 561-579. http://doi.org/10.1086/683664

Schildgen, T.F., Cosentino, D., Bookhagen, B., Niedermann, S., Yıldırım, C., Echtler, H., Wittmann, H. and Strecker, M.R., 2012. Multi-phased uplift of the southern margin of the Central Anatolian plateau, Turkey: A record of tectonic and upper mantle processes. Earth Planet. Sci. Lett. 317-318, 85-95. http://doi.org/10.1016/j.epsl.2011.12.003

Schleiffarth, W.K., Darin, M.H., Reid, M.R. and Umhoefer, P.J., 2018. Dynamics of episodic Late Cretaceous–Cenozoic magmatism across Central to Eastern Anatolia: New insights from an extensive geochronology compilation. Geosphere 14, 1990-2008. http://doi.org/10.1130/ges01647.1

Şengör, A.M.C. and Yılmaz, Y., 1981. Tethyan evolution of Turkey: a plate tectonic approach. Tectonophysics 75, 181-241. http://doi.org/10.1016/0040-1951(81)90275-4

Ṣengör, A.M.C., Lom, N., Sunal, G., Zabcı, C. and Sancar, T., 2019. The phanerozoic palaeotectonics of Turkey. Part I: an inventory. Mediterr. Geosci. Rev. 1, 91-161. http://doi.org/10.1007/s42990-019-00007-3

Şengün, F., Zack, T. and Dunkl, I., 2020. Provenance of detrital rutiles from the Jurassic sandstones in the Central Sakarya Zone, NW Turkey: U-Pb ages and trace element geochemistry. Geochemistry 80, 125667. http://doi.org/10.1016/j.chemer.2020.125667

Shaanan, U., Avigad, D., Morag, N., Güngör, T. and Gerdes, A., 2021. Drainage response to Arabia–Eurasia collision: Insights from provenance examination of the Cyprian Kythrea flysch (Eastern Mediterranean Basin). Basin Res. 33, 26-47. http://doi.org/10.1111/bre.12452

Sharief, F.A., 1986. Depositional environments of the Triassic system in central Saudi Arabia. Geol. J. 21, 403-420. http://doi.org/10.1002/gj.3350210406

Sharkov, E., Chernyshev, I., Devyatkin, E., Dodonov, A., Ivanenko, V., Karpenko, M., Lebedev, V., Novikov, V., Hanna, S. and Khatib, K., 1998. New data on the geochronology of upper Cenozoic plateau basalts from the northeastern periphery of the Red Sea Rift area (northern Syria). Trans. Russ. Acad. Sci.-Earth Sci. Sect. 358, 19-22.

Sharkov, E., Chernyshev, I., Devyatkin, E., Dodonov, A., Ivanenko, V., Karpenko, M., Leonov, Y.G., Novikov, V., Hanna, S. and Khatib, K., 1994. Geochronology of Late Cenozoic basalts in western Syria. Petrology 2, 385-394.

Sherlock, S., Kelley, S., Inger, S., Harris, N. and Okay, A., 1999. ^{40}Ar-^{39}Ar and Rb-Sr geochronology of high-pressure metamorphism and exhumation history of the Tavsanli Zone, NW Turkey. Contrib. Mineral. Petrol. 137, 46-58. http://doi.org/10.1007/PL00013777

Stampfli, G.M. and Borel, G., 2002. A plate tectonic model for the Paleozoic and Mesozoic constrained by dynamic plate boundaries and restored synthetic oceanic isochrons. Earth Planet. Sci. Lett. 196, 17-33. http://doi.org/10.1016/S0012-821X(01)00588-X

Teipel, U., Eichhorn, R., Loth, G., Rohrmüller, J., Höll, R. and Kennedy, A., 2004. U-Pb SHRIMP and Nd isotopic data from the western Bohemian Massif (Bayerischer

Wald, Germany): implications for upper Vendian and lower Ordovician magmatism. Int. J. Earth Sci. 93, 782-801. http://doi.org/10.1007/s00531-004-0419-2

Tekin, U.K., Okuyucu, C., Sayit, K., Bedi, Y., Noble, P.J., Krystyn, L. and Göncüoglu, M.C., 2019. Integrated Radiolaria, benthic foraminifera and conodont biochronology of the pelagic Permian blocks/tectonic slices and geochemistry of associated volcanic rocks from the Mersin Mélange, southern Turkey: Implications for the Permian evolution of the northern Neotethys. Isl. Arc 28, e12286. http://doi.org/10.1111/iar.12286

Tien, C.-Y., Lin, Y.-C., Chu, M.-F., Chung, S.-L. and Bingöl, A.F., 2017. A hidden Late Cretaceous arc and subsequent magmatic events in the Caucasus-Iran-Anatolia (CIA) orogenic belt: Detrital zircon U-Pb and Hf isotopic constraints, AGU Fall Meeting Abstracts, pp. T41A-0608.

Torley, J.M. and Robertson, A.H.F., 2018. New evidence and interpretation of facies, provenance and geochemistry of late Triassic-early Cretaceous Tethyan deep-water passive margin-related sedimentary rocks (Ayios Photios Group), SW Cyprus in the context of eastern Mediterranean geodynamics. Sediment. Geol. 377, 82-110. http://doi.org/10.1016/j.sedgeo.2018.09.001

Trifonov, V., Dodonov, A., Sharkov, E., Golovin, D., Chernyshev, I., Lebedev, V., Ivanova, T., Bachmanov, D., Rukieh, M. and Ammar, O., 2011. New data on the Late Cenozoic basaltic volcanism in Syria, applied to its origin. J. Volcanol. Geotherm. Res. 199, 177-192. http://doi.org/10.1016/j.jvolgeores.2010.01.013

Tripathy, G.R., Singh, S.K. and Ramaswamy, V., 2014. Major and trace element geochemistry of Bay of Bengal sediments: Implications to provenances and their controlling factors. Palaeogeogr. Palaeoclimatol. Palaeoecol. 397, 20-30. http://doi.org/10.1016/j.palaeo.2013.04.012

Tsikouras, B., Lai, C.-K., Ifandi, E., Norazme, N.A., Teo, C.-H. and Xia, X.-P., 2021. New zircon radiometric U-Pb ages and Lu-Hf isotopic data from the ultramafic-mafic sequences of Ranau and Telupid (Sabah, eastern Malaysia): Time to reconsider the geological evolution of Southeast Asia? Geology 49, 789-793. http://doi.org/10.1130/G48126.1

Ustaömer, P.A., Ustaömer, T., Collins, A.S. and Robertson, A.H.F., 2009. Cadomian (Ediacaran–Cambrian) arc magmatism in the Bitlis Massif, SE Turkey: Magmatism along the developing northern margin of Gondwana. Tectonophysics 473, 99-112. http://doi.org/10.1016/j.tecto.2008.06.010

Ustaömer, P.A., Ustaömer, T., Gerdes, A., Robertson, A.H.F. and Collins, A.S., 2012. Evidence of Precambrian sedimentation/magmatism and Cambrian metamorphism in the Bitlis Massif, SE Turkey utilising whole-rock geochemistry and U–Pb LA-ICP-MS zircon dating. Gondwana Res. 21, 1001-1018. http://doi.org/10.1016/j.gr.2011.07.012

Ustaömer, T., Robertson, A.H.F., Ustaömer, P.A., Gerdes, A. and Peytcheva, I., 2013. Constraints on Variscan and Cimmerian magmatism and metamorphism in the Pontides (Yusufeli–Artvin area), NE Turkey from U–Pb dating and granite geochemistry. In: A.H.F. Robertson, O. Parlak and U.C. Ünlügenç (Editors), Geological Development of Anatolia and the Easternmost Mediterranean Region. Geological Society of London, Special Publications, pp. 49-74.

Ustaömer, T., Ustaömer, P.A., Robertson, A.H.F. and Gerdes, A., 2016. Implications of U–Pb and Lu–Hf isotopic analysis of detrital zircons for the depositional age, provenance and tectonic setting of the Permian–Triassic Palaeotethyan Karakaya Complex, NW Turkey. Int. J. Earth Sci. 105, 7-38. http://doi.org/10.1007/s00531-015-1225-8

Ustaömer, T., Ustaömer, P.A., Robertson, A.H.F. and Gerdes, A., 2020. U-Pb-Hf isotopic data from detrital zircons in late Carboniferous and Mid-Late Triassic sandstones, and also Carboniferous granites from the Tauride and Anatolide continental units in S Turkey: implications for Tethyan palaeogeography. Int. Geol. Rev. 62, 1159-1186. http://doi.org/10.1080/00206814.2019.1636415

Uzuncimen, S., Tekin, U.K., Bedi, Y., Perincek, D., Varol, E. and Soycan, H., 2011. Discovery of the Late Triassic (Middle Carnian–Rhaetian) radiolarians in the volcano-sedimentary sequences of the Kocali Complex, SE Turkey: Correlation with the other Tauride units. J. Asian Earth Sci. 40, 180-200. http://doi.org/10.1016/j.jseaes.2010.08.004

van Hinsbergen, D.J., Torsvik, T.H., Schmid, S.M., Maţenco, L.C., Maffione, M., Vissers, R.L., Gürer, D. and Spakman, W., 2020. Orogenic architecture of the Mediterranean region and kinematic reconstruction of its tectonic evolution since the Triassic. Gondwana Res. 81, 79-229. http://doi.org/10.1016/j.gr.2019.07.009

Waldron, J., 1984. Structural history of the Antalya Complex in the ‘Isparta Angle’, Southwest Turkey. In: J.E. Dixon and A.H.F. Robertson (Editors), Geological Evolution of the Eastern Mediterranean. Geological Society of London, Special Publications, pp. 273-286.

Watson, E.B. and Harrison, T.M., 1983. Zircon saturation revisited: temperature and composition effects in a variety of crustal magma types. Earth Planet. Sci. Lett. 64, 295-304. http://doi.org/10.1016/0012-821X(83)90211-X

Weiler, Y., 1970. Mode of occurrence of pelites in the Kythrea flysch basin (Cyprus). J. Sediment. Res. 40, 1255-1261. http://doi.org/10.1306/74D7217B-2B21-11D7-8648000102C1865D

Woodcock, N.H. and Robertson, A.H.F., 1977. Origins of some ophiolite-related metamorphic rocks of the “Tethyan” belt. Geology 5, 373-376. http://doi.org/10.1130/0091-7613(1977)5<373:OOSOMR>2.0.CO;2

Woodside, J., 1977. Tectonic elements and crust of the eastern Mediterranean Sea. Mar. Geophys. Res. 3, 317-354. http://doi.org/10.1007/BF00285658

Wu, S., Yang, M., Yang, Y., Xie, L., Huang, C., Wang, H. and Yang, J., 2020. Improved in situ zircon U–Pb dating at high spatial resolution (5–16 μm) by laser ablation–single collector–sector field–ICP–MS using Jet sample and X skimmer cones. Int. J. Mass Spectrom. 456, 116394. http://doi.org/10.1016/j.ijms.2020.116394

Xiang, W., Griffin, W.L., Jie, C., Pinyun, H. and Xiang, L., 2011. U and Th contents and Th/U ratios of zircon in felsic and mafic magmatic rocks: Improved zircon ‐ melt distribution coefficients. Acta Geologica Sinica (English Edition) 85, 164-174. http://doi.org/10.1111/j.1755-6724.2011.00387.x

Xie, L., Zhang, Y., Zhang, H., Sun, J. and Wu, F., 2008. In situ simultaneous determination of trace elements, U-Pb and Lu-Hf isotopes in zircon and baddeleyite. Chin. Sci. Bull. 53, 1565-1573. http://doi.org/10.1007/s11434-008-0086-y

Xin, G.-Y., Chu, Y., Su, B.-X., Lin, W., Uysal, I. and Feng, Z.-T., 2021. Rapid transition from MORB-type to SSZ-type oceanic crust generation following subduction initiation: insights from the mafic dikes and metamorphic soles in the Pozantı-Karsantı ophiolite, SE Turkey. Contrib. Mineral. Petrol. 176, 64. http://doi.org/10.1007/s00410-021-01821-5

Yılmaz, Y., 1989. An approach to the origin of young volcanic rocks of western Turkey. In: A.M.C. Şengör (Editor), Tectonic Evolution of the Tethyan Region. NATO ASI Series (Series C: Mathematical and Physical Sciences). Springer, pp. 159-189.

Yılmaz, Y., 1993. New evidence and model on the evolution of the southeast Anatolian orogen. Geol. Soc. Am. Bull. 105, 251-271. http://doi.org/10.1130/0016-7606(1993)105<0251:NEAMOT>2.3.CO;2

Yu, Z., Colin, C., Wan, S., Saraswat, R., Song, L., Xu, Z., Clift, P., Lu, H., Lyle, M. and Kulhanek, D., 2019. Sea level-controlled sediment transport to the eastern Arabian Sea over the past 600 kyr: Clay minerals and SrNd isotopic evidence from IODP Site U1457. Quat. Sci. Rev. 205, 22-34. http://doi.org/10.1016/j.quascirev.2018.12.006

Zanchi, A., Garzanti, E., Larghi, C., Angiolini, L. and Gaetani, M., 2003. The Variscan orogeny in Chios (Greece): Carboniferous accretion along a Palaeotethyan active margin. Terra Nova 15, 213-223. http://doi.org/10.1046/j.1365-3121.2003.00483.x

Zlatkin, O., Avigad, D. and Gerdes, A., 2013. Evolution and provenance of Neoproterozoic basement and Lower Paleozoic siliciclastic cover of the Menderes Massif (western Taurides): coupled U–Pb–Hf zircon isotope geochemistry. Gondwana Res. 23, 682-700. http://doi.org/10.1016/j.gr.2012.05.006

Zoleikhaei, Y., Amini, A. and Zamanzadeh, S.M., 2015. Integrated provenance analysis of Zakeen (Devonian) and Faraghan (early Permian) sandstones in the Zagros belt, SW Iran. J. Afr. Earth Sci. 101, 148-161. http://doi.org/10.1016/j.jafrearsci.2014.09.012

Figure Caption

Fig. 1 Outline tectonic map of the Eastern Mediterranean region and its major tectonic zones, including the main tectonic units mentioned in the text. Main data source MTA (2011). Abbreviations: A, Andırın; AB, Adana Basin; AC, Antalya Complex; AM, Alanya Massif; AMt, Amanos Mountain; An, Anamas; Ak, Akseki; As, Asi (Orontes); BA, Banias; BB, Baer-Bassit; BHH, Beyşehir-Hoyran-Hadim (Bözkır) nappes; BM, Bitlis Massif; BO, Bolkar nappe; BoM, Bolu Massif; CB, Cilicia Basin; Ce, Ceyhan; CyB, Cyprus Basin; D, Divriği; Do, Doğanşehir; E, Elazığ; EB, Erciyes Basin; Ec, Ecemiş corridor; En, Engizek; F, Feke; GD, Geyik Dağı; Go, Göksu; HA, Hatay (Kızıldağ); HB, Hekimhan Basin; HeB, Herodotus Basin; IA, Isparta Angle; K, Kahramanmaraş; KA, Kazdağ; KC, Konya Complex; KD, Karacahisar dome; KO, Koçali ophiolite; KP, Karaburun Peninsula; LB, Levant Basin; LnR, Larnaca Ridge; M, Muş; Ma, Malatya; MA, Mamonia Complex; MC, Maden Complex; Mi, Misis; MM, Mersin Massif; MaM, Malatya Metamorphics; OLB, Outer Latakia Basin; OR, Orhaneli; PKO, Pozantı-Karsantı ophiolite; PM, Pütürge Massif; S, Sivas; SD, Sultan Dağı; Se, Seyhan; TM, Troodos Massif; TR, Tartus Ridge; UB, Ulukışla Basin.

Fig. 2 Simplified stratigraphy of the Kyrenia Range, N Cyprus (modified from McCay and Robertson, 2012). The paleocurrent data are from McCay (2010).

Fig. 3 (a) Eastward view on the narrow, east-west trending Kyrenia Range, here dominated by Mesozoic thrust sheets of Trypa Group meta-carbonate rocks, E of Beylerbeyi, central range; (b) Mesozoic meta-platform carbonates and unconformably overlying Upper Eocene-Miocene turbidites of the Kythrea Group, W of Karşıyaka, western range; (c) Irregular unconformity between thick-bedded marble of the Trypa Group and pinkish basal breccia and pelagic carbonates and volcanics of the Melounda Formation, S of Karşıyaka, western range; (d) Eocene-

Miocene turbidites of the Kythrea Group in the northern part of the Mesaoria Basin, with central Kyrenia Range behind, W of Değirmenlik; (e) Panoramic view of Upper Eocene-Miocene sandstone turbidites of the Kythrea Group in the northern part of the Mesaoria Basin, SW of Değirmenlik, central range.

Fig. 4 Outline geological map of the Kyrenia Range (modified from Robertson et al., 2012b). Sample locations are indicated by coloured numbers.

Fig. 5 Representative photomicrographs of sandstones analysed from the Kyrenia Range. (a) Medium to coarse-grained sandstone of the Kiparisso Vouno Member (GC19-09), with angular clasts of chert, recrystallised limestone and muscovite; (b) Detrital grains of recrystallised chert, basalt (with microphenocrysts) and metamorphic lithic fragments in the Kalograia-Ardana Formation (GC19-11); (c) Coarse-grained sandstone with angular grains of quartz (both monocrystalline and polycrystalline), together with various different rock fragments in a calcite spar cement (GC19-13; Kythrea Conglomerate); (d) Medium-grained sandstone from the Bellapais Formation (GC19-12), with abundant angular to sub-angular serpentinite grains and radiolarian chert in a calcite spar cement; (e) Medium-grained sandstone with recrystallised micritic carbonate grains, together with metamorphic lithics (e.g., mica-schist), relatively rounded quartz and felspar, from the Klepini Formation (GC19-22); (f) Medium-grained sandstone of the Flamoudi Formation (GC19-31) showing a mixed assemblage of planktonic and benthic foraminifera; (g) Fine to medium-grained sandstone of Panagra Formation (GC19-30), with grains of quartz and carbonate including foraminifera, set in a calcite spar cement; (h) Medium-grained sandstone of the Trapeza Formation (GC19-06) with subangulargrains of quartz, feldspar and micritic carbonate; (i) Poorly sorted sandstone of the Davlos Formation (GC19-33) with grains of serpentinite, muscovite, redeposited carbonate; (j) Sandstone of Mia Milia Formation (GC19-57) with redeposited micritic carbonate and biogenic grains including foraminifera; (k) Gypsiferous sandstone of the Yılmazköy Formation (GC19-53), with small quartz, metamorphic lithic and biogenic grains; (l) Reworked grains of calcareous red algae and foraminifera, plus detrital grains of quartz, micritic carbonate and sedimentary lithic fragments in sandstone of the Athalassa Formation (GC19-17). Abbreviations: Qz, quartz; RL, recrystallised limestone; Ch, chert; CA, calcite cement; Ms, muscovite; Md, mudstone; Bs, basalt; C, chert (variably recrystallised, both primary radiolarian chert and silica-replaced carbonate); Lm, metamorphic lithics; S, serpentinite (ophiolite-derived rock clast); Lv, volcanic lithics; Mc, micritic carbonate; F, foraminifera; Fsp, feldspar; Ls, sedimentary lithics; RA, reworked grain of calcareous red algae.

Fig. 6 Kernel Density Estimation (KDE) plots for detrital zircon U-Pb ages obtained for the samples from the western (red curve) and central (green curve) Kyrenia Range (concordant ages only). Bandwidths were set at 5 Ma and 20 Ma, with fixed binwidths of 10 Ma and 30 Ma for the time windows of 0-541 Ma and 0-4000 Ma, respectively.

Fig.7 Zircon Th/U ratio versus age plot for the sandstones analysed. The magmatic and metamorphic zircon fields are from Teipel et al. (2004). The fields for mafic and felsic melt-sourced zircons are from Linnemann et al. (2011). Separated Th/U data for each formation are given in Supplementary Figure S5.

Fig. 8 Kernel Density Estimation (KDE) plots for detrital zircon U-Pb ages obtained for the samples from the eastern Kyrenia Range (blue curve) and the Karpas Peninsula (purple curve) (concordant ages only). Bandwidths were set at 5 Ma and 20 Ma, with fixed binwidths of 10 Ma and 30 Ma for the time windows of 0-541 Ma and 0-4000 Ma, respectively.

Fig. 9 (a-c) U/Yb versus Nb/Yb (Grimes et al., 2015) and (d-f) Nb/Hf versus Th/U (Hawkesworth and Kemp, 2006) for the zircons analysed.

Fig. 10 $\varepsilon Hf_{(t)}$ versus age plots of the sandstones of the western (a-c), central (d-f), eastern (g-i) Kyrenia Range and the Karpas Peninsula (j-l) analysed during this work. Abbreviations: DM, depleted mantle, data after Chauvel et al. (2008); CHUR, Chondrite Uniform Reservoir, data after Bouvier et al. (2008). The arrows show the evolutionary trends of the zircons during Late Cretaceous-Pliocene, which reflect the involvement of juvenile materials which have relatively positive $\varepsilon Hf_{(t)}$ values (e.g., remnant Neotethys); recycled crustal additions have negative $\varepsilon Hf_{(t)}$ values.

Fig. 11 Simplified sedimentary log of the Middle-Upper Triassic to Pleistocene of the Kyrenia Range, together with the U-Pb zircon age populations obtained during this study, combined with published data from Chen et al. (2019), Shaanan et al. (2021) and Glazer et al. (2021). The dominant zircon morphology is indicated. The number of zircons in each age category are indicated within the two different boxes (euhedral/subhedral zircons) and the oval shapes (subrounded/rounded); black for the main peaks and white for the small peaks. The zircon data are indicated separately for the western, central and the eastern Kyrenia Range areas and for the Karpas Peninsula to facilitate regional comparisons.

Fig. 12 (a) $\varepsilon Hf_{(t)}$ versus U-Pb age plot of zircons from the Triassic Sikhari Formation, the Upper Cretaceous rhyolite block, the Middle Eocene Kalogaria-Ardana Formation, the Upper Eocene-Oligocene Bellapais Formation, the Lower Miocene Flamoudi Formation and the Lower-Upper Miocene Mia Milia Formation; data from Glazer et al. (2021) and Shaanan et al. (2021); (b) $\varepsilon Hf_{(t)}$ values of Carboniferous-Recent zircons from the Kyrenia Range, compared with literature data from possible source rocks in the region. Comparative data from Fu et al. (2015), Lin et al. (2015), Karslı et al. (2016), Ustaömer et al. (2016, 2020), Tien et al. (2017), Bingöl et al. (2018), Şengün et al. (2020), Xin et al. (2021). Abbreviations: DM, depleted mantle, data after Chauvel et al. (2008); CHUR, Chondrite Uniform Reservoir, data after Bouvier et al. (2008).

Fig. 13 Alternative tectonic models of the Kyrenia Range in the Eastern Mediterranean region showing sources of detrital zircons. (a) The Kyrenia Range is restored to the northern margin of Southern Neotethys (Robertson and Woodcock, 1986; McCay and Robertson, 2012; Robertson et al., 2012a, 2014): (a1) during rifting and passive margin phase; (a2) during Upper Cretaceous northward subduction; (a3) during Middle Eocene northward convergence; (a4) during Upper Miocene convergence to the south of Cyprus; (b) The Kyrenia Range is restored as part of the distal, N Africa continental margin (Maffione et al., 2017; McPhee and van Hinsbergen, 2019). This model focusses on the Upper Cretaceous-Upper Miocene tectonic development, while assuming the prior existence of an oceanic basin with the Kyrenia Range on its southern, passive margin (i.e., N Africa-Arabia): (b1) the Upper Cretaceous ophiolites form within S

Neotethys far to the NE; the subducting slab then rolls back and ‘invades’ the eastern Mediterranean and is emplaced southwards onto the N Africa-Arabia continental margin and northwards onto Tauride crust; (b2) the Middle Eocene remained passive, with the Kyrenia Range still attached to N Africa; (b3) northward subduction is activated south of Cyprus, similar to (aiv); (c) The Kyrenia Range is restored as a far-travelled allochthonous unit derived from the southern margin of Eurasia (Glazer et al., 2021); alternative positions are indicated by dashed circles: (c1) the model focusses on the Triassic to Mid-Eocene development of the Kyrenia Range. The Kyrenia Range is located along the Eurasian active margin, with a setting along the outer north-Gondwana margin (Anatolides) as an alternative; (c2) zircons were still able to reach the Kyrenia Range in its far-northerly position; (c3) the entire Kyrenia Range was tectonically transported to near its present position in the northeastern Mediterranean region, cutting off zircon supply from Eurasia.